UNIVERSITY OF CALIFORNIA, SAN DIEGO

Mechanisms of Spike Generation in Neocortical Neurons

A dissertation submitted in partial satisfaction of the requirements for the degree Doctor of Philosophy in Neurosciences

by

Zachary F. Mainen

Committee in charge:

Professor Terrence J. Sejnowski, Chair
Professor Martin I. Sereno
Professor Charles F. Stevens
Professor Stephen J. Heinemann
Professor Stephen L. Foote
Professor Roberto Malinow

1995

The dissertation of Zachary F. Mainen is approved, and it is acceptable in quality and form for publication on microfilm:

Chair

University of California, San Diego

1995

TABLE OF CONTENTS

LIST OF FIGURES

LIST OF TABLES

ACKNOWLEDGEMENTS

First, I wish thank my advisor, Terry Sejnowski, whose guidance and encouragement made possible this dissertation. It has been a wonderful experience to share in his vision and enthusiasm for neuroscience.

It is a pleasure to thank the members of Terry's lab at the Salk Institute, who made this an ideal place to work and play at the game of "solving the brain". A special debt of gratitude goes to Tony Bell and Misha Tsodyks, whose struggles with Terry and me to understand the "noisy neuron" ultimately inspired Chapters IV and V of this thesis. Similar thanks go to John Huguenard and Jasdan Joerges, whose electronic correspondence were essential to Chapter II. I also benefited greatly from discussions with Chuck Stevens and members of his lab downstairs, particularly Tony Zador.

Of course one must thank the hand that feeds. My graduate work was supported by a predoctoral fellowship from the Howard Hughes Medical Institute and ongoing support from the "Mainen Fund".

Finally, I am most deeply indebted to my family and to all my friends who have supported me and put up with me during my years here in San Diego. Thank you.

Please note that Chapters II–IV are based on material published or submitted for publication in which I was the primary investigator and my dissertation advisor supervised the research. Chapter II is based on material that will be published in Mainen, Z. F., Joerges, J., Huguenard, J. R., and Sejnowski, T. J. "A model of spike initiation in neocortical pyramidal neurons", *Neuron*, 15, 1995. Chapter III is based on material submitted for publication in Mainen, Z. F. and Sejnowski, T. J. "Dendritic structure determines repetitive firing properties in model neocortical neurons", 1995. Chapter IV is based on material originally published in Mainen, Z. F. and Sejnowski, T. J. "Reliability of spike timing in neocortical neurons", *Science*, 268:1503–1506, 1995.

VITA

1991	B.A. Yale University
1991	M.S. Yale University
1991–1995	Howard Hughes Medical Institute Predoctoral Fellow
1995	Ph.D. University of California, San Diego

PUBLICATIONS

Mainen, Z. F. and Sejnowski, T. J. (1995). Reliability of spike timing in neocortical neurons. *Science*, 268:1503-1506.

Mainen, Z. F., Joerges, J., Huguenard, J., and Sejnowski, T. J. (1995). A model of spike initiation in neocortical pyramidal neurons. *Neuron*, in press.

Bell, A., Mainen, Z. F., and Sejnowski, T. J. (1995). 'Balancing of conductances' may explain irregularity of cortical spiking. Technical Report 9502, Institute for Neural Computation, La Jolla, CA.

Destexhe, A., Mainen, Z. F., and Sejnowski, T. J. (1995a). Elementary kinetics provide efficient models of synaptic transmission and neuromodulation. In Bower, J., editor, *The Neurobiology of Computation*, volume 2, pages 9–14. Kluwer Academic Press, Norwell, MA.

Destexhe, A., Mainen, Z. F., and Sejnowski, T. J. (1995b). Synaptic currents, neuromodulation and kinetic models. In Arbib, M., editor, *The Handbook of Brain Theory and Neural Networks*, pages 956-959. MIT Press, Cambridge, MA.

Destexhe, A., Mainen, Z. F., and Sejnowski, T. J. (1994a). An efficient method for computing synaptic conductances based on a kinetic model of receptor binding. *Neural Computation*, 6:14–18.

Destexhe, A., Mainen, Z. F., and Sejnowski, T. J. (1994b). Synthesis of models for excitable membranes, synaptic transmission, and neuromodulation using a common kinetic framework. *J. Computational Neurosci.*, 1:195–230.

Bell, A., Mainen, Z. F., Tsodyks, M., and Sejnowski, T. J. (1994). Balancing of conductances may explain irregularity of cortical spiking. In *Proc. Joint Symposium on Neural Computation: UCSD and Caltech*, number INC-9502, pages 1–5, La Jolla, CA. Inst. for Neural Computation.

Huguenard, J., Joerges, J., Mainen, Z. F., and Sejnowski, T. J. (1994). Functional role of axon hillock and initial segment in cortical spike initiation. *Soc. Neurosci. Abstr.*, 20:1527.

Mainen, Z. F. and Sejnowski, T. J. (1994a). Reliability of spike encoding in neocortical neurons. In *Proc. Joint Symposium on Neural Computation: UCSD and Caltech*, number INC-9502, pages 24–29, La Jolla, CA. Inst. for Neural Computation.

Mainen, Z. F. and Sejnowski, T. J. (1994b). Reliability of spike initiation in neocortex. *Soc. Neurosci. Abstr.*, 20:1527.

Tsodyks, M., Bell, A., Mainen, Z. F., and Sejnowski, T. J. (1994). Why do cortical neurons spike irregularly? *Soc. Neurosci. Abstr.*, 20:1527.

Brown, T. H., Zador, A. M., Mainen, Z. F., and Claiborne, B. J. (1992). Computational models of the principal classes of hippocampal neurons. In McKenna, T., Davis, J., and Zornetzer, S., editors, *Single Neuron Computation*, pages 61–80. Academic Press, New York.

Kairiss, E. W., Mainen, Z. F., Claiborne, B. J., and Brown, T. H. (1992). Dendritic control of hebbian computations. In Eeckman, F., editor, *Analysis and Modeling of Neural Systems*. Kluwer Academic, Boston, MA.

Brown, T. H., Mainen, Z. F., Zador, A. M., and Claiborne, B. J. (1991a). Self-organization and nonlinear processing in hippocampal neurons. In Lippman, R., Moody, J., and Touretzky, D., editors, *Advances in Neural Information Processing Systems*, volume 3, pages 39–45. Morgan Kaufmann, San Mateo, CA.

Brown, T. H., Zador, A. M., Mainen, Z. F., and Claiborne, B. (1991b). Hebbian computations in hippocampal neurons. In Baudry, M. and Davis, J., editors, *Long-term Synaptic Potentiation: A Debate of Current Issues*, pages 357–390. MIT Press, Cambridge, MA.

Mainen, Z. F., Claiborne, B. J., and Brown, T. H. (1991). A novel role for synaptic competition in the development of cortical lamination. *Soc. Neurosci. Abstr.*, 17:759.

Mainen, Z. F., Zador, A. M., Claiborne, B. J., and Brown, T. H. (1990). Hebbian synapses induce feature mosaics in hippocampal dendrites. *Soc. Neurosci. Abstr.*, 16:492.

ABSTRACT OF THE DISSERTATION

Mechanisms of Spike Generation
in Neocortical Neurons

by

Zachary F. Mainen
Doctor of Philosophy in Neurosciences
University of California, San Diego, 1995
Professor Terrence J. Sejnowski, Chair

While the basic workings of the nerve impulse have been known for some time, our understanding of how action potentials are generated and used by neurons is still far from complete. In this dissertation, the techniques of *in vitro* electrophysiology and computer modeling were used to address several questions concerning spike generation in neocortical pyramidal neurons. 1. What makes the axon initial segment the natural locus of spike initiation, and what contribution is made by dendritic sodium channels to initiation and propagation of the spike? 2. What is the anatomical or physiological basis for the heterogeneity of intrinsic firing patterns observed across different types of neocortical neurons? 3. With what degree of temporal precision can a spike train encode a stream of synaptic input? 4. What impact does spike frequency adaptation have on the reliability of the encoding process? The results presented suggest the importance of the details of cell morphology and ion channel distribution to the electrical signaling properties of cortical neurons. A high density of sodium channels in the axon initial segment appears to make it a preferred and highly reliable locus for spike initiation. Meanwhile, low densities of dendritic sodium channels promote the active propagation of a somatic spike into the dendrites. The currents produced by this dendritic sodium spike, and those of the dendritic potassium channels it activates, link the characteristic firing pattern of a cortical neuron directly to its dendritic morphology. Finally, the slow potassium channels, mediating spike frequency adaptation, improve the temporal precision of spike encoding by increasing the relative sensitivity of spike generation to stimulus transients.

Chapter I

Introduction and Summary

In this dissertation, four chapters explore two themes concerning action potentials in neocortical neurons. The first two make use of detailed computer models to address mechanistic questions. The third and fourth make use of electrophysiological recordings and minimal models to address questions relating to the role of action potentials in the representation of information.

The basic mechanisms of the nerve impulse have been known since the seminal work of Hodgkin and Huxley (1952), and it is accepted that trains of impulses are an almost exclusive mode of communication between neurons in the cortex. Considerably less clear are how the detailed properties of spike trains produced by cortical neurons arise from their cellular substrates—the electrical structure of cytoplasm and membrane and the distribution of ion channels within it—and what relevance the details have to the functions they perform.

We are thus unable to list confidently the ways that spike generation by a cortical neuron differs from that in any other excitable membrane such as that of the squid giant axon. We do not know with any certainty which of the properties of these neurons are functionally significant and which are not. Consequently, with respect to the goal of describing the role of a neuron as a computational element in the brain, there does not yet exist a model that satisfactorily captures the essential aspects of spike generation.

In the first half of the thesis, the approach that we have taken to understand spike generation is a type of biophysical modeling known as "compartmental modeling" (Koch and Segev, 1989). With this technique, a neuron is decomposed into a tree of so-called equivalent electrical circuits, each representing a small length of dendrite or axon that is assumed to be isopotential. Within each compartment, the membrane is represented by a capacitance in parallel with a number of variable conductances that represent different types of ion channels. Using present desktop computers and efficient algorithms (Hines, 1993), a numerical solution for the evolution of mem-

brane potential given by the thousands of differential equations describing the equivalent circuits of a reasonably complex neuron model can be calculated at a speed typically only about one or two orders of magnitude slower than real time.

The main feature of compartmental modeling, the capacity to simulate the interactions of a multitude of currents flowing about an arbitrarily complex geometry, is both blessing and bane. The considerable disadvantage is an explosion of parameters which must be specified. In general, the more free parameters, the more ways that a model can be fit to a given set of data; the output of a compartmental model—the simulated response to some experimental stimulus—is usually vastly under-constrained by even the best electrophysiological recordings. Nevertheless, the power of the compartmental modeling approach stems from the fact that it is possible to relate each of the many parameters directly to a physical property of the neuron that can, at least in principle, be independently measured. Thus, a compartmental model can combine large amounts of isolated anatomical and physiological data in a way that tests their adequacy in explaining or predicting the behavior of the whole cell.

Interest in a better biophysical model of a cortical neuron was stirred recently by a seemingly paradoxical finding concerning action potentials in these cells. In an investigation of the locus of spike initiation, simultaneous dual somatic and dendritic recordings were made from neocortical pyramidal neurons (Stuart and Sakmann, 1994). It was found that spikes were preferentially initiated at the axon initial segment, as has long been thought for the spinal motoneuron (Coombs, Curtis and Eccles, 1957). However, it was also found that the dendritic membrane contained a density of sodium channels equal to that in the soma, and that these channels substantially boosted the propagation of the action potential into the dendrites. If the dendrite was sufficiently excitable to propagate spikes, how could the axon initial segment be the site of initiation regardless of the location of the stimulus?

Chapter II of this dissertation presents a compartmental model of spike initiation developed using a wide variety of published anatomical and physiological data from neocortical pyramidal cells. In the model, spikes are initiated preferentially at the axon initial segment due partly to its high sodium channel density; the initial segment is similar in many respects to a node of Ranvier. In addition, the small diameter and electrical isolation from the soma and dendrites facilitate local regenerative depolarization. The initiation of a dendritic spike is impeded by the much larger electrical load of the dendritic tree. By the time a stimulus to a dendrite can depolarize a large region of membrane to threshold, sodium channel inactivation has reduced the available sodium channels. A somatic spike, by comparison, encounters relatively little load as it travels outward into a dendrite. Chapter III presents an extension of the model of Chapter II from the initiation

of single spikes to the production of trains of action potentials. The main additional feature is the presence of the potassium currents responsible for spike frequency adaptation. Although these currents are not significantly activated until after the first spike, they have long been known to play a large role in the control of repetitive firing. In this model the invasion of the dendritic arbor by the sodium spike was crucial in accounting for the membrane potential trajectory between spikes and the generation of spike bursts.

An intriguing result from the repetitive firing model was that manipulating the dendritic structure, without changing the densities of dendritic or axonal channels, produced a heterogeneous set of firing patterns bearing a strong resemblance to the variety found across neocortical neurons (regular spiking, bursting, fast spiking, and many intermediate varieties; McCormick et al., 1985). Although correlations between morphology and firing pattern are well known, no causal relationship between the structure and the physiology has been determined. The controlling influence of dendritic structure in the model depended in part on the numerical ratio of dendritic and axonal potassium channels and in part on the current entering during the dendritic invasion of the sodium spike. These results provide a mechanism for a link between anatomy and function and raise the interesting possibility that the basis for the heterogeneity of neocortical firing patterns may lie chiefly in a diversity of morphologies rather than in expression of many unique sets of ion channels.

In the second half of the dissertation, we turn to the question of action potential timing and variability. Our interest in the theme of spike generation was in fact originally sparked by a conundrum that we have known as the "noisy neuron" problem. The problem stems from the observation that the patterns of spikes recorded *in vivo* from cortical neurons are remarkably irregular (e.g. Noda and Adey, 1970; Softky and Koch, 1993). That is, over a wide range of firing frequencies the sequence of interspike intervals may have a coefficient of variation of near unity: the standard deviation of the intervals is about equal to the mean. This observation immediately raises two questions. First, what are the mechanics of variability: is it predicted by existing neural models? Second, what computational role does the variability play: is it signal or noise?

A relatively simple model that predicts high variability over a wide range of firing rates is a "random walk" model (Gerstein and Mandelbrot, 1964; Shadlen and Newsome, 1994). This is a type of simple "integrate-and-fire"model. These models generally represent spike generation as the crossing of some fixed threshold. The flavor of a particular class of model depends on the nature of assumptions about the synaptic input and the equations governing the subthreshold membrane potential. In the random walk model, the synaptic input consists of a stochastic barrage of excitatory steps balanced by a nearly equal frequency of inhibitory steps. Together, these steps drive the membrane potential in a sort of Brownian motion between resting and threshold lev-

els. The frequency of firing (threshold crossing) can be elevated not only by increasing the relative amount of excitation compared to inhibition (biasing the walk), but also simply by increasing excitation and inhibition together (speeding up the walk). The latter method preserves variability of interspike intervals, avoiding the problem of decreasing variability by integration.

The random walk model provides an explanation of neuronal variability based on strong assumptions about its origin and role: the inputs to the model are stochastic sequences generated with some mean frequency, while the methods of integration and spike generation are entirely deterministic. There is indeed experimental evidence supporting the idea that noise in spike generation is unnecessary to explain the variability of firing driven by spontaneous synaptic activity (Calvin and Stevens, 1968) and also considerable evidence that central synapses often transmit in a rather unreliable fashion. Nevertheless, synapses operating with a low basal release probability are well-suited for regulation by previous activity patterns or endogenous neuromodulators. These less stochastic factors might impose considerable deterministic control on the behavior of a synapse *in vivo*. Spike generation, by the pooling of many stochastic channels, will be much closer to deterministic. It may nevertheless be affected to varying degrees by different types of spontaneous membrane conductance fluctuations or input noise. It is therefore pertinent to ask: What is the reliability of repetitive firing (or of synaptic transmission) when encoding signals resembling those seen *in vivo*? How does the mechanism determine the susceptibility to noise?

An approach to these questions, presented in Chapter IV, used electrophysiological recordings from neurons in slices of neocortex. In this *in vitro* preparation, endogenous synaptic input can be eliminated and computer-controlled stimuli provided by current injected through the recording electrode. This makes it possible to study the "encoding" process with a degree of control impossible *in vivo*. The reliability of spike timing was assessed by repeatedly presenting the same stimulus and measuring the consistency of the evoked responses. When the stimulus was a flat (d.c.) current step, as typically used in *in vitro* experiments, it was found that due to sources of uncontrolled variability, repeated steps produced spike trains with consistent mean rates but unreliable timing. However, when patterns of input with fluctuations resembling integrated excitatory and inhibitory synaptic currents were repeated, the reliability of stimulus-locked spike timing increased dramatically. By analyzing spike-triggered averages of the stimuli, it was also found that spikes tend to be preceded by a rapid hyperpolarizing–depolarizing sequence of current. This suggested that an enhanced sensitivity to stimulus transients could make neocortical neurons somewhat more reliable in the face of slow trial-to-trial variability than would otherwise be predicted. One possible mechanism would be spike frequency adaptation, a property that results in an increased sensitivity of responses to transients compared to d.c. input.

On this basis, in Chapter V, spike encoding is examined using a simple integrate-and-fire

style model analogous to the random walk model but incorporating a mechanism for spike frequency adaptation. The adaptation mechanism is based on an analysis of the kinetics of the slow voltage-dependent and calcium-dependent potassium conductances in a compartmental model similar to that of Chapter III. The addition of an adaptation conductance to an integrate-and-fire model increases the relative sensitivity of firing to stimulus variance compared to stimulus mean and decreases the effective time constant of integration. A number of consequences for the encoding of time-varying inputs result. First, when stimulated by random synaptic input, irregular spike trains can be maintatined over a larger range of firing rates, providing a better match to *in vivo* data than corresponding non-adapting models. Second, the waveform of the reverse-correlation of spike train and stimulus is predicted accurately by adapting models but not by models without adaptation. Finally, when stimulated repeatedly by a particular time-varying stimulus, it can be seen that the precision or reliability of encoding is greater in adapting models compared to non-adapting models. This is true for both low and high noise assumptions. These results suggest that adaptation conductances, already known to be important in the regulation of repetitive firing, are particularly critical to the temporal precision of spike encoding in the neocortex.

Chapter II

A Model of Spike Initiation

Neocortical pyramidal cells possess voltage-dependent dendritic sodium channels that promote propagation of action potentials into the dendritic tree but paradoxically may fail to originate dendritic spikes. A biophysical model was constructed to reconcile these observations with known anatomical and physiological properties. When dendritic and somatic sodium channel densities compatible with electrophysiological measurements were combined with much higher densities in the axon initial segment then, regardless of the site of stimulation, spikes initiated at the initial segment and subsequently invaded the dendrites. The lower initial segment threshold arose from high current density and electrical isolation from the soma. Failure of dendritic channels to initiate spikes was due to inactivation and source-load considerations, which were more favorable for conduction of back-propagated spikes.

Introduction

The dendrites of central neurons contain a variety of voltage-gated ion channels that may be critical to the processing of electrical signals. In particular, the presence of fast voltage-dependent Na^+ channels in neocortical pyramidal cell dendrites (Huguenard, Hamill and Prince, 1989; Stuart and Sakmann, 1994) suggests that these channels may not only underlie long-distance axonal propagation but also shape dendritic function. In the subthreshold regime, dendritic Na^+ channels can be activated by local excitatory synaptic potentials (Magee and Johnston, 1995), indicating that active Na^+ currents may amplify distal synaptic events. In the superthreshold regime, synaptic potentials may not only serve to initiate Na^+ spikes at various loci, but may themselves be affected by action potentials invading the dendrites (Jester, Campbell and Sejnowski, 1995). A full grasp of the interplay between synaptic and voltage-gated currents will clearly require a de-

tailed understanding of the nature of spike initiation and propagation.

Two recent studies of neocortical pyramidal cells have provided conflicting evidence concerning the impact of dendritic Na^+ channels on the initiation of action potentials in neocortical pyramdial neurons. Using voltage-clamp techniques, Regehr et al. (1993) concluded that distal synaptic activation can initiate dendritic spikes far from the soma. By contrast, Stuart and Sakmann (1994), using simultaneous dendritic and somatic recordings, found little evidence for dendritic spike initiation following either electrical or synaptic stimulation of the dendrite. Nevertheless, dendritic Na^+ conductances substantially boosted the invasion of action potentials from the soma back into the dendrites (Stuart and Sakmann, 1994).

To help resolve these issues, we constructed a computer model of action potential generation using independent constraints from anatomical, physiological, and molecular data on neocortical pyramidal cells. Our main goals were to explain the paradoxical ability of dendritic Na^+ channels to support propagation but not initiation of dendritic spikes, to examine the role of the axon initial segment in spike initiation, and to determine the conditions that might lead to ectopic spike initiation.

Methods

A multicompartmental single-neuron model was implemented using the simulation program NEURON (Hines, 1993). The fully-implicit backward Euler integration method was used with a time step of 25 μsec (unless otherwise noted).

Dendritic Anatomy

The dendritic morphology was based on a layer 5 pyramidal neuron from a postnatal day 19 rat (D. Smetters and S. Nelson, unpublished data) filled with biocytin and digitally reconstructed using the Eutectics tracing system (Figure II.1A). A spatial discretization of ≤ 50 μm per compartment was observed for all dendritic segments except the main apical trunk, which was discretized at ≤ 10 μm per compartment.

The geometry of this cell was similar to measurements from other rat layer 5 pyramidal cells. The soma area was 1578 μm^2, comparable to a reported average area of 1393 μm^2 (Mason and Larkman, 1990). The apical trunk tapered from 4.5 to 1.4 μm between 100 and 600 μm from the soma, again similar to reported measurements (Larkman and Mason, 1990). This required a slight correction of the trunk diameter of the original reconstruction to obtain a more uniform taper. The total dendritic length was 13,654 μm (6,704 μm basal, 4,167 μm apical oblique, 2,226 μm apical tuft, 557 μm apical trunk). The median overall dendritic diameter was approximately 0.75 μm.

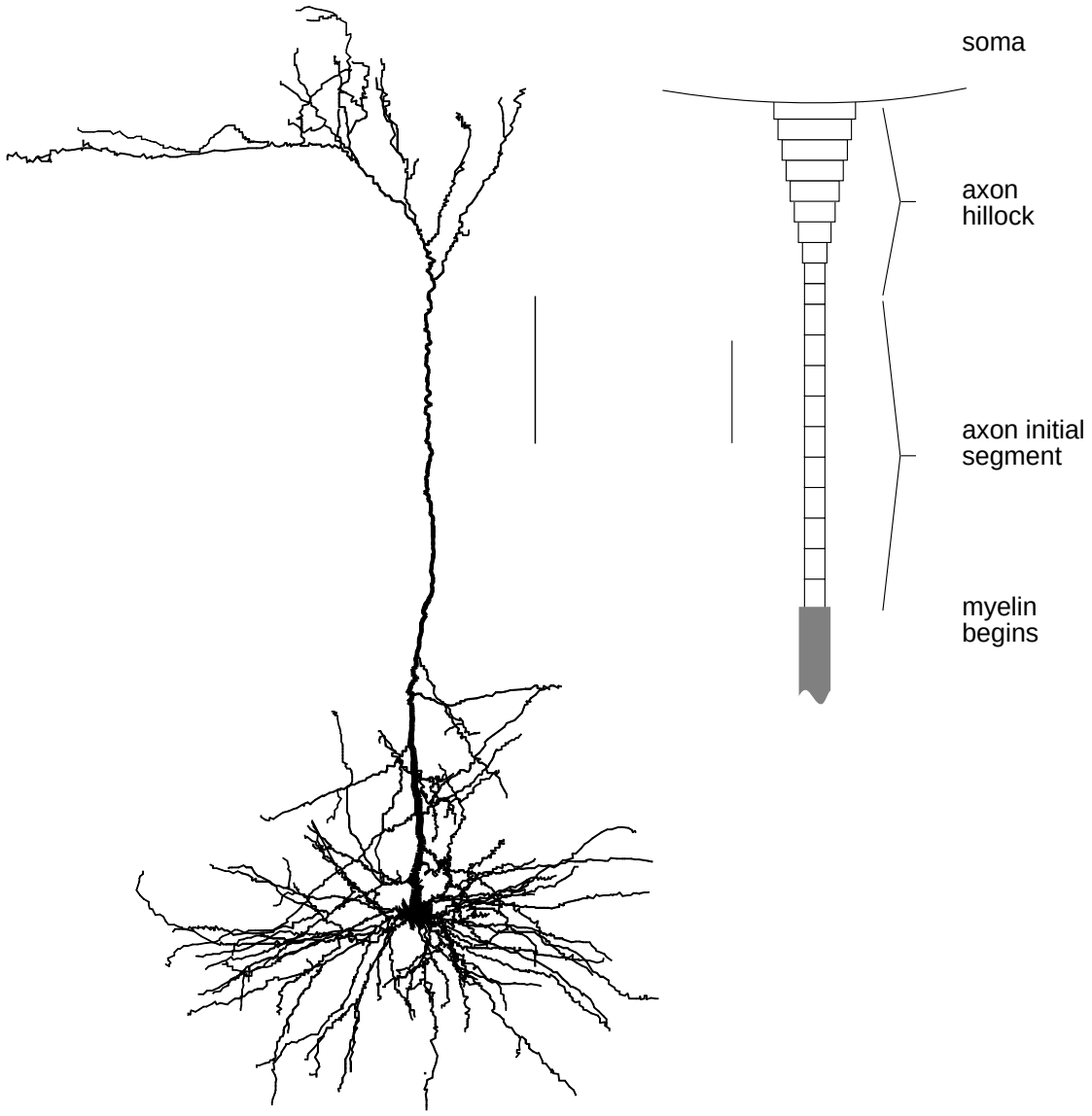

Figure II.1: Anatomy of dendritic arbor and axon hillock and initial segment. Left. Dendritic morphology of a rat layer 5 pyramidal cell recorded, filled and reconstructed by D.K. Smetters and S. Nelson (unpublished). Right. Geometry of the initial segment used in the model, based on three-dimensional serial EM reconstructions from cat layer 5 pyramidal cells (Farinas and DeFelipe, 1991). We refer to the proximal 10 μm of the initial segment, which tapers from 4 μm in diameter to 1 μm as the "hillock" and the distal 15 μm as the "initial segment". Scale bars are 100 μm (left) and 5 μm (right).

Dendritic spines were taken into account by increasing the effective membrane area (Stratford et al., 1989), see Electrical Properties below. Single spine area was 0.83 μm (Harris and Stevens, 1989). Densities were assigned to different areas based on spine counts per linear μm from rat layer 5 pyramids (Larkman, 1991). The total dendritic membrane area was 36,344 μm^2 before and 54,080 μm^2 after incorporation of spines.

Axonal Anatomy

A myelinated axon was attached to the soma of the neuron. The geometry of the initial segment (the unmyelinated segment of the axon closest to the soma) and axon hillock (the transitional zone between the soma and and initial segment proper (Palay et al., 1968); here used to refer to the proximal, tapering portion of the initial segment) have been documented in serial electron microscopic reconstructions for cat cortical pyramidal cells (Fariñas and DeFelipe, 1991). The average length of the initial segment from this study is about 20 μm and the average diameter about 1 μm, tapering from the proximal to the distal end. Similar diameters have been reported in rat neocortex (Westrum, 1970). Based on these data, our standard model consisted of a 10 μm hillock tapering from 4 to 1 μm followed by a 15 μm initial segment of 1 μm diameter (Figure II.1B). Both hillock and initial segment were divided lengthwise into 10 segments for simulation.

Myelination begins immediately at the end of the initial segment (Fariñas and DeFelipe, 1991). Measurements of cerebral axon diameters are in the range of 0.5 to 2 μm (Haug, 1968). The initial segment (and nodes of Ranvier) are generally narrower than myelinated, internodal segments of the axon (Palay et al., 1968). We assumed an internode diameter of 1.5 μm and node diameter of 1 μm. Internode lengths were 100 μm, comparable to measurements of the terminal arbors of cat cortical axons (Deschênes and Landry, 1980). Nodes themselves were 1 μm in length. Internodes were divided into 25 segments and nodes a single segment.

Electrical Properties

Membrane capacitance (C_m) is often assumed to be 1 μF-cm^{-2}, but is probably lower, in the range 0.6-0.8 μF-cm^{-2}(Major et al., 1994). We used a value of 0.75 μF-cm^{-2}. A membrane resistance of 40 kΩ-cm^2 and axial resistance of 200 Ω-cm are in line with recent modeling studies based on patch recordings (Spruston, Jaffe and Johnston, 1994; Major et al., 1994). These values gave a membrane time constant of 30 msec and an input resistance of 74.2 MΩ. Simulations were run to examine the sensitivity of the results to the specific electrical constants and were found to be insignificant to the results described.

The electrical properties of the axon are more difficult to estimate. In the absence of better

Current	Variable	Function	A	$V_{1/2}$	k
I_{Na}	m	α	0.182	-35	9
		β	0.124	-35	9
	h	α	0.024	-50	5
		β	0.0091	-75	5
		∞	-	-65	6.2
I_K	m	α	0.02	20	9
		β	0.002	20	9

Table II.1: Parameters for the equations describing the Na^+ and K^+ currents (refer to Equations II.3 and II.4 in the text).

evidence, we assumed identical parameters to the dendritic membrane, with two exceptions. First, capacitance of the myelinated segments is much lower than unmyelinated membrane (Black, Kocsis and Waxman, 1990). Second, the resistance of the nodes is believed to be substantially lower than other membrane (Black, Kocsis and Waxman, 1990), helping to repolarize the membrane following an action potential in the absence of a delayed rectifier current. In line with other axon models (Graham and Redman, 1994), we chose $R_{m-node} = 50\,\Omega$-cm^2 and $C_{m-myelin} = 0.04\,\mu$F/cm^2. The electrical properties are summarized in Table II.1.

Channel Kinetics

We assumed that the primary contribution to the initiation and propagation of single action potentials is made by the fast Na^+ channel. Although there are also dendritic voltage-dependent Ca^{2+} channels (Amitai et al., 1993; Yuste et al., 1994), these were not included in the model. As the model was not required to produce repetitive firing, other K^+ channels which sculpt such behavior were omitted. We used a single non-inactivating, voltage-dependent K^+ current to provide spike repolarization. No other channels were included.

The kinetics of the Na^+ currents were based on data obtained from acutely isolated rat neocortical neurons (Huguenard, Hamill and Prince, 1988; Hamill, Huguenard and Prince, 1991) and were very similar to those reported in rat brain Na^+ channel expressed in oocytes (Stühmer et al., 1987) and rat and human neocortex (Cummins, Xia and Haddad, 1994). We reanalyzed the original data of Hamill et al. (1991) to obtain the kinetics used. As these measurements and the experiments of Stuart and Sakmann (1994) and Regehr et al. (1994) were performed at room temperature, no adjustment of kinetics for temperature was necessary. The voltage dependence of the kinetics was uniformly shifted ~5 mV depolarized in order to obtain a higher threshold.

The equations for the Na^+ current were based on those of Hodgkin-Huxley (1952) and

were similar but not identical to those used by McCormick and Huguenard (1992). The Na^+ current was calculated using the standard ohmic relation

$$I_{Na} = \bar{g}_{Na}\, m^3\, h\, (V_m - E_{Na}), \tag{II.1}$$

where I_{Na} is the Na^+ current, V_m is the membrane potential, E_{Na} is the equilibrium potential for Na^+ (assumed to be +60 mV), m and h are the activation and inactivation state variables, respectively. The variable m ranges from 0 (not activated) to 1 (fully activated) and h ranges from 0 (fully inactivated) to 1 (no inactivation). The maximal conductance is the product $\bar{g}_{Na} = \gamma_{Na}\, \rho_{Na}$, where γ_{Na} is the single channel conductance and ρ_{Na} is the channel density. I_{Na} activation was described by the usual first order kinetic reaction, $open \rightleftharpoons closed$, which yields steady-state value m_∞ and time constant τ_m given by

$$\begin{aligned} m_\infty &= \frac{\alpha}{\alpha+\beta} \\ \tau_m &= \frac{1}{\alpha+\beta}\ , \end{aligned} \tag{II.2}$$

where α and β, the forward (opening) and backward (closing) reaction rates, respectively, are functions of the local membrane potential. Specifically,

$$\begin{aligned} \alpha(V_m) &= \frac{A\,(V_m - V_{1/2})}{1 - e^{-(V_m - V_{1/2})/k}} \\ \beta(V_m) &= \frac{-A\,(V_m - V_{1/2})}{1 - e^{(V_m - V_{1/2})/k}}\ , \end{aligned} \tag{II.3}$$

where the A is a rate constant, $V_{1/2}$ is the half-activation voltage, and k determines the slope of the activation curve. In contrast, I_{Na} inactivation was best described with independent functions for time constant and steady state values. Thus, τ_h was described analogously to τ_m, but h_∞ was given directly by

$$h_\infty = \frac{1}{1 + e^{(V_m - V_{1/2})/k}}. \tag{II.4}$$

The parameters for Equations II.3 and II.4 were derived from the data of Hamill et al. (1991) and are given in Table II.2. The steady-state and time constant voltage dependencies are shown in Figure II.2. The peak open probability (P_{open}) was 0.53 (during a step from -90 to +50 mV). A peak current of ~ 1 pA/μm^2 occurred during voltage clamp steps from -90 to -10 mV. At rest (-70 mV) 31 percent of channels were inactivated.

The equations we used to describe the Na^+ activation function were similar in form to those used in most modeling studies. However, the steepness of the activation curve was notably shallower than in many others (Lytton and Sejnowski, 1991; Bernander et al., 1991; Traub et al., 1994; Rhodes and Gray, 1994; De Schutter and Bower, 1994). The decreased slope in the present

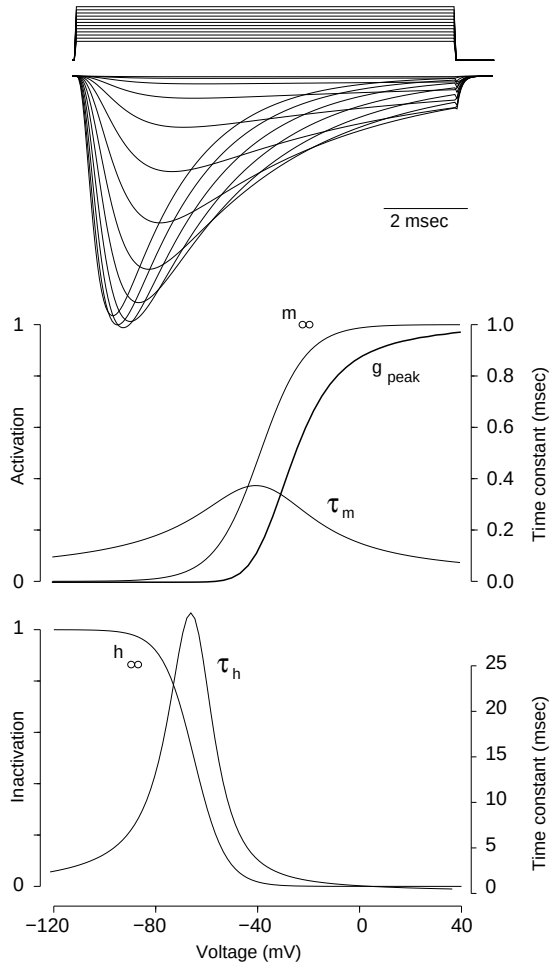

Figure II.2: I_{Na} kinetics. Top: Simulation of Na^+ currents from a series of voltage clamp steps (V_{hold} = 90 mV, V_{clamp} = -60 to 0 mV). The current amplitude scale is arbitrary. For the Na^+ channel density used in the standard model in the dendrites and soma (30 pS/μm^2), the peak current observed was $\sim$ 1 pA/μm^2. Middle: Steady-state (m_∞) and time constant (τ_m) of Na^+ channel activation are plotted as a function of membrane voltage (see Equations II.2 and II.3 in text). The voltage-dependence of peak Na^+ conductance (thick line), derived from the simulation above, is also shown. Bottom: The voltage dependence of steady-state Na^+ inactivation and inactivation time constants.

Parameter	Symbol	Region	Value	Units
Resting potential	V_{rest}		-70	mV
Axial resistivity	R_{ax}		200	Ω-cm
Membrane capacitance	C_m	soma/dend	0.75	μF/cm^2
		node	0.75	μF/cm^2
		myelin	0.04	μF/cm^2
Membrane resistivity	R_m	soma/dend	40,000	Ω-cm^2
		node	50	Ω-cm^2
		myelin	50	Ω-cm^2
Na^+ conductance density	$\bar{g}_{Na}$	soma/dend	30	pS/μm^2
		node	30,000	pS/μm^2
		myelin	30	pS/μm^2
K^+ conductance density	$\bar{g}_K$	soma/basal	100	pS/μm^2
		elsewhere	0	pS/μm^2

Table II.2: Membrane parameters used in the standard model. "Node" indicates the axon hillock, initial segment and nodal membranes.

study is in accord with the data we analyzed (Hamill, Huguenard and Prince, 1991) as well as other experimental reports (Huguenard, Hamill and Prince, 1988; Stühmer et al., 1987; Cummins, Xia and Haddad, 1994; Sah, Gibb and Gage, 1988; Belluzzi and Sacchi, 1986). Although the steeper slope apparently is adequate for most purposes, a shallower slope had significant effects in the more detailed model examined here, increasing the disparity between axonal and dendritic threshold levels.

A non-inactivating K^+ current was described by

$$I_K = \bar{g}_K \, m \, (V_m - E_K), \tag{II.5}$$

where E_K was -90 mV. Activation kinetics were analogous to the Na^+ activation variable (Equations II.2 and II.3), with parameters given in Table II.2.

Channel Distributions

Comparisons between dendritic and somatic Na^+ channel densities in neocortical pyramids have been made by whole cell (Huguenard, Hamill and Prince, 1989) and patch recordings (Huguenard, Hamill and Prince, 1989; Stuart and Sakmann, 1994). Neither study found a difference between somatic and dendritic densities. We therefore assumed a uniform density of Na^+ channels throughout the soma and dendritic membrane. Somatic and dendritic channel density in the model were adjusted in order to match the amplitude and latency distributions reported by Stuart and Sakmann (1994). We arrived at a maximal Na^+ conductance of 30 pS/μm^2. A three-fold

higher density (90 pS/μm^2) was used to reproduce results of Regehr et al. (1993). These values are comparable to estimated somatic/dendritic Na^+ conductance densities of 40 to 120 pS/μm^2 (Stuart and Sakmann, 1994; Huguenard, Hamill and Prince, 1989).

Given the relatively low channel open probability during simulated voltage clamp steps, the effective Na^+ current density in the model appears to be lower than experimental reports: model current density of 1–3 pA/μm^2 compared to 4.6 pA/μm^2 in cell attached patches (Stuart and Sakmann, 1994). At least three factors may contribute to this quantitative discrepancy. (1) Na^+ current densities in outside-out patches may be larger than in intact cells because Na^+ concentrations in the patch pipette (2 mM; Stuart and Sakmann, 1994) are significantly lower than normal intracellular concentrations (10-30 mM; Ericsinska and Silver, 1989). (2) measurements of area of patches in which Na^+ currents were measured were not available, and an area of 1.5 μm^2 (Stuart and Sakmann, 1994) may underestimate the true patch area. (3) Na^+ channels are downregulated by protein kinase C, cAMP-dependent protein kinase, and phosphoprotein phosphotases (Murphy et al., 1993; Li et al., 1992). The absence of these enzymes in the outside-out patch configuration may therefore lead to an increase in channel activity in patches compared to intact cells.

Na^+ channel density in the initial segment and nodes of Ranvier have been shown to be large compared to the internodal, somatic and dendritic membrane (Wollner and Catterall, 1986; Chiu and Schwarz, 1987; Angelides et al., 1988; Black, Kocsis and Waxman, 1990; Waxman and Ritchie, 1993). We assumed an internodal density identical to the somatic/dendritic density of 30 pS/μm^2. Conventional estimates for nodal Na^+ channel density are around 1000–2000 chan/-nels /μm^2 (reviewed in Waxman and Ritchie, 1993). Assuming a similarity between initial segment and nodes of Ranvier, which have the same ultrastructural features (Peters, Proskauer and Kaiserman-Abramof, 1968; Palay et al., 1968), we used a value of 30,000 pS/μm^2 for the initial segment and nodal membrane, corresponding to 1500-2000 channels/μm^2 at 15-20 pS single channel conductance (Alzheimer, Schwindt and Crill, 1993; Stühmer et al., 1987).

K^+ channel densities are less well known. We assumed a uniform low density throughout the soma and basal dendrites: 100 pS/μm^2. This was chosen to give weak but complete spike repolarization with minimal activation below action potential threshold in order not to interfere with initiation. No significant differences in the results were found when K^+ channels were restricted to the soma and/or initial segment (data not shown). It was necessary to exclude fast K^+ channels from the apical dendrites in order to reproduce the recordings of Stuart and Sakmann (1994), which show extremely slow repolarization of dendritic action potentials. However, appropriate dendritic repolarization and very similar overall results could also be obtained when low densities of much more slowly activating ($\tau > 25$ msec), non-inactivating, voltage-dependent K^+

channels were present in the apical dendrites (not shown). Because of the large leak conductance in the nodes of the axon, no voltage-dependent K^+ current was necessary for action potential repolarization in the axon (Kaars and Faber, 1981; Graham and Redman, 1994). The channel densities used in the model are summarized along with electrical constants in Table II.1.

Results

We examined many different combinations of Na^+ channel kinetics and distributions in an effort to reproduce the findings of Stuart and Sakmann (1994), and arrived at a model that could account for their main observation, active back-propagation without local initiation of dendritic spikes. The model combined detailed reconstructions of dendritic (D.K. Smetters and S. Nelson, unpublished data; Figure II.1A) and axonal anatomy (Fariñas and DeFelipe, 1991; Figure II.1B) of neocortical pyramidal cells with Na^+ channel kinetics measured in dissociated neocortical neurons (Huguenard, Hamill and Prince, 1988; Hamill, Huguenard and Prince, 1991; Figure II.2). A very high density of Na^+ channels in the axon initial segment compared to the soma and dendrites was suggested by a variety of data and proved to be critical to the results.

Current injection at either the soma or at points along the apical dendritic shaft evoked action potentials that originated near the soma and then invaded the dendritic site (Figure II.3A). The speed of the dendritically-propagating spike and the decrement of its amplitude with distance from the soma (Figure II.3B and C; compare to Stuart and Sakmann (1994) Figures 1d and 2d) were used to calibrate the somatic/dendritic Na^+ channel density in the model. The value obtained in this manner (2-3 μm^2) was comparable to those estimated by outside-out dendritic patch recordings (Stuart and Sakmann, 1994; see Experimental Procedures for a discussion of these density estimates). That this density of Na^+ channels greatly enhanced the invasion of back-propagating spikes can be seen by comparing the peak dendritic depolarization produced by a back-propagating action potential in models with active and passive apical dendrites (Figure II.4).

The ability of low densities of Na^+ channels to conduct but not to initiate action potentials can be partly explained by considering Na^+ channel inactivation (Figure II.5). Because the density of Na^+ channels in the somatic and dendritic membrane was low relative to the passive electrical load, threshold voltage in these regions was high. Because Na^+ channel inactivation began at voltages below this threshold with a speed comparable to the membrane time constant, substantial Na^+ inactivation occurred while the dendrite was being charged, greatly reducing the number of available Na^+ channels. In contrast, a spike invading the dendrite from the soma depolarized the membrane more rapidly, thus mitigating the effects of inactivation. This behavior is illustrated by plotting the time course of Na^+ channel inactivation (the Hodgkin-Huxley "h"

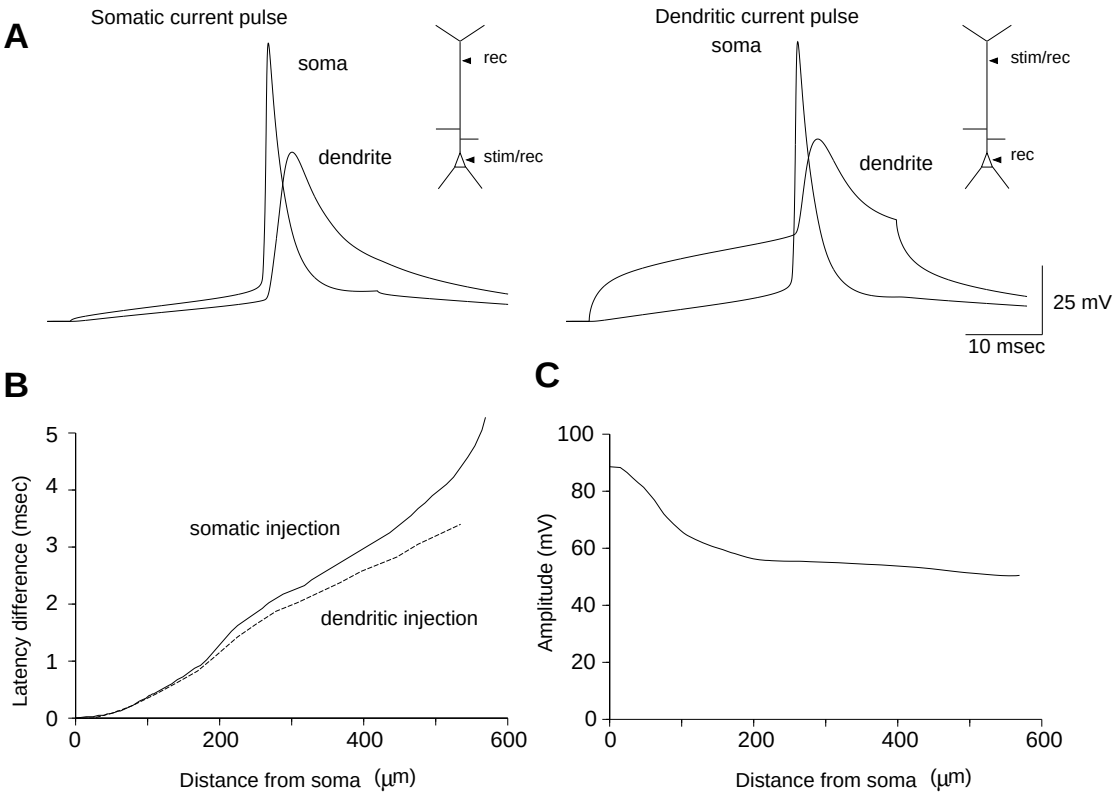

Figure II.3: Site of action potential initiation. A. Voltage traces from the soma and apical dendrite. The dendritic site was on the main apical trunk 416 μm from the soma. The same site was also used in all subsequent figures involving dendritic recording unless otherwise noted. Action potentials were evoked by current steps to either the soma (left; 170 pA) or dendrite (right; 210 pA). The insets in this and following figures show a schematic diagram of the simulated recording and stimulation sites. B. Plot of the latency difference between peak somatic and peak dendritic potential at different distances from the soma. Action potentials were elicited by somatic (solid line; 170 pA) or dendritic (dashed line; 100 pA) current injection. Latencies were measured using time to peak amplitude. C. Action potential amplitude plotted as function of distance from the soma under the same conditions as (B) following somatic injection. Amplitudes were measured from threshold to peak. Threshold level was determined using the second derivative of membrane potential.

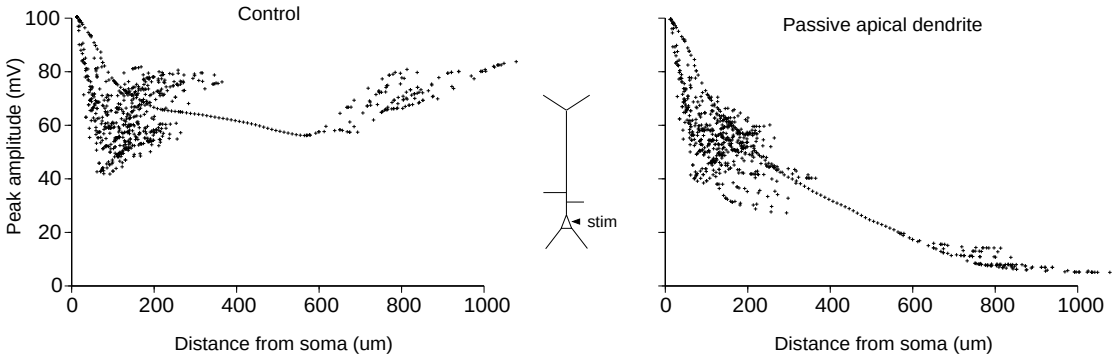

Figure II.4: Dendritic back-propagation. Left. A current step (170 pA) was injected into the soma of the standard model. For each dendritic segment of the model, the peak voltage is plotted. The scatter of points reflects the different amounts of attenuation at locations in different dendritic branches. Right. The same protocol is applied when Na^+ channels are removed from the apical dendrite (but not the basal dendrites or soma).

parameter) at the dendrite and soma during dendritic vs. somatic stimulation (Figure II.5).

Inactivation does not completely account for these observations in that large and brief dendritic current pulses (1-20 nA, 0.5 msec) also failed to initiate dendritic action potentials (Fig. II.6). Although these stimuli can easily produce dendritic voltage transients larger than those produced by a back-propagating action potential, they do not mimic well the electrical effects of the action potential. A spike initiated in the axon charges the soma and proximal dendrites before reaching more distal sites in the apical dendrite, while a dendritic current pulse first charges the local dendritic membrane. When comparable dendritic voltages are reached, in the former case a large portion of the cells membrane has been depolarized while in the latter only the local dendritic region has been. Low densities of dendritic Na^+ channels are sufficient to boost a spike traveling from a depolarized region, but not to produce equally strong regenerative currents from a resting state.

Contribution of the Axon Initial Segment

The actual site of action potential initiation, as determined by simultaneous somatic and axonal recordings (Stuart and Sakmann, 1994), is in the axon, some distance from the soma. Consistent with this observation, in the model the site of initiation was approximately 25 μm from the soma, toward the end of the initial segment near the first myelinated internodal segment (Figure II.7). Depending on the electrical space constant of the axon, about which there is some amount of uncertainty, this locus moved further out in the axon or closer to the soma. This is consistent with previous suggestions that the site of initiation in spinal motoneurons may sometimes be at

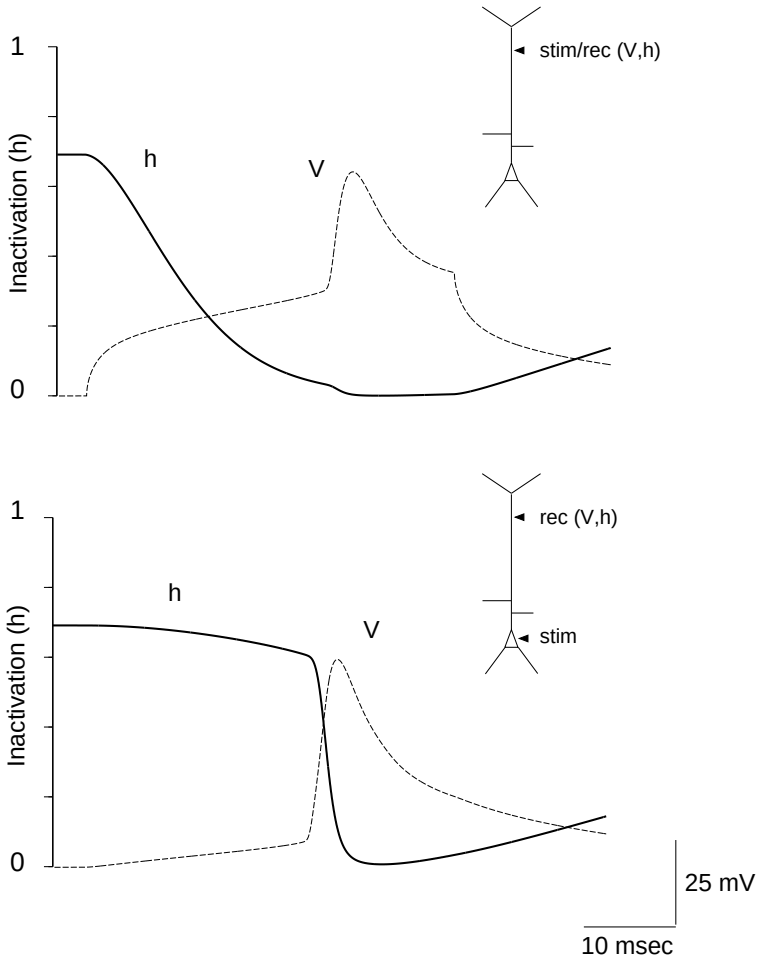

Figure II.5: Effect of Na^+ channel inactivation on action potential initiation. A current step was applied to either the soma (bottom, 170 pA) or dendrite (top, 210 pA). Membrane potential and Na^+ inactivation at the same dendritic site are shown for these two stimulus locations. The inactivation trace corresponds the Hodgkin-Huxley "h" parameter, which has a range from 0 to 1 (0 indicates all channels are inactivated). The fraction of available Na^+ channels at the time the spike is triggered is much greater when the action potential is evoked by somatic compared to dendritic current injection.

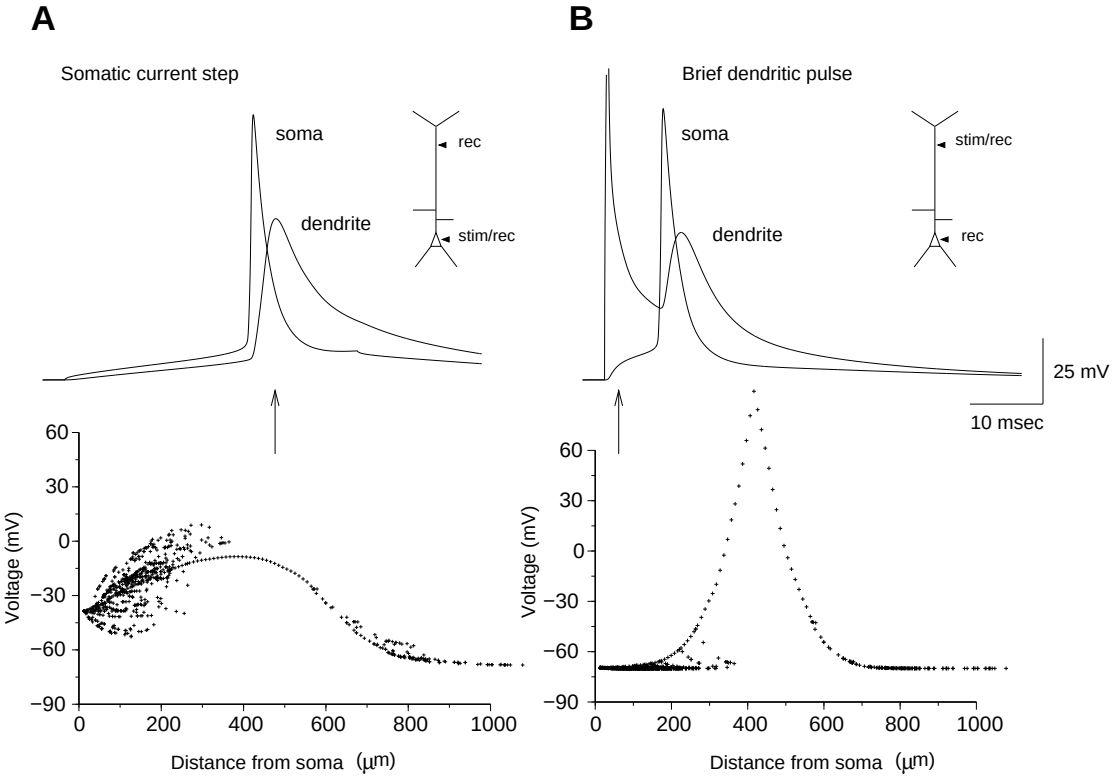

Figure II.6: Comparison of back-propagating spike and dendritic current pulse A. A somatic current step (as Fig. II.3A) evoked an action potential that was actively propagated from the soma into the apical dendrite. The somatic and dendritic voltage time courses are shown. Bottom: The voltage at segments throughout the neuron at the time of the peak dendritic voltage (arrow) as a function of distance from the soma. B. A strong (5 na) and brief (0.5 msec) dendritic pulse generated a large local depolarization but failed to initiate a local action potential. Note that the voltage throughout the neuron (bottom) at the end of the dendritic pulse (arrow) has a large local dendritic peak, but is substantially less depolarized overall compared to (A), particularly the proximal dendrites.

the first node rather than the initial segment (Coombs, Curtis and Eccles, 1957; Gogan, Gueritaud and Tyc-Dumont, 1983). There was relatively little dependence of the site of initiation on the location of stimulation, consistent with the similarity of behavior with somatic and dendritic current injection.

The axon hillock and initial segment contributed significantly to the size and shape of the action potential seen at the soma. The somatic membrane of the model contained a low density of Na^+ channels, equal to the density in the dendritic membrane (see Huguenard, Hamill and Prince, 1988; Stuart and Sakmann, 1994). The current underlying an action potential in the soma was actually supplied largely by Na^+ channels in the initial segment, particularly the proximal portion (or "hillock") which was closest electrotonically to the soma. This could be demonstrated by simulations in which the hillock Na^+ channel density was set to zero. In addition, the sharpness of the voltage inflection at the beginning of the action potential was a consequence of initiation in the initial segment. Simulations in which the axon was truncated after the hillock produced slowly rising action potentials that originated in the hillock. Simulations in which Na^+ channels in the basal dendrites were removed showed that these channels also contributed to the somatic action potential amplitude, although their contribution was small compared to that of the initial segment.

Because of the lower threshold for spike initiation, it has been suggested that initial segment Na^+ kinetics may have a voltage-dependence that is more negative than those those of the soma (Coombs, Curtis and Eccles, 1957; Dodge and Cooley, 1973). We therefore examined the effect of shifting the voltage dependence of dendritic and somatic Na^+ channel kinetics +5 to +15 mV. We found that such shifts increased the amplitude of dendritic action potentials but were not sufficient in themselves to account for the data in Figure II.3 without a large difference in dendritic and axonal channel density.

The low threshold of the initial segment can be understood by comparing the passive (capacitive) load to the magnitude of the source current (Na^+ conductance) (Moore, Stockbridge and Westerfield, 1983). The larger the ratio of source to load, the more quickly the source may charge and thereby depolarize the local membrane. The high density of Na^+ channels in the initial segment provided a very large source current while its small diameter gave minimal local capacitive load and strong electrical isolation from the load of the soma. By systematically varying the initial segment properties, it was possible to assay which electrical and anatomical features were most important in its contribution to reduced threshold (Figure II.7C). Threshold depended mainly on the axial resistivity (R_{ax}), length, diameter and Na^+ channel density of the initial segment. The relationships between these parameters and threshold level were similar to those expected on the basis of the steady-state electrotonic attenuation between the soma and the distal end of the initial segment. In contrast, threshold level was insensitive to the specific membrane capacitance

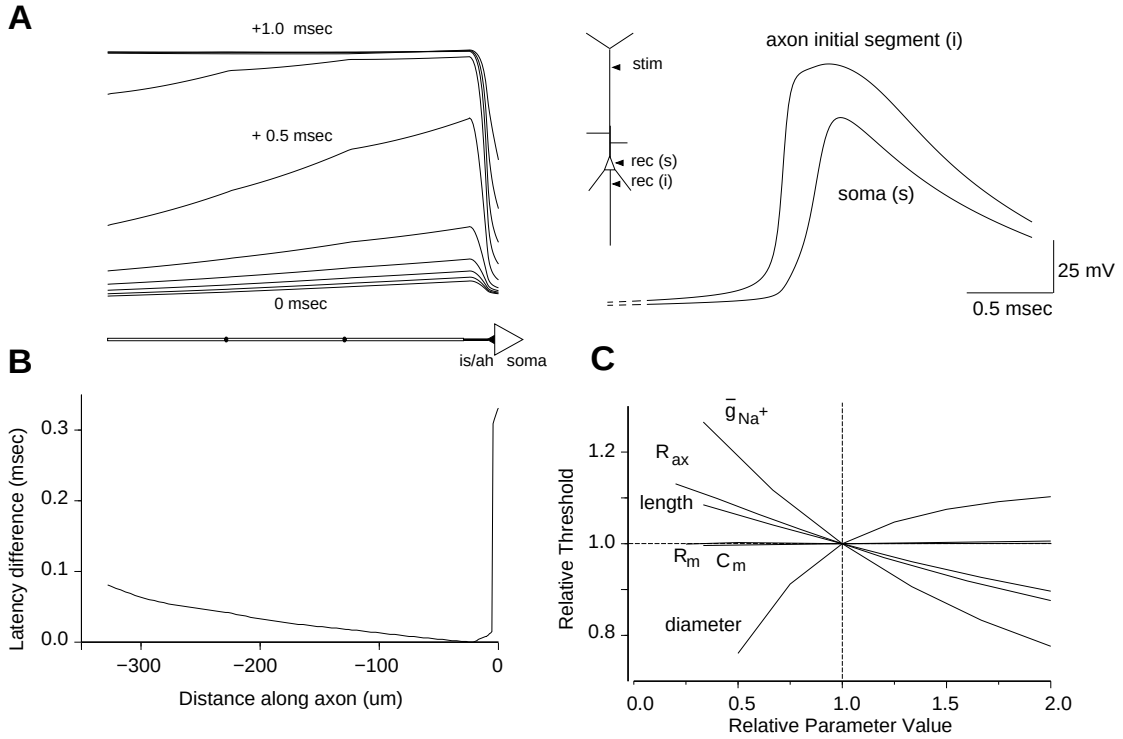

Figure II.7: Role of initial segment in action potential initiation. A. Plot of membrane potential as a function of time (right) and space (left). Action potentials were initiated by current injection into the dendrite. The traces on the left plot membrane potential across the axon at a series of time points to show the site of initiation. The traces on the right show the membrane voltage time course at the soma and the distal end of the initial segment. The label "is/ah" indicates the initial segment and axon hillock. B. Plot of the difference in action potential latency as a function of distance from the soma along the axon. Latency was determined using the peak curvature of the voltage on the rising phase of the action potential. Simulations were run with a time step of 1 μsec. C. Effects of initial segment properties on action potential threshold. Current steps were injected into the soma and the model parameters (length, diameter, axial resistivity R_{ax}, membrane resistivity R_m, and membrane capacitance C_m as indicated) of the initial segment were varied to produce the curves shown. The threshold level and the parameter values are shown normalized to the standard model (see Table 2). Similar results were obtained using dendritic rather than somatic current injection. Threshold was measured as the somatic voltage at maximum somatic voltage curvature and had a value of 11.6 mV in the standard model. The total number of Na^+ channels (the product of membrane area and channel density) was conserved when length and diameter were varied.

(C_m) and the membrane resistivity (R_m) of the initial segment within an order of magnitude range around the standard parameter values. This observation indicates that the load of the soma and basilar dendritic tree on the initial segment is much larger than the local load of the initial segment itself.

The electrical isolation of the initial segment from the soma may have significant physiological and experimental consequences. Uncontrolled action potentials were initiated readily in the initial segment by simulated somatic voltage clamp steps to superthreshold potentials (Figure II.8A). These action potentials always propagated down the axon. Although the amount of voltage escape of the somatic membrane potential from the command potential depended on the series resistance of the clamp, initiation in the initial segment occurred even during "perfect" somatic clamp (series resistance approaching 0). Uncontrolled action potential initiation in the initial segment could also be seen when the soma was clamped during dendritic current injection (see below).

Dendritic Back-propagation

For an action potential initiated in the axon, the junction between axon and soma in the pyramidal neuron presents an enormous increase in electrical load and drop in Na^+ current source. The ratio of soma area to initial segment area ($\sim$ 1500:125 μm^2) and the ratio of soma diameter to initial segment diameter ($\sim$ 15:1 μm) exceed an order or magnitude. When the basal dendrites are taken into account, the load increase is even larger. Nevertheless, action potentials have been reported to invade readily the somata of pyramidal neurons from the axon even when the soma is not otherwise depolarized (e.g. Cowan and Wilson, 1994).

In the model, action potentials initiated at a distant axonal location successfully invaded the soma when the cell was at rest (Figure II.9, top). The localization of Na^+ channels in the initial segment was crucial to this behavior. When the same total channel count (product of channel density and membrane area) was redistributed uniformly through the soma, hillock, and initial segment, antidromic invasion of the soma did not occur (Figure II.9, middle). The geometry of the initial segment was also important to antidromic invasion. When the normal taper of the axon hillock was replaced by a uniform cylinder abutting the soma the action potential amplitude in the soma decreased substantially (Figure II.9, bottom). This manipulation caused a similar reduction in action potential amplitude when spikes were evoked by dendritic or somatic current injection. Thus "orthodromic" action potentials were really "antidromic" in some sense, being triggered in the initial segment and subsequently invading the soma and then dendrites. The amplitude of the action potential a few hundred micrometers from the soma into the apical dendrite was not significantly reduced even when the somatic spike amplitude was greatly attenuated, indicating an

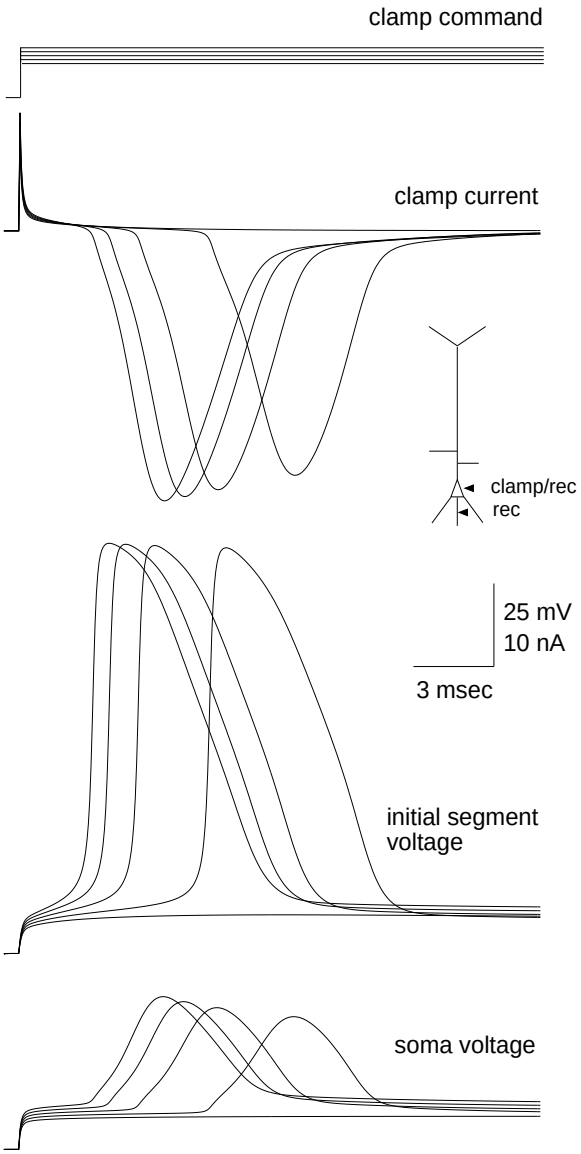

Figure II.8: Voltage clamp fails to prevent action potential initiation in initial segment. Somatic voltage clamp steps of +10 to +15 mV from resting potential (from -70 mV to -60 through -55 mV) were simulated. Despite low (1 MΩ) series resistance, the clamp showed large current responses (top) due to triggering of action potentials in the initial segment which was not clamped due to its electrical isolation from the soma. The somatic membrane potential also showed voltage escape due to the finite series resistance of the clamp. Single electrode voltage clamp was simulated by injecting a current proportional to the difference between the command potential (V_{com}) and the membrane potential (V_m): $i = (V_{com} - V_m)/R_s$, where R_s is the series resistance of the clamp.

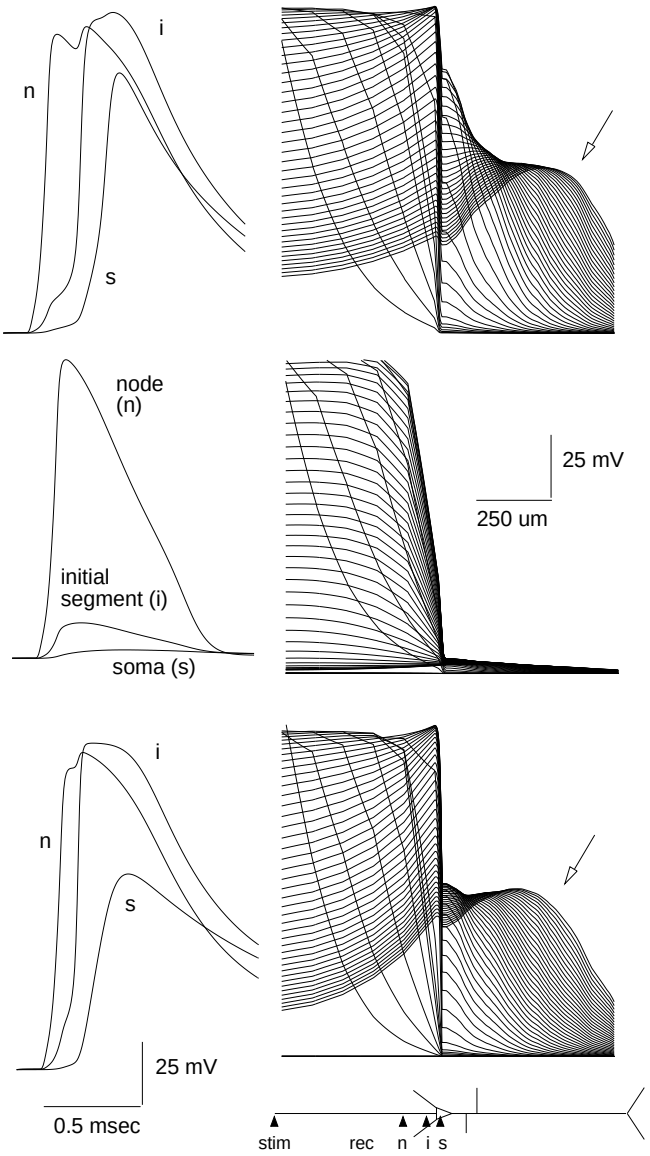

Figure II.9: Antidromic invasion. A current step (0.5 nA, 0.5 msec) was applied to the tip of the axon (> 500 μm) to evoke an antidromic action potential. Traces on the left show voltage time courses at the first node of Ranvier ("node" or "n", the distal end of the initial segment "i" or the soma "s". Curves on the right show voltage as a function of distance from the soma at time steps of 0.1 msec. Top: In the standard model, full invasion of the soma occurs. Middle: Na^+ channels are redistributed evenly through the soma and initial segment rather than being concentrated in the initial segment. Somatic invasion fails. Bottom: The taper of the hillock is eliminated and its Na^+ density increased to compensate. Note that somatic spike amplitude is decreased, but dendritic invasion is not compromised (compare top and bottom at arrows).

"all-or-none" aspect to the dendritic invasion of the action potential.

Scenarios for Dendritic Spike Initiation

In contrast to Stuart and Sakmann (1994), Regher et al. (1993) described synaptically-triggered action potentials in the dendrites of cortical pyramidal neurons. Their experiments were performed by voltage clamping the soma; the presence of dendritically-initiated action potentials was inferred by the ability of synaptic stimulation to elicit unclamped active currents, presumably occurring in distal, unclamped dendritic regions. We approximated these experimental conditions by injecting current into the apical dendrite while simulating a somatic voltage clamp. In this situation, an action potential could indeed be initiated in the very distal part of the apical dendrite. However, the action potential failed to propagate down the apical dendrite and the corresponding voltage clamp current recorded at the soma was minimal, indicating a mismatch between model and experiment.

The study of Regehr et al. (1993) was performed using older animals than that of Stuart and Sakmann (1994) (14-27 days compared to 14 days), and during the second and third weeks of maturation, significant increases in Na^+ channel density are known to occur (Huguenard, Hamill and Prince, 1988; Hamill, Huguenard and Prince, 1991; Cummins, Xia and Haddad, 1994). We reasoned that increased dendritic Na^+ channel density could be partly responsible for the discrepancy between the two studies; we therefore examined the impact of such an increase by performing simulations with increased somatic and dendritic Na^+ channel density. With a three-fold increase in somatic and dendritic channel density (to 90 pS/μm^2), the results of simulations were in much closer accord with the data of Regehr et al. (1993) (Figure II.10A). Dendritic current steps evoked either small or large regenerative currents. The small currents corresponded to dendritically-initiated action potentials while the large currents corresponded to axonally-initiated action potentials. As reported by Regehr et al. (1993), the series resistance of the clamp was critical to whether or not an axonally-initiated spike occurred. With better voltage control, the somatic clamp prevented the initial segment from depolarizing sufficiently to reach threshold. Developmental increases in other channels may be expected to accompany increases in Na^+ channel density (Hamill, Huguenard and Prince, 1991). Therefore, we performed the same voltage-clamp simulations with a complementary 3-fold increase in somatic and dendritic K^+ channel density. Similar results to those in Figure II.10 were found.

With the increased dendritic Na^+ channel density, dendritic current steps in the absence of voltage clamp readily evoked action potentials of dendritic origin (Figure II.10B, compare to Figure II.3A). Following dendritically originated spikes the initial segment eventually reached threshold to produce a secondary spike which subsequently propagated back into the dendrites. Thus,

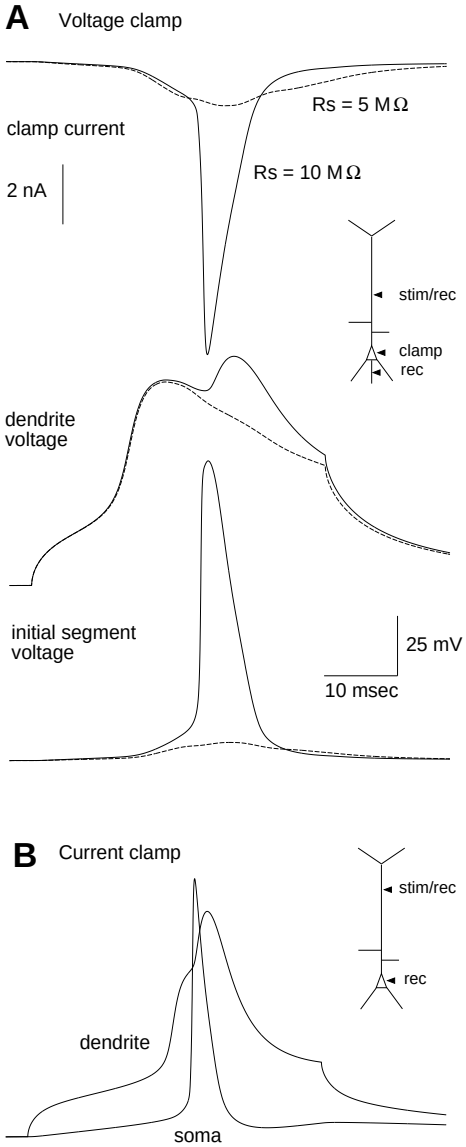

Figure II.10: Voltage clamp during dendritic current injection. With higher dendritic Na^+ channel density (90 pS/μm^2) an action potential was initiated in the apical dendrite by current injection (300 pA). A. A somatic voltage clamp showed a small regenerative current caused by the dendritic spike or a much larger regenerative current caused by a subsequent initial segment spike depending on the series resistance of the clamp (top: voltage clamp current, middle: dendritic voltage at injection site, bottom: voltage at initial segment; solid line, 5 MΩ; dashed line 10 MΩ). Note strong voltage escape at both dendritic and initial segment sites. B. The same dendritic Na^+ channel density and stimulus under current clamp recording elicited an action potential in the apical dendrite which preceded that in the axon.

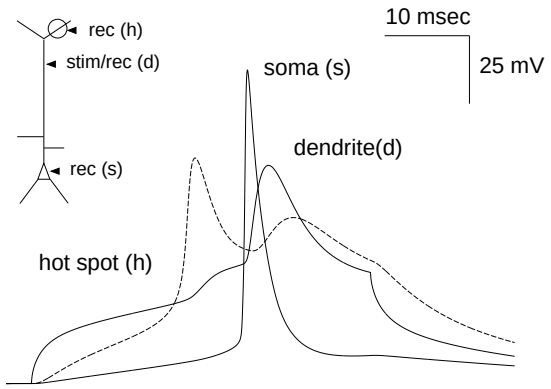

Figure II.11: A "hot spot" of high Na^+ channel density (300 pS/μm^2) was placed on a fine branch in the distal apical tuft (0.8 μm diameter, 34 μm length; 719 μm from the soma). Current injection into the main apical trunk (210 pA) initiated an action potential at the hot spot. Note that the spike failed to propagate into the apical trunk and several milliseconds later a spike was initiated in the initial segment.

the dendritic recording showed a characteristic biphasic waveform, with the first component corresponding to the direct dendritically-initiated action potential and the second component corresponding to the back-propagated axonal action potential. Interestingly, the back-propagated action potential produced a greater peak depolarization in the dendrite than the original dendritically--initiated action potential. In general, with the higher density of dendritic channels, action potential amplitude did not attenuate with distance from the soma and was actually larger in dendritic than in somatic regions.

Because the density of Na^+ channels in fine caliber dendrites has not been measured directly, localized "hot spots" of Na^+ channels in these dendritic branches are an alternative mechanism for dendritic spike initiation (Softky, 1995). Such hot spots would be likely sites for initiation due to considerations of current source to electrical load similar to those that make the initial segment a likely initiation site. To explore the behavior of the model in such conditions, we simulated loci of high channel density (ten times the normal dendritic density) in small diameter dendritic branches and applied current steps to the apical dendrite (Figure II.11). Action potentials could be easily initiated at hot spots located in distal apical dendrites but not readily at hot spots in more proximal oblique apical or basal branches. Spikes initiated at distal hot spots were small but visible in the apical dendrite but barely visible at the soma.

Discussion

We have presented a model of action potential initiation in neocortical pyramidal cells that is consistent with the known physiological and anatomical properties of these cells. In this model, the axon initial segment is the usual trigger zone for spikes by virtue of its geometry and high Na^+ channel density. The surprising ability of dendritic Na^+ channels to substantially boost back-propagation of action potentials while failing to support dendritic initiation (Stuart and Sakmann, 1994) could be explained by the fast time constant of Na^+ channel inactivation relative to the membrane time constant and by the asymmetry of membrane charging from dendrite versus soma.

The contradictory conclusions of Regehr et al. (1993), that spikes may be dendritically initiated, could be reconciled with the model by invoking a maturational increase in dendritic Na^+ channel density (Huguenard, Hamill and Prince, 1988; Cummins, Xia and Haddad, 1994) that might accompany the difference in the ages of rats used in the two studies. With regard to the resolution of this issue, the model makes a number of specific predictions: (1) with dendritic spike initiation, the form of dendritic spikes should be biphasic (Figs. II.10, II.11); (2) conditions that favor dendritic spike initiation should lead to non-decremental amplitude spikes in dendrites; (3) when it becomes possible to measure accurately the initial segment Na^+ channel density, it should be orders of magnitude larger than the somato-dendritic density; (4) if it were possible to inactivate the axon hillock and initial segment, a profound change in spike initiation should should be seen. The last experiment may be extremely difficult due to the close apposition of the hillock to the soma.

Most recent models of cortical and hippocampal pyramidal cells and Purkinke cells have neglected the axon initial segment, typically assigning high density of Na^+ channels to the soma (Bernander et al., 1991; Traub et al., 1991; Lytton and Sejnowski, 1991; Rhodes and Gray, 1994; De Schutter and Bower, 1994). In this study we have found that the axon hillock and initial segment are of critical importance for spike initiation.

A primary distinguishing feature of the initial segment of the neocortical pyramidal cell, shared with the nodes of Ranvier, is the presence of an electron-dense undercoating (Peters, Proskauer and Kaiserman-Abramof, 1968). It has long been speculated that this undercoating is related to electrical conduction (Peters, Proskauer and Kaiserman-Abramof, 1968; Palay et al., 1968), possibly relating to an elevated density of Na^+ channels. The existence of a diffusional barrier in the membrane between between axon hillock and soma (Srinivasan et al., 1988; Kobayashi et al., 1992) could provide the molecular basis for the trapping of channels in the initial segment.

The initial segment was proposed some time ago as the site for action potential initia-

tion in spinal motoneurons (Coombs, Curtis and Eccles, 1957; Frank and Fuortes, 1957). Yet the demonstration of active currents in the dendrites of cortical pyramidal neurons left the applicability of the classical model to these cells uncertain. Our model expands upon the pioneering models of Dodge and Cooley(Cooley and Dodge, 1966; Dodge and Cooley, 1973) and Moore et al. (Moore, Stockbridge and Westerfield, 1983) concerning the locus of spike initiation in the spinal motoneuron. Dodge and Cooley (1973) used a high Na^+ channel density in the initial segment and changed the Na^+ (and K^+) kinetics to reduce threshold there. A shift in the voltage dependence of channel kinetics could theoretically be caused by polarization differences between somatic and neuritic membrane (Bedlack et al., 1994) or by differences in Na^+ channel subtype expression (Westenbroek, Merrick and Catterall, 1989) or phosphorylation state (Murphy et al., 1993; Li et al., 1992). Experiments by Moore and Westerfield (1983) argued against such axonal specialization. Accordingly, Moore et al. (1983) used identical kinetics and channel densities to the soma and initial segment and found the initial segment could be the site of initiation solely due to the large ratio of the Na^+ conductance to the passive electrical load of there.

A recent model of the hippocampal CA3 pyramidal cell by Traub and coworkers (Traub et al., 1994) incorporated an initial segment with high Na^+ channel density and Na^+ channel kinetics distinct from those in the soma and dendrites. In the CA3 model, as in the present study, dendritic stimuli produced spikes that originated at the initial segment and antidromically invaded the dendritic tree. However, in contrast to our results, axonal initiation in the CA3 model was only demonstrated with channel distributions that restricted Na^+ conductances to the promixal dendrites and only when the size of stimuli was limited (Traub et al., 1994).

In the present model, the initial segment was critical in spike initiation. Because of the very high Na^+ channel density (compared to the soma or dendrites), the initial segment actually supplied a significant fraction of the depolarizing current observed at the soma during an action potential. Without the contribution of current from the initial segment, the amplitude of action potential generated in the soma was quite small. This result may be comparable to recordings of dissociated pyramidal cells in acute cultures (Hamill, Huguenard and Prince, 1991), which often showed small action potentials and lack of sustained firing. In these studies a correlation between spike amplitude and the presence of an apparent axon was noted (J.H., unpublished observations).

The electrical isolation and high Na^+ current density of the initial segment from the soma made voltage control of spike initiation very difficult. Once the initial segment became depolarized sufficiently to activate its Na^+ channels, somatic voltage clamp was completely ineffective in preventing spike initiation. Because spike initiation does not occur in the soma (as tends to be casually assumed) a somatic voltage clamp suffers a severe space clamp problem in controlling large regenerative Na^+ currents even under optimal voltage clamp conditions (Regehr et al., 1993).

Thus, the properties of the spike generation zone make interpretation of the locus of origin of unclamped regenerative events difficult (see e.g. Regehr et al., 1992). It is also important to point out that when the soma has been voltage clamped at potentials sufficiently depolarized to inactivate Na^+ channels in the initial segment, unclamped action potentials continue to be generated from more distal nodes in the axon where passive electrical attenuation brings the membrane potential just to a threshold level. The apparent cessation of somatic action potentials when a neuron is clamped to positive potentials—as for example during a pairing procedure used to induce long-term potentiation (e.g. Malinow and Tsien, 1989; Schuman and Madison, 1994)—does not indicate that the cell has stopped firing.

The geometry of the axon hillock and initial segment and the high axonal Na^+ channel density enhanced the security with which action potentials from the axon successfully invaded the soma and dendritic compartments. The properties of the myelinated axon beyond the initial segment may also be important to antidromic invasion, as suggested by Moore et al. (1983). The security of antidromic invasion may be functionally significant if action potentials are naturally generated axonally. Although we do not know of any direct evidence for this phenomenon, distal spike initiation followed by retrograde invasion is one possible interpretation of several studies reporting unexplained retrograde synaptic effects (Vincent and Marty, 1993; Pitler and Alger, 1994; Schuman and Madison, 1994).

Finally, the nature of the spike initiation zone may influence the reliability of spike initiation. Because of the stochastic nature of single channel behavior and finite channel numbers, action potential currents might theoretically be affected by single channel conductance fluctuations (Skaugen, 1980). Modeling studies predict that these effects would be greatest in situations involving few channels and small electrical compartments (Skaugen, 1980). Although the initial segment is small and isolated electrically from the soma, the very high total number of Na^+ channels would be expected to effectively wash out single channel stochasticity. This prediction is in accord with the observed reliability of action potential generation in neocortical neurons (Mainen and Sejnowski, 1995b). It remains possible that dendritic spike initiation, in regions with a much lower channel density, would be subject to greater stochastic effects.

This chapter is based on material that will be published in Mainen, Z. F., Joerges, J., Huguenard, J. R., and Sejnowski, T. J. "A model of spike initiation in neocortical pyramidal neurons", *Neuron*, 15, 1995. The dissertation author was the primary investigator and the dissertation advisor supervised the research for this chapter.

Chapter III

A Model of Repetitive Firing Properties

Neocortical neurons express a variety of intrinsic firing patterns (McCormick et al., 1985) and characteristic interspike membrane potential trajectories (Calvin, 1974; Stafstrom, Schwindt and Crill, 1984). These behaviors are generated by ion channels that are known to be distributed inhomogeneously (Angelides et al., 1988; Westenbroek, Merrick and Catterall, 1989; Sheng et al., 1992) across the dendritic, somatic and axonal membrane, yet the significance of morphology in shaping the interactions between ionic currents in repetitive firing is poorly understood. Using computer simulations, we demonstrate that the spatiotemporal interactions between nonuniformly distributed ionic currents link the intrinsic firing pattern and interspike voltage trajectories of a neuron directly to its anatomical structure. Simplified models show that variation in dendritic length can produce a range of firing patterns similar to those of neocortical neurons. Anatomically detailed models show that the known correlations between dendritic morphology and firing properties (McCormick et al., 1985; Chagnac-Amitai, Luhmann and Prince, 1990; Mason and Larkman, 1990) can be captured with a single channel distribution. Morphological diversity could therefore account for much of the electrophysiological heterogeneity of neocortical neurons without requiring specialization of the types and distributions of ion channels.

Methods

Standard compartmental modeling techniques (Hines, 1993) were used to simulate spatially extended neurons with passive electrical structure, four voltage-dependent currents (fast Na^+, I_{Na} (Hamill, Huguenard and Prince, 1991; Mainen et al., 1995); fast K^+, I_{K_V} (Hamill, Hugue-

nard and Prince, 1991; Mainen et al., 1995); slow non-inactivating K^+ (the "M" current), I_{K_M} (Gutfreund, Yarom and Segev, 1995); and high-voltage activated Ca^{2+}, I_{Ca}(Reuveni, Friedman and Amitai, 1993)) and one Ca^{2+}-dependent current, $I_{K_{Ca}}$ (Reuveni, Friedman and Amitai, 1993). All currents were calculated using conventional Hodgkin-Huxley style kinetics: current I from channel type each was computed given by the Ohmic relation: $I = \bar{g}a^x b(v - E)$ where $\bar{g}$ is the local conductance density, a is an activation variable with x order kinetics, b in an optional inactivation variable, v is the local membrane potential, and E is the reversal potential for the ionic species (E_K = -90 mV, E_{Na} = 50 mV). I_{Ca} was computed using the Goldman-Hodgkin-Katz current equation rather than Ohm's law. Extracellular Ca^{2+} concentration, $[Ca^{2+}]_o$, was 2 mM and internal concentration was computed using entry via I_{Ca} and removal by a first order pump: $d[Ca^{2+}]_i/dt = (-1 \cdot 10^5 \cdot I_{Ca}/2F) - ([Ca^{2+}]_i - [Ca^{2+}]_\infty)/\tau_R$, where $[Ca^{2+}]_\infty$ = 10 nM, and τ_R = 700 msec. All channel activation and inactivation variables were expressed in terms of a steady-state value, $a_\infty(v)$, and a time constant $\tau_a(v)$ which were calculated from a first order reaction scheme with forward rate α and backward rate β, giving $a_\infty(v) = \alpha/(\alpha(v) + \beta(v))$, $\tau_a = 1/(\alpha + \beta)$.

The specific rate functions for each current were I_{Na} activation m^3: $\alpha_m(v) = 0.182(v + 25)/(1 - e^{-(v+25)/9})$, $\beta_m(v) = -0.124(v + 25)/(1 - e^{(v+25)/9})$; I_{Na} inactivation h time constant: $\alpha_h(v) = 0.024(v + 40)/(1 - e^{-(v+40)/5})$, $\beta_h(v) = -0.0091(v + 65)/(1 - e^{(v+65)/5})$; with steady-state inactivation calculated by $h_\infty(v) = 1/(1 + e^{(v+55)/6.2})$; I_{K_V} activation n: $\alpha_n(v) = 0.02(v - 25)/(1 - e^{-(v+25)/9})$, $\beta_n(v) = -0.002(v - 25)/(1 - e^{(v+25)/9})$; I_{K_M} activation q: $\alpha_q(v) = 2 \cdot 10^{-4}(v + 35)/(1 - e^{-(v+35)/9})$, $\beta_q(v) = -2 \cdot 10^{-4}(v + 35)/(1 - e^{(v+35)/9})$; I_{Ca} activation r^2: $\alpha_r(v) = 0.055(v + 27)/(1 - e^{-(27+v)/3.8})$, $\beta_r(v) = 0.94e^{-(v+75)/17}$; I_{Ca} inactivation s: $\alpha_s(v) = 4.57 \cdot 10^{-4}e^{-(v+13)/50}$, $\beta_s(v) = 0.0065/(1 + e^{-(v+15)/28})$; $I_{K_{Ca}}$ activation w: $\alpha_w([Ca^{2+}]_i) = 5 \cdot 10^6([Ca^{2+}]_i)^4$, $\beta_w = 0.075$.

The time constants and maximal conductances were developed in models based on room temperature and were therefore scaled from 23 to 37 ^{o}C using a Q_{10} of 2.3 or 2 ($I_{K_{Ca}}$ and I_{Ca}). Specific membrane capacitance was 0.75 μF/cm^2; specific membrane resistance was 40 kΩ-cm^2; specific axial resistance was 200 Ω-cm. An integration time step of 100 – 250 μsec was used.

The simplified model consisted of 10 cylindrical compartments (length and diameter): soma (20 × 10 μm), basal dendrite (150 × 10 μm), apical dendrite (25 – 1000 × 6.5 μm), axon hillock (10 × 2.5 μm), axon initial segment (15 × 1 μm). The apical dendrite comprised 6 compartments.

Dendritic reconstructions were provided by J. Anderson, K. Martin and R. Douglas (pyramids and spiny stellates), L. Cauller (smooth stellates, pyramids and spiny stellates), D.K. Smetters (pyramid, not shown), and N. Spruston and G. Stuart (pyramids, not shown). All dendritic branches were divided into cylindrical compartments with a maximal length of 50 μm. An axon, which was not present in the reconstructed anatomy, was attached to the soma of each cell. The axon consisted of a conical hillock and a cylindrical initial segment region, each divided into 5

compartments. We took into account an observed correlation between soma diameter and initial segment diameter (Sloper and Powell, 1978), which tends to decrease the effects of dendritic geometry by scaling the axonal currents along with increased somatic/dendritic area. Initial segment diameter, d, was scaled as a function of the soma area, a, by $d = 0.1\sqrt{a/(4\pi)}$. Soma areas ranged from 340 to 1750 μm^2. The hillock diameter tapered from $4d$ at the soma to d at the initial segment. Hillock and initial segment length were 10 and 15 μm. Note, as axonal size had significant effects on the repetitive firing properties observed, uncertainties in soma measurements and correlation with axon geometry complicate the interpretation of these results. Channel kinetics and somatic/dendritic conductance densities were identical to those in the simplified model. Axonal conductance densities were $\bar{g}_{K_V}$ = 1500 pS/μm^2 and $\bar{g}_{Na}$ = 40,000 pS/μm^2.

Results

We used compartmental models to explore the effects of anatomy on the repetitive firing properties of neocortical neurons. In models with simplified dendritic structure (Fig. III.1A) the length of the apical dendrite dramatically altered the firing generated in response to somatic current pulses (Fig. III.1B), producing patterns conventionally ascribed to "fast-spiking", "regular-spiking" and "intrinsically bursting" neocortical cell types (Connors and Gutnick, 1990). Changes in the shape of spike repolarization paralleled changes in firing pattern (Fig. III.1C), illustrating that altering the ratio of axonal to dendritic membrane area altered the relative contributions of slow and fast K^+ currents to the somatic membrane potential between action potentials. In contrast, spike width and amplitude were not altered by changes in dendritic load (Fig. III.1D), indicating that fast currents always dominated the spike waveform itself.

A spatially heterogeneous distribution of channels was necessary to produce the results described. First, fast voltage-dependent Na^+ channels must be present in the dendrites and a much higher density (~1000-fold) Na^+ channels concentrated at the axon initial segment (Mainen et al., 1995). There is good molecular (Wollner and Catterall, 1986; Angelides et al., 1988) and physiological (Huguenard, Hamill and Prince, 1989; Waxman and Ritchie, 1993; Stuart and Sakmann, 1994) evidence for such distributions of Na^+ channels. Second, fast voltage-dependent K^+ channels must be concentrated near the soma and initial segment (and excluded from the dendrites). There is also evidence for spatial segregation of K^+ channels (Sheng et al., 1992), but the distributions of these channels are less well established. Finally, low densities of much slower K^+ channels must be present in the dendrites. The presence (or absence) of low densities of these channels in the soma and axon is not important due to the relatively small areas of these compartments. Within these guidelines, the link between dendrite size and firing pattern was remarkably robust, being

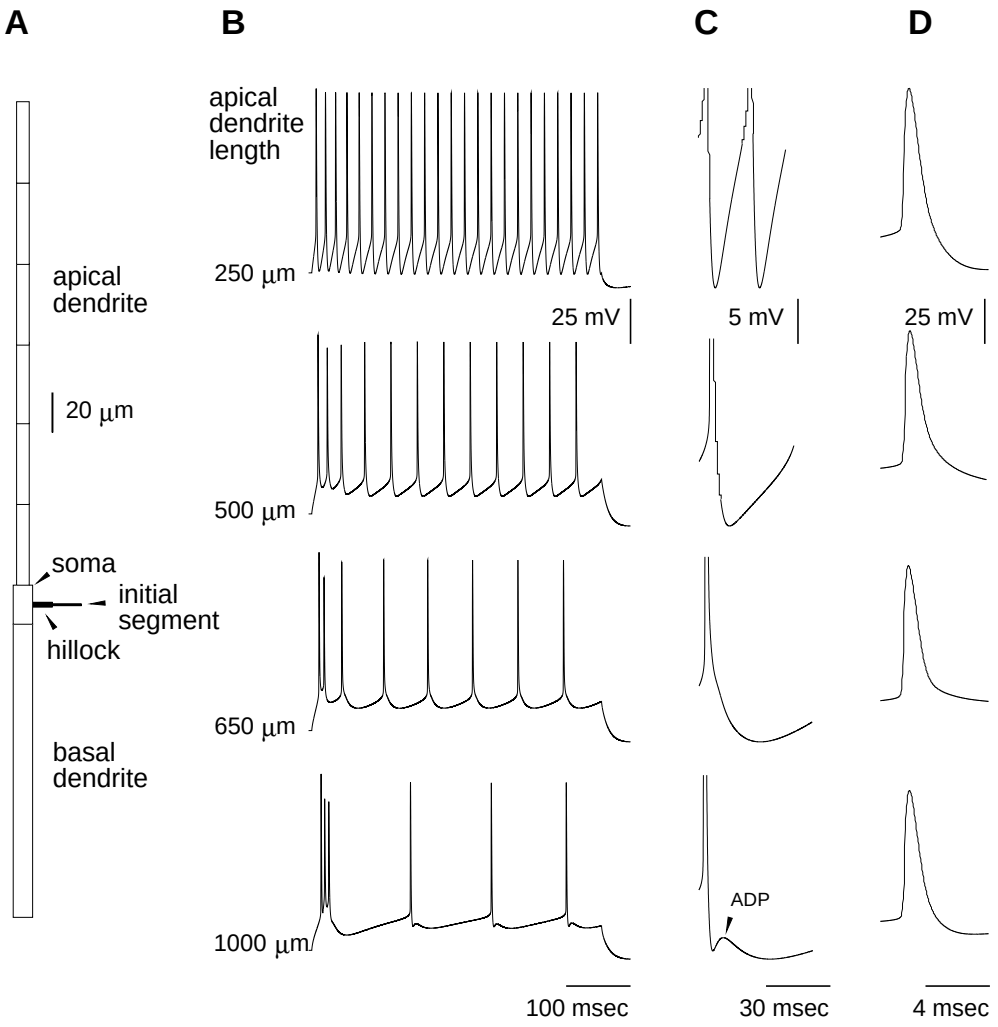

Figure III.1: Effects of dendritic length on firing pattern in simplified neural models. A. A simple model consisting of soma, apical and basal dendrites, and axon hillock and initial segment. The soma and dendrites contain the currents (densities in pS/μm^2): I_{Na} (15), I_{Ca} (0.03), I_{K_M} (1), and $I_{K_{Ca}}$ (0.05). The axonal compartments contained I_{Na} (30,000) and I_{K_V} (1000). B. Varying the length of the apical dendrite alters the repetitive firing patterns elicited by current injection in the soma (0.25 nA, 250 msec, not shown). For each trace, the length of apical dendrite is indicated to the left. Top trace, "fast-spiking" pattern with little adaptation occur at short dendritic lengths. Second and third traces, "regular spiking" patterns occur at intermediate lengths. Fourth and bottom traces, "intrinsic bursting" pattern. C. Changes in the shape of individual spike afterhyperpolarization (AHP) patterns accompany changes in firing pattern. Top trace, a short dendrite, producing a deep monophasic AHP. Middle trace, intermediate length dendrites produce shallower, biphasic AHPs with fast and slow components. Bottom trace, long dendrites produce triphasic AHPs with prominent fast and slow AHPs as well as an afterdepolarizing potential (ADP). D. Lack of spike shape change at different dendritic lengths.

independent of particular choices of channel types and kinetics and precise channel densities. For example, qualitatively identical results were obtained using either slow voltage–dependent K^+ channels (not shown) or a combination of voltage–dependent K^+ and Ca^{2+}–dependent K^+ channels and voltage-dependent Ca^{2+} channels (as illustrated).

Spatial heterogeneity of ion channels produce spatiotemporal voltage gradients between different regions of a neuron (Fig. III.2). The presence of such gradients can be tested experimentally using two-electrode recordings (Stuart and Sakmann, 1994) and reveal key properties of the proposed channel distributions. First, the axonal membrane potential leads that of the soma on both the depolarizing and repolarizing phases of the spike (Fig. III.2A). Channels in the axon generate the bulk of the action potential currents seen in the soma regardless of the dendritic length. Second, dendritic Na^+ channels promote active backpropagation of spikes into the dendrites (Fig. III.2B). In neurons with longer dendrites, backpropagation can produce spike bursts and afterdepolarizations (ADPs) by prolonging the dendritic depolarization following a spike (Granit, Kernell and Smith, 1963; Calvin, 1974). The effects of active dendritic propagation depend on (1) the distance which the dendritic action potential travels and its velocity, (2) the number of activatable dendritic Na^+ channels, and (3) factors which modulate the duration of dendritic depolarization (e.g. dendritic Ca^{2+} and K^+ currents). Third, the larger the dendritic membrane, the larger the fraction of hyperpolarizing current during interspike intervals is provided by dendritic rather than axonal K^+ channels (Fig. III.2C). The ratio of dendritic to axonal membrane sets the balance between fast axonal and slow dendritic K^+ currents and hence the amount of spike frequency adaptation (Fig. III.2D). Bursting occurs as an extremum on a continuum from non-adapting to strongly adapting firing patterns as a consequence of a succession of superthreshold afterdepolarizing potentials (Kandel and Spencer, 1961; Calvin, 1974).

To test whether this theory might account for the physiological differences between neocortical neurons, we modeled dendritic arbors reconstructed from neurons of several types (Fig. III.3A) with the same distribution of channels used in the simpler geometry. Somatic current steps produced distinct firing patterns which varied greatly depending on the anatomy (Fig. III.3B,C). We examined a total of 18 reconstructed neurons: layer 5 aspiny stellates (n=4) produced spike trains with weak spike frequency adaptation; layer 4 spiny stellates and layer 2/3 pyramidal neurons (n=7) gave non-bursting spike trains with moderate to strong adaptation; and layer 5 pyramidal neurons (n=7) showed either intrinsic bursting (n=4) or adapting spike trains (n=3). While the behavior of the pyramidal and spiny stellate neurons was consistent with the known anatomy-physiology correlations (McCormick et al., 1985; Mason and Larkman, 1990), smooth stellate neurons showed non-physiological spike frequency adaptation, particularly noticeable at low firing frequencies. This suggests the absence or diminished magnitude of slow K^+ currents in these cell

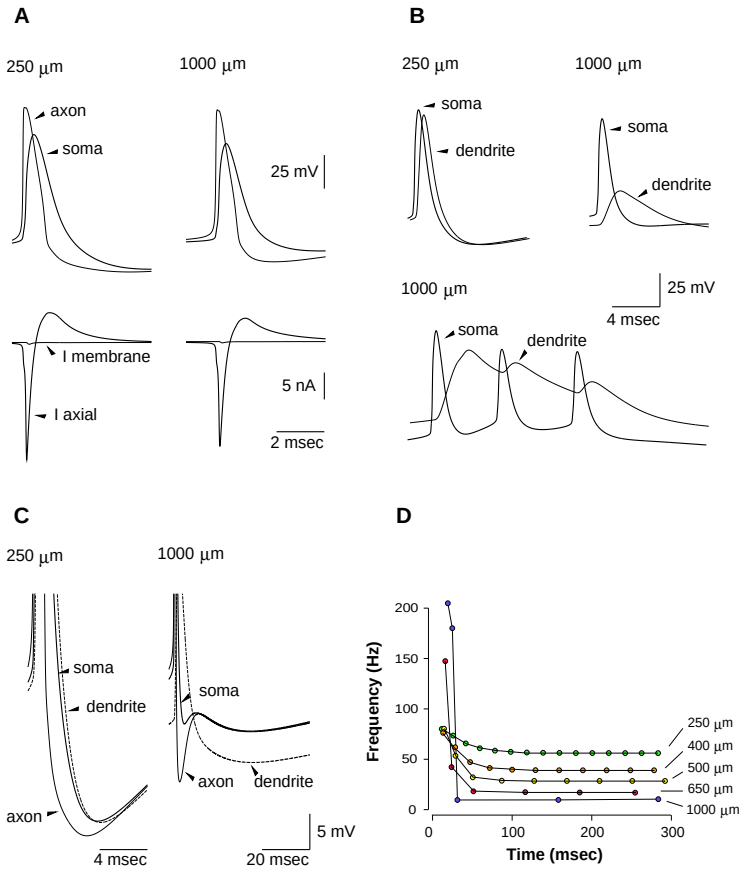

Figure III.2: Spatiotemporal voltage gradients and dendritic spike propagation underlie diversity of firing patterns. A. Top, membrane potential at the soma ("soma", thick lines) and axon ("axon", thin lines) during action potentials in two simplified models (lengths indicated). Bottom, net current flowing across the membrane of the soma ("I membrane", thin lines) and axial current flowing from the axon hillock to the soma ("I axial", thick lines) during action potentials in the same models. The time calibration bar applies to all traces. The current and voltage traces are aligned in time. The simulations in this and subsequent examples were identical to those shown for the respective models in Fig. III.1 and the single action potentials illustrated are the 4th in the spike train. B. Membrane potential at the soma (thick lines) and apical dendrite ("dendrite", thin lines) during single action potentials (top) and a burst (bottom). Note the first dendritic action potential of the burst outlasts the somatic action potential by several msec, thereby causing the spike burst in the axon. The diminution of subsequent dendritic spikes is due to inactivation of dendritic Na^+ channels during the relatively broad dendritic spikes and the slow activation of dendritic K^+ channels. The dendritic membrane potential was measured at the midpoint of the apical dendrite. C. Membrane potential at the soma (thick solid lines), apical dendrite (thin dashed lines), and axon (thin solid lines) during the spike afterhyperpolarization (interspike interval). Note that for the short dendrite model (left) the axon drives hyperpolarization throughout most of the interval whereas for the long dendrite model (right) the axon drives the initial hyperpolarization during the fast AHP but the dendrites drive hyperpolarization during the remainder during the slow AHP. D. Firing frequency (reciprocal interspike interval) as a function of time during somatic current injection (300 msec, 0.25 nA) for different dendritic lengths (indicated). Note the increase of initial firing and decrease of steady-state firing rate with increasing apical dendrite length.

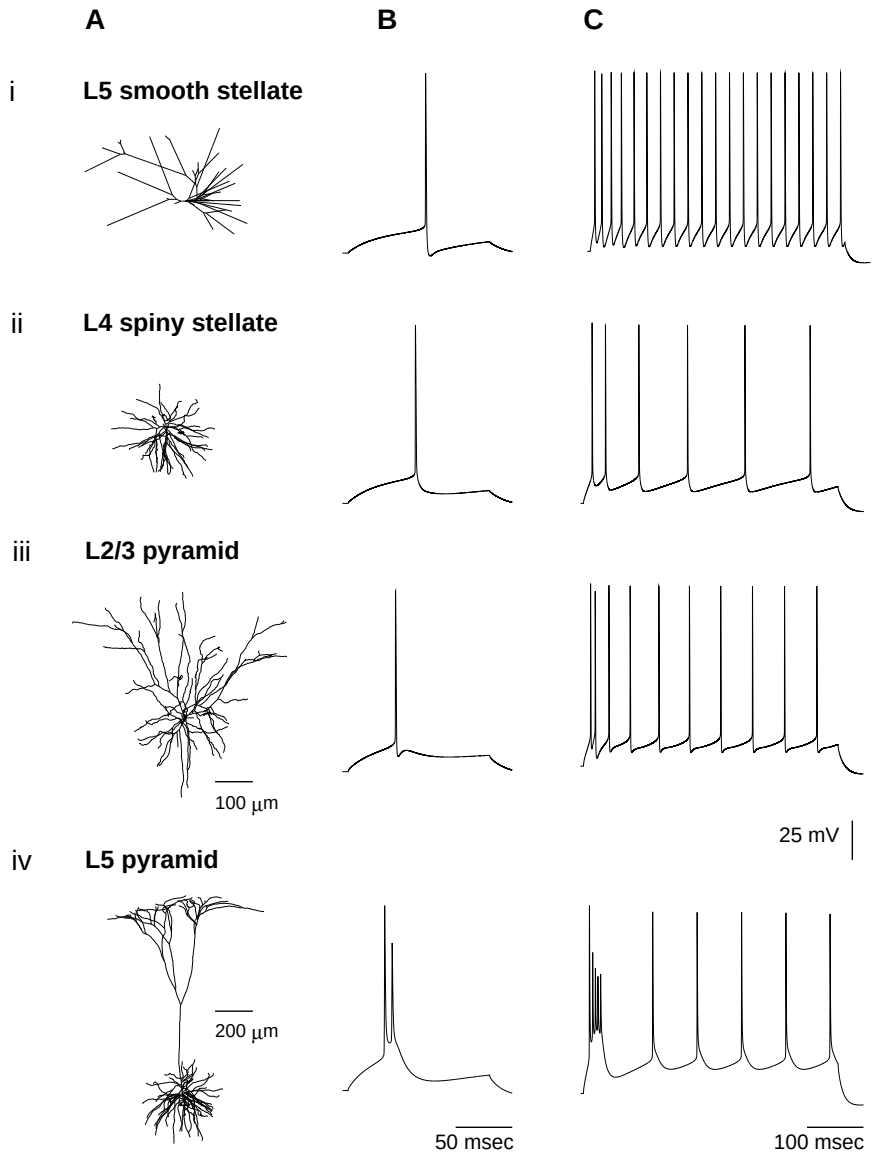

Figure III.3: Dendritic anatomy generates diverse intrinsic firing patterns. A. Digital reconstructions of dendritic arbors of neurons from rat somatosensory cortex (i) and cat visual cortex (ii-iv). The laminar position and morphological type of each neuron is indicated. The 100 μm scale bar applies to cells in the upper 3 rows. Cell (i) shows only the branch lengths and connectivity and cells (ii-iv) show a two-dimensional projection of the three-dimensional reconstruction. B. Somatic current injection (125 msec, amplitude adjusted to rheobase for each cell: from top to bottom, 21, 60, 100 and 310 pA) evoked single spikes with characteristic afterhyperpolarization shape (i-iii) or a two-spike burst (iv). C. Somatic current injection (ii-iv: 450 msec, 2x rheobase amplitude bottom traces; i: 4x rheobase amplitude) evoked repetitive firing with characteristic low adaptation (i), moderate to strong adaptation (ii, iii) or bursting (iv).

types. Smooth stellate cells also have narrower spike widths than found in our model; we therefore conclude that the physiological differences between the fast spiking neurons and the majority population of regular firing and bursting neurons are not solely due to differences in morphology.

A number of predictions concerning the mechanism of bursting can be made by the model. Bursting in a large layer 5 cell (Fig. III.4A) was abolished by pruning of basal and apical dendrites, as may occur commonly in slice preparations, but not by severing the main apical trunk (Fig. III.4B) (Rhodes and Gray, 1994). Bursting was also eliminated by blocking dendritic Na^+ currents but not by blocking Ca^{2+} currents (Fig III.4C). It is therefore possible that active dendritic backpropagation of Na^+ spikes (Stuart and Sakmann, 1994) in addition to dendritic Ca^{2+} spikes (Wong and Prince, 1978) can account for the generation of spike bursts. Finally, changing the strength of all K^+ currents by altering the K^+ reversal potential had strong effects on bursting (not shown), as seen in hippocampal neurons (Jensen, Azouz and Yaari, 1994). Modulating the strength of just the slow K^+ currents had a similar modulatory effect (Fig. III.4D), as demonstrated in experiments on neuromodulatory control of neocortical firing pattern (Wang and McCormick, 1993).

Discussion

We have demonstrated that neural structure may profoundly shape the dynamic interactions between nonuniformly distributed ion channels. Spatiotemporal channel interactions can account for several fundamental aspects of the heterogeneous firing patterns and interspike voltage dynamics observed in neocortical neurons solely in terms of their anatomical variety. It is therefore possible that many neurons in the neocortex share a relatively stereotyped channel distribution and that their functional differentiation follows largely from their various morphologies. Due to the wide variety of morphologies that have been observed (Peters and Jones, 1984), our findings support the idea of a spectrum of firing patterns at least among spiny stellate and pyramidal neurons (McCormick et al., 1985; Connors and Gutnick, 1990). Among the strongest predictions are the channel distributions outlined above and a strong correlation between firing pattern and dendritic length (Chagnac-Amitai, Luhmann and Prince, 1990). It should be possible to test the theory directly by recording from a neuron before and after ablation of dendritic branches.

This chapter is based on material submitted for publication in Mainen, Z. F. and Sejnowski, T. J. "Dendritic structure determines repetitive firing properties in model neocortical neurons", 1995. The dissertation author was the primary investigator and the dissertation advisor supervised the research for this chapter.

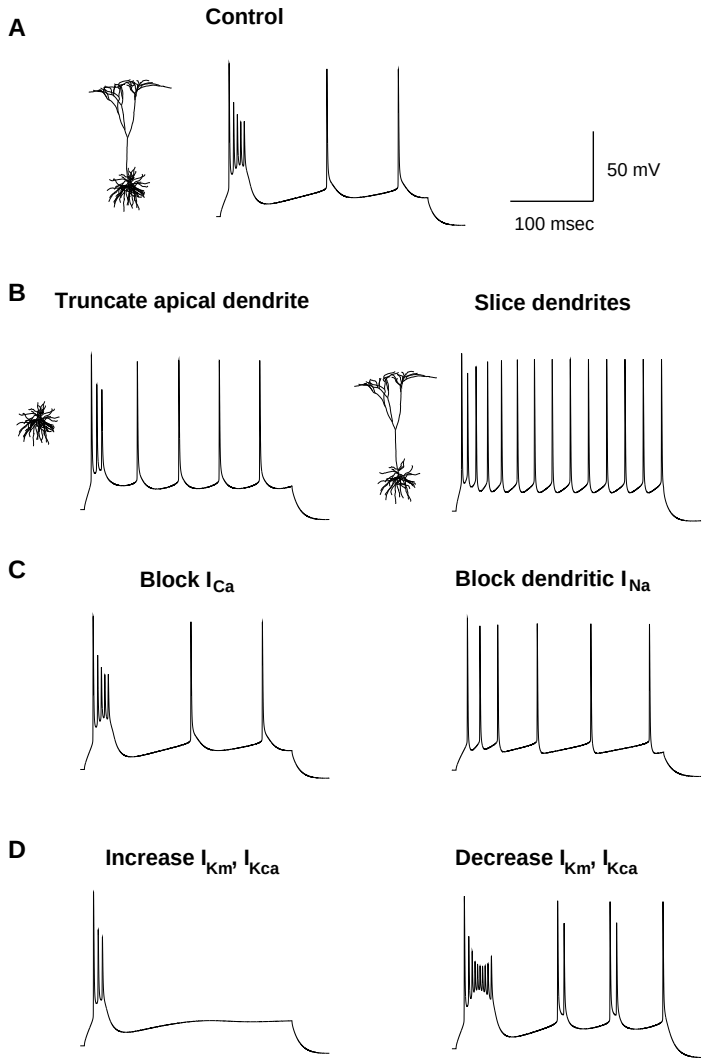

Figure III.4: Burst generation is altered by dendritic pruning and modulation of intrinsic currents. A. Layer 5 pyramidal neuron (Fig. III.3, iv) with intrinsic burst firing in response to current pulse injection (250 msec, 600 pA). The same stimulus was used in B-D. B. Truncation of the entire main apical dendrite (left) resulted in a smaller change to the firing pattern (compare to A) than did planar truncation of basal and apical dendrites (right). The apical dendrite was removed less than 100 μm from the soma. The basal and apical dendrites were pruned by removing all dendrites passing a plane 50 μm in front of soma in the z-axis of the reconstruction (parallel to the plane of the page). The latter procedure removed ~25% of the total dendritic arbor and simulates dendritic loss possible in slice recordings from surface cells. Note the apparent intactness of the dendritic tree despite significant physiological effects. C. Blocking Ca^{2+} currents had little effect on bursting (left), but blocking dendritic (not axonal) Na^{+} currents abolished it (right). D. Bursting was sensitive to modulation of slow K^{+} currents. Increasing slow voltage-dependent and Ca^{2+}-dependent K^{+} currents by 25% slowed firing and reduced initial burst duration (left). Reducing these same slow K^{+} currents by 50% increased burst duration and produced spike doublets (resembling the so-called "extra spike mode" of pyramidal tract neurons (Calvin, 1974)).

Chapter IV

Reliability of Spike Timing In Vitro

It is not known whether the variability of neural activity in the cerebral cortex carries information or reflects noisy underlying mechanisms. In an examination of the reliability of spike generation using recordings from neurons in rat neocortical slices, the precision of spike timing was found to depend on stimulus transients. Constant stimuli led to imprecise spike trains, whereas stimuli with fluctuations resembling synaptic activity produced spike trains with timing reproducible to less than 1 millisecond. These data suggest a low intrinsic noise level in spike generation, which could allow cortical neurons to accurately transform synaptic input into spike sequences, supporting a possible role for spike timing in the processing of information by the neocortex.

Introduction

Neurons transmit information by transforming continuously varying input signals into trains of discrete action potentials. The coding scheme used in this process is an unresolved issue that is critical to computational theories of brain function. Codes which utilize spike timing (Strehler and Lestienne, 1986; McClurkin et al., 1991; Tovee, Rolls and Bellis, 1993; Middlebrooks et al., 1994; Singer and Gray, 1995; Vaadia et al., 1995) can make more efficient use of the capacity of neural connections than those that simply rely on the average rate of firing (Stein, 1967; Bullock, 1970; Bialek et al., 1991). The simplest spike timing code would be one input pulse, one output pulse, but synaptic currents in the cortex are too small and intracellular recordings in vivo look very noisy (Ferster and Jagadeesh, 1992; Douglas, Martin and Whitteridge, 1991). Furthermore, cortical activity is characterized by highly irregular interspike intervals in both spontaneous (Noda and Adey, 1970) and stimulus-evoked conditions (Tomko and Crapper, 1974; Tolhurst, Mov-

shon and Dean, 1983; Softky and Koch, 1993). These observations have led some to conclude that only statistical averages of many inputs carry useful information between cortical neurons (Burns, 1968; Barlow, 1972; Shadlen and Newsome, 1994). Another possibility, which we explore here, is that cortical neurons may respond reliably to relatively weak input fluctuations. Irrregularity in spike timing may then reflect the presence of information. This is possible only if the intrinsic noise within neurons is small. Although some previous studies have suggested that neurons may have low intrinsic noise (Calvin and Stevens, 1968; Korenberg, Sakai and Naka, 1989; Lass and Abeles, 1975; Bryant and Segundo, 1976), others have argued to the contrary (Burns, 1968; Schellart and Spekreijse, 1973; Levine, Saleh and Yarnold, 1988; Croner, Purpura and Kaplan, 1993).

Methods

The aim of the present report was to determine directly the temporal precision with which cortical neurons are capable of encoding a stimulus into a spike train. A cortical slice preparation was chosen so that the state of a single neuron and its input could be well-controlled experimentally.

Coronal slices of occipital cortex (400 μm) were prepared from 14-24 day old Sprague-Dawley rats deeply anesthetized using ether and decapitated. After 1-6 hours incubation in an interface chamber, a slice was transferred to a submerged chamber (22-24 °C) for recording and continuously perfused with oxygenated (95% O_2 / 5% CO_2) ringer solution containing (in mM) 126 NaCl, 1.25 NaH_2PO_4, 10 D-glucose, 2.5 KCl, 2 MgCl, 2 $CaCl_2$, 26 $NaHCO_3$. Tight-seal whole-cell recordings were obtained from pyramidal-shaped neurons of layer 5 under visual control (Stuart, Dodt and Sakmann, 1993). Patch pipettes (3-8 MΩ, thin-walled borosilicate, wax-coated to reduce capacitance) contained (in mM): 100 K-gluconate, 25 KCl, 5 NaCl, 10 HEPES, 0.2 EGTA, 4 ATP, 0.3 GTP; pH 7.2 with KOH. Whole-cell potentials were recorded using a patch clamp amplifier (Axopatch 200a) in "fast" current-clamp mode, filtered at 1 kHz and digitized at 4-16 kHz.

As the purpose was to isolate the process of spike generation from synaptic transmission and dendritic integration, care was taken to eliminate sources of variability extrinsic to spike generating currents themselves. To reduce spontaneous synaptic activity, D-APV (20 μM) and DNQX (10 μM) were used to block glutamate receptors and BMI (5 μM) was used to block $GABA_A$ receptors. To mitigate the effects of possible long term drift in recording conditions, reliability was measured over blocks of consecutive trials recorded during a period of less than 2 minutes, and blocks showing obvious instability (membrane potential or input resistance fluctuations) were not included in the analysis. Data are reported for cells in which recordings were sufficiently stable and long-lasting to examine repeated responses to stimuli of a range of parameters. Nevertheless,

even under these conditions, relatively small sources of uncontrolled noise were still obviously present. For instance, the background voltage noise measured over 200 msec periods at resting potential (-68.4 ± 5.1 mV, n = 10) was in the range of 0.05 to 0.5 mV RMS (root mean squared).

Somatic whole-cell recordings were made in the current-clamp configuration, and spike trains were elicited with current injected through the recording electrode, near the presumed site of action potential generation (Stuart and Sakmann, 1994). Reliability was assessed by repeatedly presenting the same stimulus and evaluating the consistency of the evoked spike sequences. Trials were 1024 msec in duration and were collected at intervals of 3 to 4 s. Bridge balance was performed digitally offline using 50–100 pA hyperpolarizing pulses preceding each trial. Spike times were detected using thresholding of the first or second time derivative of voltage. All data collection and analysis were done using Sun workstations using custom software written in C++ based on NEURON (Hines, 1993).

The arrival of many uncorrelated excitatory and inhibitory synaptic events will deliver a total current to a neuron which may be treated approximately as shot noise (Rice, 1954). The event rates and their amplitude waveforms determine the mean, variance and frequency spectrum of the net current. Accordingly, the stimuli used were realizations of Gaussian white noise with chosen mean (μ_s) and standard deviation (σ_s) of fluctuations. Convolution with the function $f(t) = t\exp(-t/\tau_s)$ gave low-pass filtering with a time constant τ_s, as could be expected from synaptic time courses and dendritic filtering. Unless otherwise noted, τ_s was 3 msec. The range of σ_s investigated, 0 to 100 pA, produced voltage transients up to about 25 mV peak to peak.

Results

First, repetitive firing was evoked with flat (d.c.) current pulses (0-250 pA, 0.9 sec; Fig. IV.1A). The variability of spike counts from trial to trial was small (coefficient of variation, CV = 0.10 ± 0.13; mean ± standard deviation, SD; n = 10 cells). However, the small variances in interspike intervals (ISIs) summed to increase the desynchronization of corresponding action potentials over the course of the stimulus. The first spike of each train was tightly locked to the onset of the pulse (standard deviation = 0.62 ± 0.25 msec; n = 8), while the timing of the last spike in the train was highly variable (standard deviation = 31 ± 19 msec; n = 8). Thus, responses to flat pulse stimuli indicate reliability of spike count or average firing rate, but lack of reliability in precise timing, as measured relative to stimulus onset.

Intracellular recordings from cortical neurons in vivo reveal large and rapid fluctuations of the membrane potential from many synaptic events (Ferster and Jagadeesh, 1992; Douglas, Martin and Whitteridge, 1991). The integration of many independent excitatory and inhibitory synap-

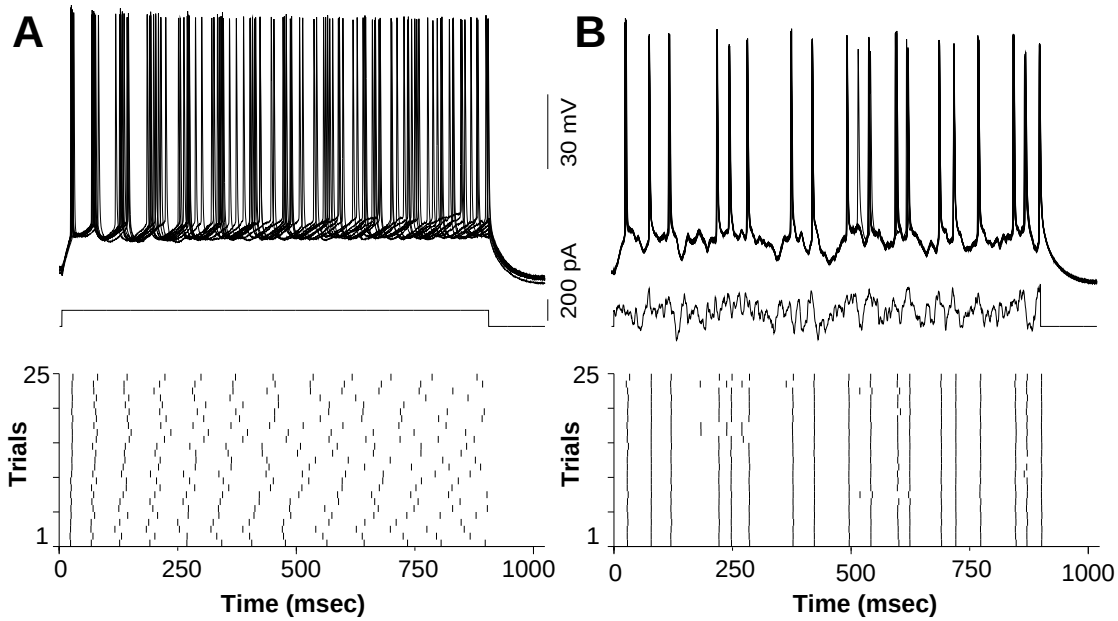

Figure IV.1: Reliability of firing patterns of cortical neurons evoked by constant and fluctuating current. A. In this example, a superthreshold d.c. current pulse (150 pA, 900 msec; lower trace) evoked trains of action potentials (approximately 14 Hz) in a regular-firing layer 5 neuron. Responses are shown superimposed (first ten trials, upper traces) and as a raster plot of spike times over spike times (25 consecutive trials, bottom traces). B. The same cell in (A) was again stimulated repeatedly, but this time with a fluctuating stimulus (Gaussian white noise, μ_s=150 pA, σ_s=100 pA, τ_s=3 msec).

tic currents would be expected to approach a Gaussian distribution at the soma. Accordingly, sequences of filtered Gaussian white noise generated by computer were added to the constant depolarizing pulse (see Methods). As with flat pulse stimuli, spike count showed little variability (CV = 0.052 ± 0.029, n= 10). In contrast to flat pulse responses, when any particular fluctuating current waveform was repeatedly injected, the pattern of spikes elicited showed precise and stable timing throughout the length of the trial (Fig. IV.1B). Occasionally, from trial to trial, spikes could appear, disappear, or abruptly shift tens of milliseconds. In some cases, a single dropped or added spike disrupted the timing of several consecutive following spikes. This behavior made it problematic to compute directly the variability in ISIs or the timing of a particular spike number; therefore, further analysis was performed using the peri-stimulus time histogram (PSTH; IV.2A).

Highly reproducible firing patterns were a robust phenomenon in the presence of stimulus fluctuations. Two measures of spike timing were calculated from the PSTH, which we termed the *reliability* and the *precision* (Fig 2A). According to these measures, the cells analyzed were all capable of responding to fluctuating input currents with nearly 100% of spikes (high reliability) in clusters with a standard deviation of less than 1 msec (high precision; Fig 2B). The reliability of spike patterns was strongly correlated with the amplitude of stimulus fluctuations (σ_s, IV.2C). The firing rate also increased with amplitude of fluctuations, particularly for cells showing strong adaptation to d.c. stimulation (not shown). The precision of spike timing depended on the time constant of stimulus fluctuations (τ_s, IV.2D). Precision and reliability dropped as stimuli were filtered at time constants increasing from 1 to 25 msec. The precision of most responses was in the range of 1 to 2 msec, a time scale much smaller than both the maximum firing rate of these cells and the time constant of fluctuations in the stimuli. There was no systematic relationship between μ_s and reliability over the range of values investigated (50 to 300 pA producing firing rate of 4 to 32 Hz), although in some cells, reliability did increase or decrease with μ_s. The decrease in precision was paralleled by a reduction of reliability (not shown).

These results indicate that a particular cell encodes a given input pattern into a consistent spike pattern based on generation of spikes in response to particular input transients. However, it was not the case that all cells generated similar patterns in response to the same stimulus waveform (Fig. IV). Intrinsic cell properties and state may lead to differing "translations" of identical incoming signals.

The reproducibility of spike patterns suggested that spikes were triggered preferentially by particular patterns of depolarizing and hyperpolarizing current in the stimulus. A reverse correlation of spike train and stimulus (spike-triggered average of the stimulus; the reverse correlation reported is similar to the first order response kernel of the neuron (Marmarelis and Marmarelis, 1978)) can reveal the stimulus waveform that tends to precede the generation of an action

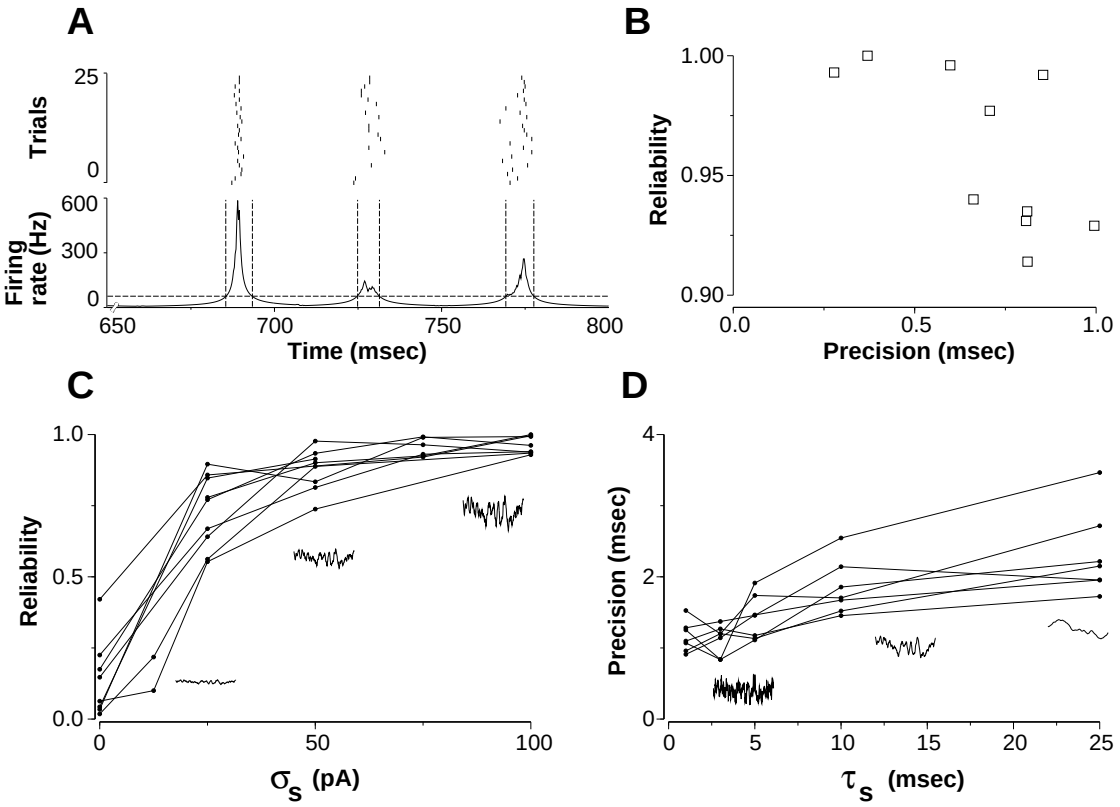

Figure IV.2: Dependence of reliability and precision of spike timing on stimulus current statistics. A. The peri-stimulus time histogram (PSTH) of spikes collected over 20 to 25 successive presentations of a particular stimulus waveform was used to quantify the consistency of spike patterns evoked by fluctuating stimuli of different types. Spikes during the first 100 msec following stimulus onset, during which most spike frequency adaptation occurred, were discarded. The PSTH was smoothed using an adaptive filter (centered on each time step and widened to capture 10 spikes) to yield an estimate of the instantaneous firing rate. A threshold (horizontal dotted line; set at 3 times the mean firing rate of the cell over a given block of responses) was used to select dramatic elevations in instantaneous firing rate, or "events". Since the minimum ISI was long compared to the duration of these events, at most one spike occurred during any event on any trial. We defined *reliability* as the fraction of total spikes which occurred during such periods of elevated firing rate. We defined temporal *precision* as the SD of spike times within any event, averaged over all events during a response. B. Each square represents the most consistent block of responses recorded in one of 10 cells (8 regular firing, 2 intrinsic bursting). For these responses, a stimulus mean, μ_s, between 100 and 300 pA and fluctuation amplitude, σ_s, between 50 and 100 pA were used, yielding firing rates between 14 and 24 Hz. C. Estimates of reliability for stimuli with various amplitudes of stimulus fluctuations. Each line on the graph connects measurements made for one of 9 cells examined at 4 or 5 different values of σ_s (μ_s for these blocks was 100 to 300 pA, giving firing rates between 8 and 24 Hz). The input resistance of neurons examined was 222 $\pm$ 85 MΩ; peak to peak voltage transients produced by these currents were less than 25 mV. D. The temporal precision of responses obtained in 7 cells for stimuli filtered at different time constants (τ_s = 1 to 25 msec, σ_s = 25 - 50 pA, μ_s = 100 -200 pA). The average membrane time constant for these cells was 29.7 $\pm$ 5.9 msec.

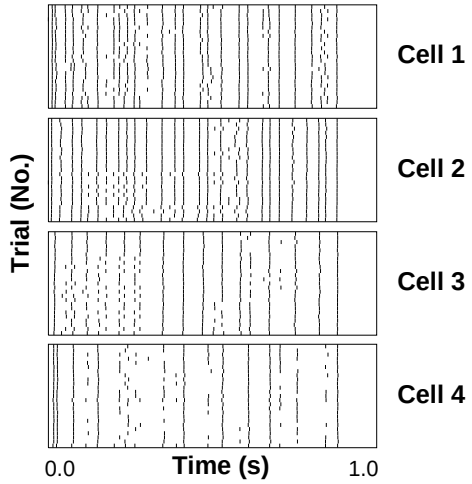

Figure IV.3: Intrinsic cell properties affect response pattern. Although individual cells show stereotyped spike patterns for a given stimulus, the identical stimulus does not generate the same pattern of spikes in different neurons. The response of four different pyramidal neurons to 25 presentations of the same current stimulus (μ_s=200 pA,σ_s=50 pA,τ_s=3 msec) are shown.

potential and give an indication of the length of stimulus history that is relevant. Reverse correlations showed a strong tendency for spikes to be preceded by a depolarizing transient. At greater mean input currents (μ_s), the average depolarizing transient was reduced while a preceding hyperpolarizing transient was introduced (Fig. IV.4A). Varying the stimulus filter time constant revealed a preference for maximum stimulus slope 5-10 msec preceding the spike (Fig. IV.4B). Therefore, the time course of the reverse correlations was broadened by filtering of the stimulus, but the basic shape was preserved. Transients of this amplitude correspond to the arrival of about 10 excitatory postsynaptic currents of 5 to 10 pA within 10 msec.

Discussion

These data demonstrate that repetitive firing in neocortical neurons is sufficiently reliable that currents resembling synaptic input may be repeatably encoded into spike patterns with millisecond precision. Therefore, it is likely that the intrinsic variability of the spike-generating currents and their susceptibility to non-synaptic background noise has minimal contribution to interspike interval variability under *in vivo* conditions.

Spike-triggered stimulus averages suggest that consistent temporal coding follows in part from a greater sensitivity of spike generation to transients than to steady state depolarization. This analysis also indicates that properly-timed hyperpolarizing events may increase firing probability, possibly through reduction of sodium channel inactivation. Stimuli without transients may

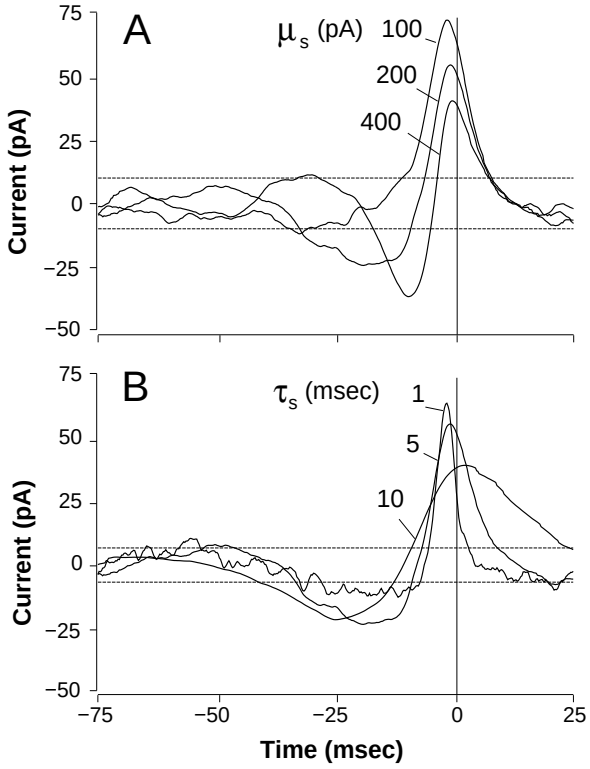

Figure IV.4: Reverse correlations (spike-triggered stimulus averages) were computed over 25 consecutive trials for which stimuli were generated with equivalent parameters (μ_s, σ_s, τ_s) but different random seed. A. Reverse correlations from blocks of trials with mean amplitudes shown (σ_s = 50 pA, τ_s = 3 msec). Firing frequency ranged from 10 to 25 Hz (corresponding to 225 to 554 spikes averaged). B. Reverse correlations obtained with the different time constants of stimulus filtering shown (μ_s = 200 pA and σ_s = 50 pA; 282-322 spikes averaged). For A and B, the trigger point (t = 0, vertical line) was at the inflection in the rising phase of the spike. The current values shown are relative to the mean current (μ_s). For a neuron generating spikes randomly, the average stimulus preceding a spike is not expected to differ from the average stimulus in general, which approaches a flat line with increasing samples. Departure from this expectation reveals a preference for particular stimulus waveforms. Confidence limits (dashed lines) were calculated as described in Bryant and Segundo (1976) , and only the widest limits are shown. The data are from a single neuron in which reverse correlations were collected at a variety of stimulus parameters. Similar results were seen in all 3 other cells examined.

be encoded reliably with respect to mean rate, but not with respect to the exact timing of spikes. The behavior observed is roughly compatible with a deterministic leaky-integrator or Hodgkin-Huxley model with a fixed level of additive background noise. However, other mechanisms such as spike frequency adaptation may contribute to the observed reliability (Mainen and Sejnowski, 1995a).

We have deliberately isolated one step in the sequence of electrical and chemical events involved in the propagation of a neural signal. Although we find that reliable spike trains may be elicited by injected currents resembling integrated synaptic inputs, we have not addressed unreliability at other steps in the signaling process, particularly in synaptic transmission (Hessler, Shirke and Malinow, 1993; Rosenmund, Clements and Westbrook, 1993; Otmakhov, Shirke and Malinow, 1993; Allen and Stevens, 1994; Thomson, Deuchars and West, 1993). Such variability would be expected to erode the fidelity of temporal coding, but may be mitigated by particular activity patterns. For example, bursts of action potentials may significantly increase the reliability (release probability) of a synapse through the mechanism of paired-pulse facilitation (Zucker, 1989; Stevens and Wang, 1995). Evidence for rapid modulation of firing rate (Maunsell and Gibson, 1992; Snowden, Treue and Andersen, 1992; Phillips, Johansson and Johnson, 1992; Bair et al., 1994) and repetition of particular spike interval patterns (Vaadia et al., 1995; Strehler and Lestienne, 1986) suggests that it is possible for the neocortex to overcome these sources of noise.

Neurons in the peripheral auditory system can encode information based on the timing of individual spikes (Carr and Konishi, 1990; Suga, Olsen and Butman, 1990). Although our finding that neocortical neurons also have the ability to generate precisely-timed firing patterns does not prove that this timing has a physiological significance, it is consistent with theories of cortical information processing in which spike timing is important.

This chapter is based on material originally published in Mainen, Z. F. and Sejnowski, T. J. "Reliability of spike timing in neocortical neurons", *Science*, 268:1503–1506, 1995. The dissertation author was the primary investigator and the dissertation advisor supervised the research for this chapter.

Chapter V

Adaptation and the Reliability of Spike Encoding

Spike frequency adaptation is a hallmark of the electrophysiology of excitatory neurons in the cortex. Adaptation decreases a neurons response sensitivity to sustained input relative to its sensitivity to input transients. We examined models of the voltage-dependent and calcium-dependent conductances underlying adaptation in order to clarify their mechanism and explore their functional consequences for spike encoding by single neurons. By treating subthreshold and suprathreshold behavior separately, either type of adaptataion conductance could be described using a simple mechanism in a integrate-and-fire style model. Simulations of this model were used to document the impact of adaptation conductances on the spike encoding of simulated synaptic input. When driven by random input, adaptation conductances produced characteristic changes in reverse correlation and autocorrelation spike train analyses and increased the irregularity of interspike intervals. When driven by time-varying signals in the presence of additive noise, adaptation conductances greatly enhanced the reliability of stimulus-locked spike timing. These results suggest that adaptation conductances will increase the precision of temporal aspects of information processing in the neocortex.

Introduction

The mechanism of spike train generation in neurons of the central nervous system differs from that of the squid giant axon due largely to the contribution of slow K^+ conductances to repolarization of the membrane (see reviews by Storm, 1990; Brown, 1990). These slowly increasing outward currents give rise to the adaptation of spike frequency characteristic of excitatory neurons

in the cortex (Schwindt et al., 1988).

There are two general classes of slow potassium currents. One type, exemplified by the "muscarinic" K current (I_M), is voltage dependent like the squid delayed rectifier studied by Hodgkin and Huxley, but operates with a time constant 1 to 2 orders of magnitude slower (10 - 100 msec). The other type ($I_{K(Ca)}$) is gated by intracellular Ca^{2+} rather than by voltage and operates at time constants of up to seconds.

The significance of slow potassium currents for the regulation of repetitive firing has been recognized for some time (Baldissera and Gustafsson, 1971). Likewise, the importance of adaptation in peripheral sensory coding is well-known. Recent modeling studies have shown that adaptation of firing rate has implications for dynamic neural control (Lisberger and Sejnowski, 1992), associative memory networks (Cartling, 1993), and cortical visual processing (Xing and Gerstein, 1994). Furthermore, the strength of adaptation currents are subject to control by numerous neuromodulatory transmitters (reviewed in Brown, 1990), suggesting that these processes will be regulated in an ongoing fashion.

The aim of the present study was to explore the effects of adaptation by slow potassium currents on the encoding of time-varying signals by the spike trains of individual cortical neurons. We begin by studying a relatively detailed kinetic model of repetitive firing in order to derive a simplified model for the dynamics of adaptation currents. The simplified adaptation mechanism, a conductance with first-order kinetics, can be used to augment a standard "integrate-and-fire" model, much as a passive leak conductance is added to the perfect integrator model to produce a leaky integrator model, which will be called the adapting integrator model. We then perform a series of simulations using artificial "synaptic noise" stimuli in order to analyze the contributions of adaptation to spike encoding. The standard leaky integrator model is used effectively as a control.

Methods

Standard compartmental modeling techniques (Hines, 1993) were used to simulate repetitive firing in single-compartment neurons. A fast Na^+ current, I_{Na} (Hamill, Huguenard and Prince, 1991) and delayed rectifier K^+ current, I_{Kdr}, identical to those published in a model of neocortical spike initiation (Mainen et al., 1995) were used. In addition we simulated a slow, non-inactivating K^+ current, I_{K_M} (Gutfreund, Yarom and Segev, 1995), a high-voltage activated Ca^{2+} current, I_{Ca}(Reuveni, Friedman and Amitai, 1993), and a Ca^{2+}-dependent current K^+ current, $I_{K(Ca)}$ (Reuveni, Friedman and Amitai, 1993). These currents were calculated using conventional Hodgkin-Huxley style kinetics with the following rate equations:

First order I_{K_M} activation: $\alpha(v) = 2 \cdot 10^{-4}(v+35)/(1-e^{-(v+35)/9})$, $\beta(v) = -2 \cdot 10^{-4}(v+35)/(1-e^{(v+35)/9})$; second order I_{Ca} activation: $\alpha(v) = 0.055(v+27)/(1-e^{-(27+v)/3.8})$, $\beta(v) = 0.94e^{-(v+75)/17}$; first order I_{Ca} inactivation: $\alpha(v) = 4.57 \cdot 10^{-4}e^{-(v+13)/50}$, $\beta(v) = 0.0065/(1+e^{-(v+15)/28})$; first order $I_{K(Ca)}$ activation: $\alpha([Ca^{2+}]_i) = 2 \cdot [Ca^{2+}]_i$, $\beta = 0.075$.

For Na^+ and K^+ currents an ohmic current–voltage relationship with E_{Na} = 50 mV and E_K = -90 mV was assumed. I_{Ca} was computed using the Goldman-Hodgkin-Katz current equation rather than Ohm's law. Extracellular Ca^{2+} concentration was 2 mM and internal concentration was computed dynamically, with entry via I_{Ca} and removal by a first order pump:

$$d[Ca^{2+}]_i/dt = (-1 \cdot 10^5 \cdot I_{Ca}/2F) - ([Ca^{2+}]_i - [Ca^{2+}]_\infty)/\tau_R \tag{V.1}$$

where $[Ca^{2+}]_\infty$ = 0.1 μM, τ_R is a parameter for decay rate, and F is Faraday's constant.

Specific membrane capacitance was 0.75 μF/cm^2, specific membrane resistance was 30 kΩ-cm^2. All densities were based on an area of 12,000 μm^2. The time constants and maximal conductances were developed in models based on room temperature and were therefore scaled from 23 to 37 ^{o}C using a Q_{10} of 2.3 or 2 ($I_{K(Ca)}$ and I_{Ca}). An integration time step of 100 μsec was used.

A leaky integrator threshold-crossing model was the basis for simplified models of adaptation. This model consisted of a subthreshold regime following

$$c_m \dot{v} = -\bar{g}_l v + i_s \ , \tag{V.2}$$

where $\bar{g}_l$ is the leak conductance (resting potential is 0 mV) and i_s is the stimulus current. When v (mV) exceeds threshold level, θ_v, a spike is assumed to occur and v is reset to v_r. Standard parameters were g_l = 10 nS (input resistance, r_m = 100 MΩ) and θ_v = 20 mV. v_r and τ_m are specified for different models below; τ_m was scaled by changing c_m in order to preserve r_m.

Results

The M current (I_M) is a common variety of slow voltage-activated K^+ current ($I_{K(v)}$). I_M activates and deactivates mono-exponentially with τ of around 50 msec and shows little or no inactivation (Adams, Brown and Constanti, 1982). A compartmental model incorporating $I_{K(v)}$ (Fig. V.1A) does not show a gradual slowing of firing rate at low stimulus intensities because the current activates fully by the second spike. Relatively fast adaptation currents like $I_{K(v)}$ give rise to the "scooped" shape of the voltage trajectory between spikes seen commonly in cortical pyramidal neurons in vitro (e.g. McCormick et al., 1985; Connors and Gutnick, 1990).

Calcium-activated K^+ current ($I_{K(Ca)}$) kinetics are thought to be limited mainly by Ca^{2+} dynamics (Lancaster and Zucker, 1994), generally with a slower τ than $I_{K(v)}$, on the order of 100

msec to 1 sec or more. The behavior of $I_{K(Ca)}$ depends strongly on properties of Ca^{2+} entry, buffering and removal that have not been well established. We therefore used a relatively simple model in which high-voltage activated Ca^{2+} channels provide Ca^{2+} influx and all Ca^{2+} buffering and removal mechanisms are lumped into a decay term with time constant τ_R. A compartmental model incorporating $I_{K(Ca)}$ with τ_R = 500 msec produces slowly accumulating spike frequency adaptation (Fig. V.1B). $I_{K(Ca)}$ contributes less to the shape of the inter-spike voltage trajectory that does the fast $I_{K(v)}$.

The conductances ($g_{K(Ca)}$ and $g_{K(v)}$) underlying the slow K^+ currents show stereotyped patterns of activation during an action potential and between action potentials. A spike transiently activates I_{Ca} (Fig. V.1A, middle), leading to a jump in $[Ca^{2+}]_i$ and consequent step in $g_{K(Ca)}$ activation (Fig. V.1A). In the subthreshold regime, $g_{K(Ca)}$, tracking $[Ca^{2+}]_i$, decays exponentially to an asymptote near zero (Fig. V.1A, bottom). Although resulting from an entirely different mechanisms, the dynamics of $g_{K(v)}$ are surprisingly similar. With each spike, $g_{K(v)}$ experiences an abrupt, transient increase in steady-state activation value (Fig. V.1B, middle) and concomitant decrease in time constant that result in a stereotyped step increase in activation (Fig. V.1B, bottom). Between spikes, the time constant is longer and the steady-state values smaller, leading generally to exponential decay following a spike. The chief difference between the two conductances is that $g_{K(v)}$ can be activated by subthreshold depolarizations whereas $g_{K(Ca)}$ is activated predominantly by spikes (Madison and Nicoll, 1984). Thus $g_{K(Ca)}$ is more truly an "impulse-dependent" adaptation, whereas g_{Km} may have a significant "impulse-independent" component.

Following from this description, $I_{K(v)}$ or $I_{K(Ca)}$ can be modeled by introducing an activation variable, a, with subthreshold dynamics governed by

$$\dot{a} = \frac{(a_\infty - a)}{a_\tau} \quad . \tag{V.3}$$

For $I_{K(Ca)}$, a_∞ is the asymptotic Ca^{2+} level and τ_a is the Ca^{2+} removal rate. For $I_{K(v)}$, a_∞ and τ_a can be computed as a function of v(t) (as given in the Methods section). For either current, on the occurrence of an action potential, a is incremented by a fixed amount, a_s (neglecting possible conductance saturation thought to give rise to so-called "secondary range" firing (Baldissera, Gustafsson and Parmiggiani, 1978)). The value of a_s is arbitrary for $I_{K(Ca)}$ but must be chosen for $I_{K(v)}$ with respect to the amount of subthreshold activation. Empirically, a_s = 1 for either current gave a good match to dynamics in the compartmental model. Assuming a K^+ reversal potential equal to leak reversal potential (0 mV), the adaptation current is given by $i_a = \bar{g}_a \cdot a \cdot v$, leading to an adapting integrator model, following

$$c_m \dot{v} = -(\bar{g}_l + \bar{g}_a a)v + i_s \quad . \tag{V.4}$$

Simulations of the leaky integrator model showed that the features of either fast (50 msec)

or slow (500 msec) adaptation could be reproduced closely with either voltage-dependent or voltage-independent kinetics for a. The $I_{K(Ca)}$-style adaptation model is shown in Fig. V.1C and D. Due to the similar behavior of the two models for suprathreshold activation, in the following analysis, we show only simulations performed with the simpler voltage-independent adaptation kinetics. Nearly identical results in all simulations were obtained with the voltage-dependent kinetics, but we emphasize that we did not search for conditions in which response differences between these two mechanisms might arise.

Spike frequency adaptation reduces the dependence of the average spike rate on the mean of the input current, turning a "tonically" responding neuron into a "phasically" responding one. Thus, when the adaptation current is added to a non-adapting leaky integrator model, a plot of steady-state firing rate as a function of input current (the "FI" curve) remains linear but shows a significant decrease in slope (Fig. V.2A). This results in a larger effective range of mean stimulus intensities. That is, a much broader domain of input levels can be represented within the same dynamic range of firing frequencies (taking the maximal sustained firing rate for an excitatory neuron in the cortex to be $\leq$ 100 Hz). In order to achieve a similar effective input domain without adaptation, it is necessary to reduce either the time constant and/or increase the difference between threshold and reset level.

The initial response of leaky integrator model (defined as the reciprocal of the first interspike interval (ISI)) is identical to the final frequency (i.e. there is no adaptation). However, the initial responses of adapting models are close to that without adaptation (Fig. V.2B). For physiological strengths of adaptation, the ratio of initial (first interval) to adapted frequencies are in the range of 10-fold (Fig. V.2C; Mason and Larkman, 1990).

We explored the effects of slow and fast adaptation currents on spike encoding by comparing the responses of fast adapting integrator and slow adapting integrator models to a leaky integrator model with comparable steady-state FI relationships. The leaky integrator model therefore had a greater "reset" following a spike (v_r = 20 vs. 5 mV) and a longer time constant (τ_m = 50 vs. 25 msec) than the adapting integrator models.

For stimuli, we used randomly-generated patterns of "synaptic noise" current (Mainen and Sejnowski, 1995b). These were based on the assumption that the net input to a neuron is approximated by the summation of many uncorrelated excitatory and inhibitory synaptic events. Such an input will deliver a total current to a neuron that may be treated as shot noise (Rice, 1954). That is, the amplitude distribution of the net current will be Gaussian and the rates of excitatory and inhibitory postsynaptic currents and their amplitude waveforms will determine the mean, variance and frequency spectrum. Accordingly, we used randomly-generated sequences of Gaussian white noise that were convolved with an alpha function, $f(t) = t\exp(-t/\tau_s)$, to give low-pass

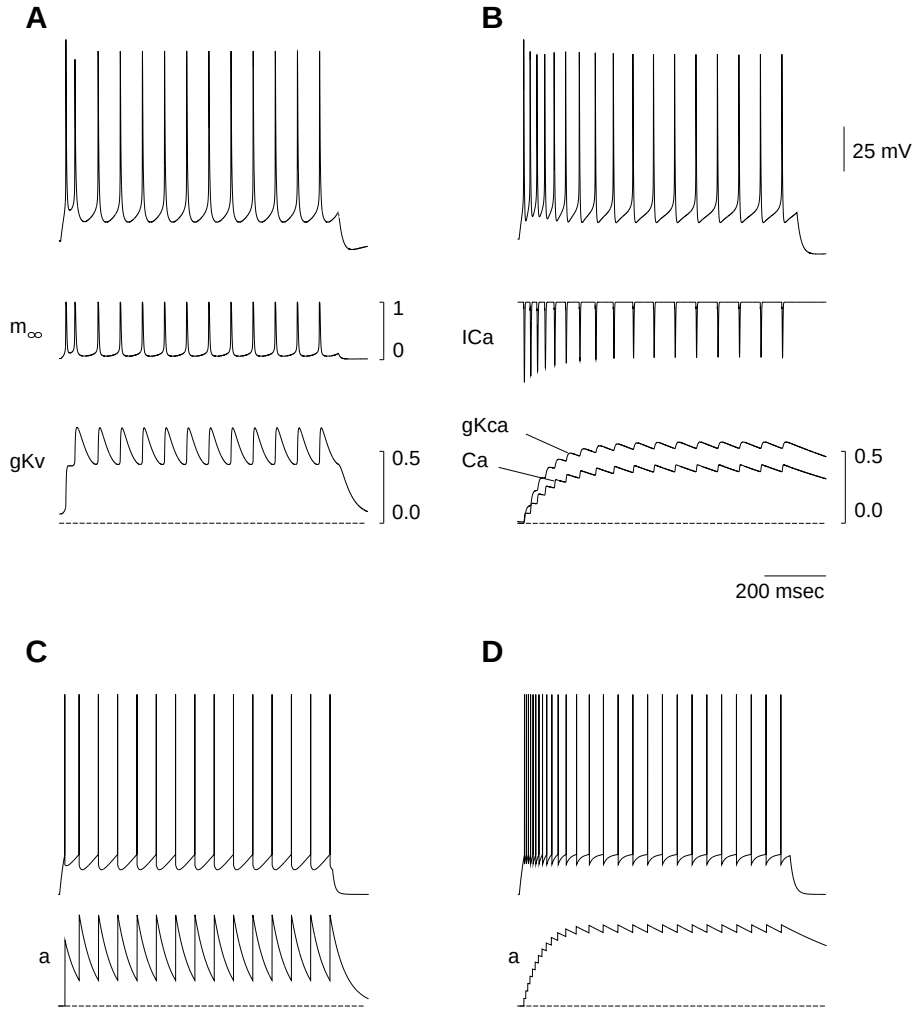

Figure V.1: Use of Hodgkin-Huxley style compartmental models to obtain simplified mechanisms for spike frequency adaptation in integrate-and-fire style threshold models. A. A compartmental model incorporating a voltage-dependent K^+ adaptation current, $I_{K(v)}$. Upper: voltage response to a current step (0.25 nA). Middle: steady-state value ("m_∞(v)") for the activation of $I_{K(v)}$. Note that the time constant for activation also becomes faster as $m_{\infty(v)}$ approaches 1. Lower: conductance waveform of $I_{K(v)}$ ("gKv"). Note the step-like increases during spikes and exponential decay between spikes. For this model, maximum conductance densities were $\bar{g}_{Na}$ = 150, $\bar{g}_{Kdr}$ = 1.2, $\bar{g}_{K(v)}$ = 0.6 (pS/μm^2). B. Compartmental model with a slow Ca^{2+}-dependent K^+ current, $I_{K(Ca)}$, and a high-voltage activated Ca^{2+} current. Upper: voltage response to 0.25 nA current step. Middle: Ca^{2+} current ("Ica"). Lower: intracellular calcium concentration ("Ca") and the conductance waveform of $I_{K(Ca)}$ ("gKca"). For this model, maximum conductance densities were $\bar{g}_{Na}$ = 150, $\bar{g}_{Kdr}$ = 2.5, $\bar{g}_{Ca}$ = 0.01, $\bar{g}_{K(ca)}$ = 0.05 (pS/μm^2). C,D. Leaky integrator models incorporating fast (C) or slow (D) adaptation mechanism (Eqns. V.3,V.4). Upper: voltage response (with spikes drawn in for illustration) to a current step x(0.4 nA). Lower: activation of the adaptation variable ("a"; compare to "gKv" in (A) and "gKca" in (B)). For both simulations, τ_m = 25 msec, v_r = 15 mV. In C, $\bar{g}_a$ = 20 μS, τ_a = 50 msec. In D, $\bar{g}_a$ = 2 μS, τ_a = 500 msec.

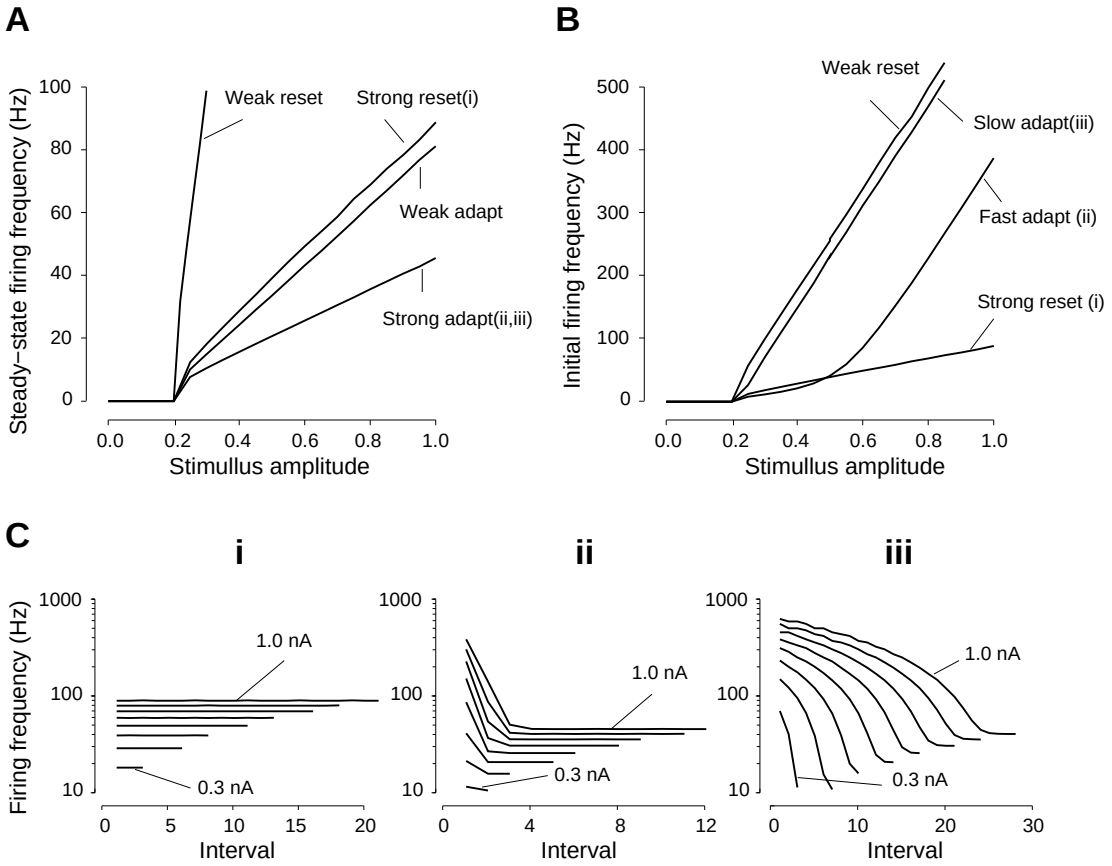

Figure V.2: Comparison of responses to current steps for adapting and non-adapting leaky integrator models. A. Steady-state firing frequency as a function of d.c. stimulus amplitude. Shown are non-adapting models with two different firing sensitivities ("weak reset": v_r = 15 mV, τ_m = 25 msec; and "strong reset": v_r = 0 mV, τ_m = 50 msec) and two adapting models with different strengths of adaptation current ("weak adapt": $\bar{g}_a$ = 10, τ_a = 50 msec; and "strong adapt": $\bar{g}_a$ = 20, τ_a = 50 msec). The adapting models were otherwise identical to the "weak reset". B. Initial firing frequency as a function of d.c. stimulus amplitude. Shown are the "weak reset" and "strong reset" leaky integrator models and adapting models with two rates of adaptation ("slow adapt": $\bar{g}_a$ = 2, τ_g = 500 msec; "fast adapt": $\bar{g}_a$ = 20, τ_g = 50 msec). Both adapting models are based on the "weak reset" leaky integrator model. Note that adapting models such as these, having equal values of the product $\tau_a \cdot \bar{g}_a$, have similar steady-state firing frequencies. C. Instantaneous spike frequency as a function of spike interval for leaky integrator (i), fast adapting integrator (ii) and slow adapting integrator (iii) models. Each line is obtained from a separate 250 msec spike train. Responses to current input steps from 0 to between 0.3 and 1.0 nA are shown.

filtering with a time constant, $\tau_s = 3$ msec, a minimum which could be expected from synaptic time courses and dendritic filtering. The noise was then scaled and offset to obtain a chosen mean (μ_s) and standard deviation (σ_s). The stimuli were thus simple to generate and manipulate (compared, e.g., to simulations of individual synaptic currents), but were limited as a model of true synaptic input in neglecting non-linear interactions (notably saturation at synaptic reversal potentials (Bush and Sejnowski, 1994) and membrane time constant effects (Bernander, Koch and Usher, 1994; Bell, Mainen and Sejnowski, 1995)) that can occur for true synaptic conductances.

Recordings of cortical neurons in vivo show a striking irregularity of spike timing at a wide range of firing rates (Burns and Webb, 1976; Softky and Koch, 1993). Pinpointing the origin of this irregularity has sparked recent controversy (Shadlen and Newsome, 1994; Bell, Mainen and Sejnowski, 1995; Softky, 1995). One measure of irregularity of firing is the coefficient of variation (CV = $\sigma\mu^{-1}$) of the set of the interspike interval distribution. Comparing the ISI CV of leaky integrator and fast adapting integrator models driven at similar rates by "synaptic noise" of equal σ_s shows that adaptation currents can enhance irregularity by this measure, particularly at high firing rates (Fig. V.3A). Increased variability is partly due to the greater sensitivity of the fast adapting integrator model to the high-frequency components of the stimulus which tend to cause irregular spike times compared to the d.c. component which tends to produce regular interspike intervals. A further contribution to irregularity is made by the lower effective τ_m of the fast adapting integrator model compared to the leaky integrator model. Output distributions tend to become regular when the mean ISI becomes small relative to τ_m; therefore decreasing τ_m increases the frequencies at which regularity sets in.

The effects of adaptation can be seen more closely by examining the spike train autocorrelation histogram (Fig. V.3B) or ISI distribution (Fig. V.3C). In comparison to the leaky integrator model, the fast adapting integrator model shows a much narrower central trough in the autocorrelation histogram and a corresponding peak in the ISI distribution at short intervals. These effects are particularly pronounced for larger σ_s. While the leaky integrator shows a characteristic unimodal distribution, the fast adapting integrator distribution is bimodal and is broader, as expected by the greater CV.

Insight into the origin of responses to noise stimuli can be provided by calculating a "reverse correlation" between the spike train and the stimulus (a spike-triggered stimulus average). The reverse correlation does not reveal the best stimulus for triggering a spike, but rather asks, given that a spike occured, "what was the most likely stimulus to have preceded it?". In the leaky integrator model, the reverse correlation rises monotonically from a baseline equal to the stimulus mean to a peak at 0 msec (Fig. V.4i). The peak indicates that threshold crossings tend to occur more frequently through integration of depolarizing fluctuations in the stimulus. At the limit of

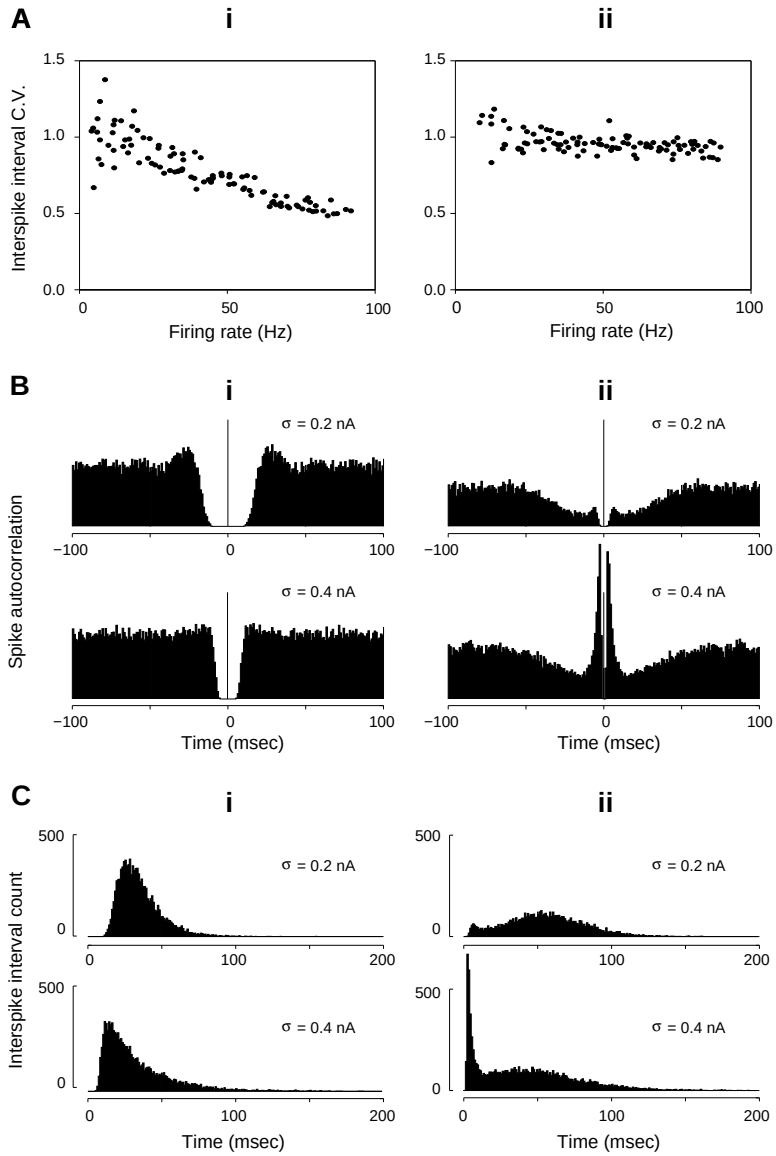

Figure V.3: Comparison of several spike interval statistics for leaky integrator (i) and fast adapting integrator (ii) models driven by random synaptic noise. For all statistics, the first 500 msec was discarded from each trial. A. Irregularity of firing as measured by the CV of interspike intervals. The CV was calculated from 100 trials of 4 sec duration, σ_s = 0.5 nA, μ_s = 0 to 1 nA (non-adapting model) or 0 to 1.75 nA (adapting model). Note the drop in CV at higher firing frequencies for the integrate and fire but not the fast adaptation model. B. Spike autocorrelation histograms computed over $\geq$ 10,000 spikes driven by synaptic noise (μ_s = 0.4 nA) of two difference variances (upper, σ_s = 0.2 nA; lower, σ_s = 0.4 nA). C. The distribution of interspike intervals computed over the same data set as (B). Note that the distributions for the adapting model are bimodal.

ISIs much greater than τ_m (top), the reverse correlation waveform rises exponentially with a time constant equal to that of the membrane. With increasing mean, the firing rate due to integration of the d.c. component of the stimulus increases, diminishing the ratio of peak to baseline amplitude. Many more spikes are "accounted for" by the mean input current than by fluctuations in that current. Furthermore, at firing rates for which many ISIs are less than τ_m (middle, lower), the effective integration time is reduced. A spike occurs within a short interval from the last whether or not a positive fluctuation in the stimulus occurs.

The addition of adaptation currents to the integrate and fire model (Fig. V.4 ii, iii) changes the reverse correlation in an interesting fashion. At zero mean (top), mono-exponential rise similar to the leaky integrator model is seen. However, at greater firing frequencies (middle, lower), the reverse correlation waveform becomes bi-phasic, with a dip in amplitude preceding the final peak. Similar waveforms have been observed in reverse correlations obtained in a similar manner from neocortical neurons in slice (Mainen and Sejnowski, 1995b). The time-course of the trough is directly related to τ_a, as seen by comparing fast adapting integrator (ii) and slow adapting integrator (iii) models. Also apparent is that the peak of the reverse correlation is substantially less diminished by increasing mean than is that of the leaky integrator model. Because the adapting models are less sensitive to the d.c. component of the input, a larger fraction of spikes are consistently accounted for by fluctuations about the mean.

Simulations in which repeated trials of synaptic noise are used to generate an estimate of the instantaneous firing rate show that adaptation currents have a striking effect on the coding of synaptic drive (Fig. V.5).

While the firing rate of the leaky integrator model (i) simply changes in proportion to the mean input (μ_s), the fast adapting integrator (ii) and slow adapting integrator (iii) models change their firing rate proportional to both μ_s the mean and its time derivative $\dot{\mu}_s$ (Fig. V.5A). "Differentiating" behavior can be seen dramatically as μ_s is stepped abruptly in positive and negative blocks. Note that $\dot{\mu}_s < 0$ cause abrupt cessation of firing just as positive $\dot{\mu}_s > 0$ cause a transient increase in firing.

Simulations of a small signal within very large background noise demonstrates that adaptation currents enhance the response to individual brief synaptic events (Fig. V.5B). A brief synaptic event contributes a small fraction of the μ_s averaged over τ_m and therefore has little effect on the firing rate of the leaky integrator model (Fig. V.5Bi). The fast adapting integrator and slow adapting integrator models are more sensitive to phasic events (Fig. V.5Bii and Biii), readily generating a strong and short-lasting response to the same events. The effective response τ for these models is lower due both to the parameter τ_m (25 msec vs. 50 mec) and due to the decrease in time constant caused by the adaptation conductance.

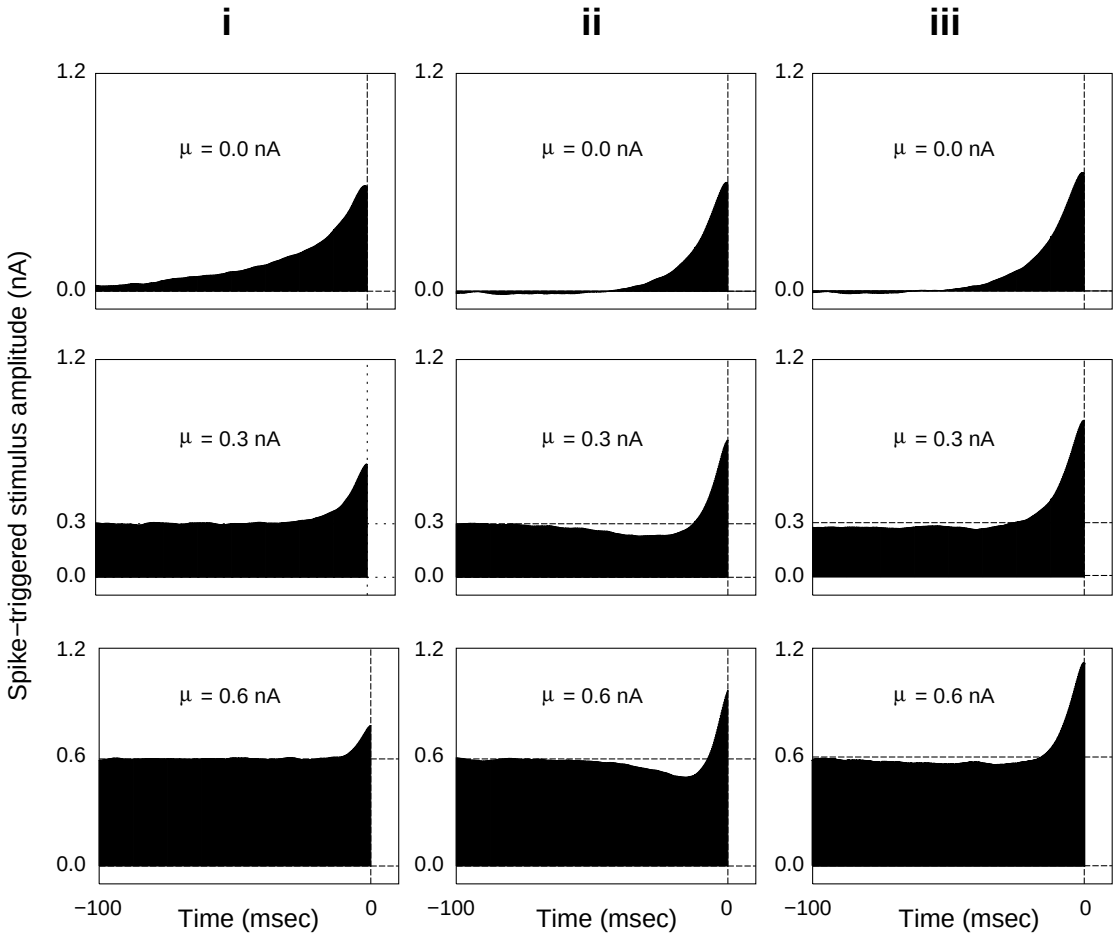

Figure V.4: Spike triggered stimulus averages (reverse correlations) for responses obtained with synaptic noise stimuli (σ_s = 0.3 nA, μ_s = 0, 0.3, 0.6 nA as indicated). For each reverse correlation, $\geq$ 5,000 spikes were averaged. The leaky integrator (i), fast adapting integrator (ii) and slow adapting integrator (iii) models are shown. Note the increase in base area and decrease in peak area with increasing μ_s. Also note the b-iphasic waveform of the reverse correlation and smaller reduction in peak area for the adapting models.

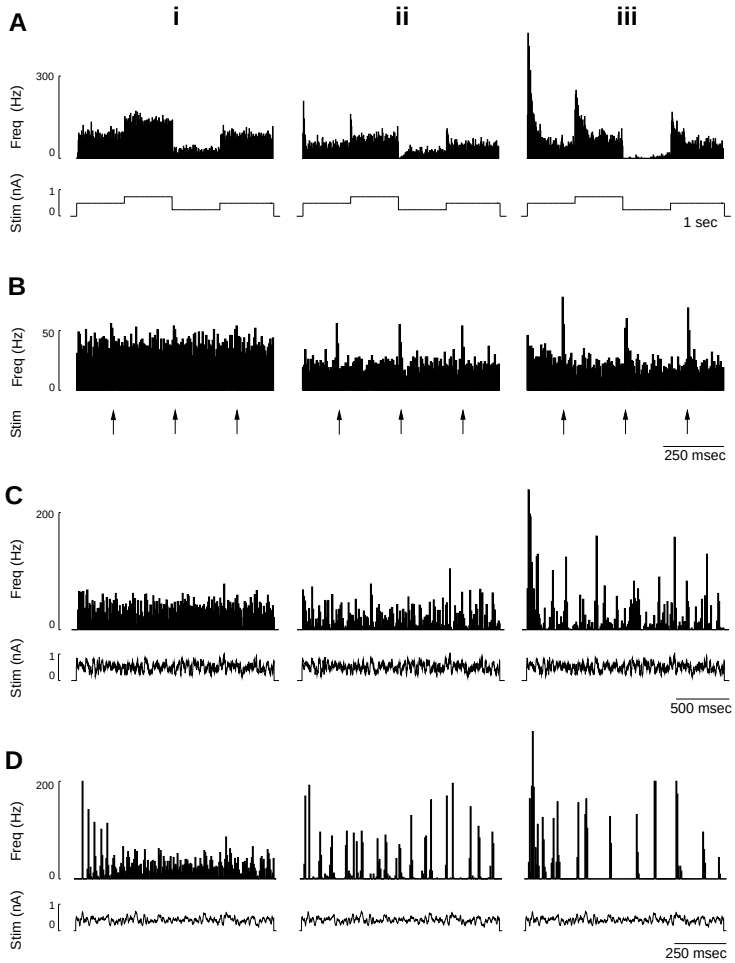

Figure V.5: Peri-stimulus firing rate histograms for three models driven by artificial "synaptic noise" (see Methods). The leaky integrator (i) fast adapting integrator (ii) and slow adapting integrator (iii) models are shown. A. Sensitivity to time derivative of input mean. The mean of the noise was stepped abruptly through several amplitudes: $\mu_s = 0.5, 0.75, 0.25$ and back to 0.5 nA (as indicated below the histograms). Histograms were computed over 100 trials; $\sigma_s = 0.2$ nA. B. Sensitivity to small brief events within large background noise. Three time-locked stimuli (arrows below histograms) were superimposed on background synaptic noise ($\sigma_s = 0.2$ nA, $\mu_s = 0.5$ nA; 200 trials). Each event had an alpha function amplitude waveform with $t_{peak} = 3$ msec, $t_{peak} = 0.18$ nA. C. Firing rate modulation by a time-varying signal within background noise. A fluctuating input signal ($\mu_s = 0.5$ nA, $\sigma_s = 0.1$ nA, shown below histograms) was applied for 100 trials in the presence of random background noise ($\mu_s = 0$ nA, $\sigma_s = 0.1$ nA) with the same variance and spectrum as the signal. D. Precision of spike timing in low noise conditions. The input was a fluctuating signal ($\mu_s = 0.4$ nA, $\sigma_s = 0.1$ nA, shown below histograms). Two types of random background noise were applied over 100 trials: (1) a fluctuating component with the same frequency spectrum as the signal ($\mu_s = 0$, $\sigma_s = 0.005$ nA) and (2) an random d.c. offset that varied from trial to trial (normal distribution with $\mu_s = 0$, $\sigma_s = 0.01$ nA).

When one random synaptic input current is considered "signal" rather than "noise" (the identical waveform is repeated over and over from trial to trial rather than being randomly regenerated as usual), then it is possible to assay the encoding of this "signal" within an equal background of noise with identical statistics (Fig. V.5C). In these simulations, the leaky integrator model shows little modulation of firing rate over time, consistent with encoding of μ_s, which is constant over the trial (Fig. V.5Ci). The fast adapting integrator model, however, shows a rapid, signal-locked modulation of the firing rate (Fig. V.5Cii). This effect is even more profound for the slow adapting integrator model (Fig. V.5Diii). Thus, the adapting models encode the features of a relatively fast time-varying input with greater temporal precision.

Finally, the encoding of a fluctuating "synaptic signal" within a background of much lower noise can be considered (Mainen and Sejnowski, 1995). A small background noise source and trial-to-trial variation in mean amplitude were used to perturb the response to a repeated stimulus (Fig. V.5D). Under identical noise conditions, the fast adapting integrator and slow adapting integrator models generate a more reliable encoding of a given time-varying signal than the leaky integrator model. Adaptation currents increase the robustness of the response pattern to slow drift or fluctuations in stimulus mean or equivalent model parameters such as threshold or resting level.

Discussion

The transduction of synaptic input into a spike train is a more complex process than spike generation in an axon. There is a fundamental difference of functions: transduction of an input signal vs. simple propagation of an impulse. Although we do not fully understand the strategy of the transduction process, a major requirement is likely to be the ability to map a large domain of inputs levels into a limited spike frequency range. Spike frequency adaptation fulfills this function while at the same time preserving sensitivity to rapid changes in input.

In this report, we developed and simulated a simple model for adaptation incorporated in a leaky integrator style threshold-crossing model. The adaptation mechanism was a true membrane conductance rather than a dynamically-varied threshold level. A similar combination of a first-order subthreshold dynamics and step increase in activation by a spike was found to be suitable for the dynamics of both voltage-dependent and Ca^{2+}-dependent adaptation conductances. While the former and not the latter are regularly activated at subthreshold voltages, we failed to find significant differences in their behavior in the simulations reported. As we concentrated on responses to depolarizing currents that were well suprathreshold, it is possible that larger differences would be apparent in examination of near threshold or subthreshold currents.

Current to spike transduction or "encoding" makes use of K^+ currents not only to repo-

larize the membrane following action potentials but also to sink current in order to limit the time before the next spike. Although these two functions can be subserved by the same current, the use of several K^+ conductances with different activation kinetics appears to be the strategy taken by neurons in the central nervous system. Slow voltage– and Ca^{2+}–dependent K^+ currents provide important forms of negative feedback that prevent excitatory input from driving a neuron to depolarized levels at which it would cease to fire due to Na^+ channel inactivation. At the same time, the slow kinetics of these conductances also extend the output range by permitting firing at much lower frequencies than possible with only the combination of leak conductance and fast action potential repolarization.

K^+ currents, such as the voltage-dependent I_M, with an activation time constant in the range of 50 msec, may reach equilibrium with one or two spike intervals (Schwindt et al., 1988). Such currents will therefore not be seen as a gradual slowing of spike frequency commonly associated with adaptation. Nevertheless, the presence of adaptation currents can be distinguished in other ways. We have noted that K^+ currents of this kinetic range produce "scooped" interspike voltage trajectories during responses to current steps, indeed a prominent feature of cortical neurons in vitro (McCormick et al., 1985; Connors and Gutnick, 1990). In responses to noisy stimuli, models repolarized by these currents have little sign of afterhyperpolarization. A lack of obvious spike "undershoot" is a regular feature of intracellular recordings of cortical neurons in vivo (e.g. Douglas et al., 1991). . Finally, strong adaptation currents might be detected extracellularly through their tendency to produce bimodal features in autocorrelation or interspike interval histograms(Fig. V.3). However, the superposition of multiple K^+ conductances with a variety of time constants (Schwindt et al., 1988; Foehring and Surmeier, 1993) may obscure this tendency.

While decreasing the sensitivity of firing rate to absolute stimulus amplitude, adaptation currents increase sensitivity to the rate of change of amplitude. Firing rates proportional to stimulus slope have been reported in cortical neurons using intracellular injection of ramp stimuli (Baldissera, Campadelli and Piccinelli, 1982). This property can also be seen as high-pass filtering of the input. The output of neurons whose firing is dominated by adaptation currents is therefore sensitive to fluctuations of the input at the expense of comparatively reduced sensitivity to a slower time-average input.

The K^+ conductances activated during spike frequency adaptation are substantially larger than the passive leak conductance. In addition to limiting firing by reducing the effective input resistance, this conductance decreases the effective time constant of the membrane. As moderate stimulus intensities, in the simulations shown, adaptation conductances resulted in a reduction by more than half of the effective time constant. A shorter membrane time constant allows the membrane voltage to change more abruptly and decreases the integration time between spikes. A

change in input leads more quickly to an increase or decrease in firing rate (Fig. V.3A).

By increasing relative sensitivity to stimulus fluctuations and decreasing the effective time constant, adaptation increases the irregularity of responses driven by noisy input (Fig. V.3A). Such variability of firing is indeed particularly prominent in the neocortex (Softky and Koch, 1993). If higher-frequency fluctuations about the mean input reflect synaptic"noise" (Shadlen and Newsome, 1994), then the resulting irregularity in spike timing may simply be the price of representing a wide range of input intensities within a limited range of firing frequencies. It is becomes less important to control the precise ratio of excitatory and inhibitory synaptic input (Shadlen and Newsome, 1994), because some of the role of balance is delegated to the spiking mechanism itself.

Adaptation currents can also be seen as enhancing a potentially useful tendency for a neuron to behave as a coincidence detector. The abrupt depolarization produced by the conjunction of several inputs will lead with much greater security to a spike than will the same inputs desynchronized in time. By further increasing the rate of change in input, a rapid hyperpolarization--depolarization sequence will be particularly effective in producing a spike. The mechanism of spike frequency adaptation by slow K^+ conductances contrasts with other mechanism for coincidence detection that call for strong dendritic Na^+ conductances (Softky, 1995).

In this vein, our simulations document several ways that adaptation conductances may increase reliability of the encoding of a temporally-structured input signal. First, in the presence of large amounts of background noise, an adapting neuron model is relatively more sensitive to the occurrence of a brief but relatively large synaptic event (Fig. V.5B)–it is a more non-linear "coincidence detector" (Abeles, 1982).

A second scenario in which adaptation dramatically affects the nature of encoding is the response to a time-varying signal within background noise of similar amplitude and statistics (Fig. V.5C). This would correspond, for example, to a signal transmitted across synapses with imperfect reliability. This result is particularly interesting in light of a recent report showing a similar modulation of firing rate in recordings from neurons in the visual cortex of awake monkeys (Bair et al., 1994).

Finally, the present results provide insight into the precision of spike timing in low noise conditions, as recently described in recordings from neurons in neocortical slices (Mainen and Sejnowski, 1995b). The bi-phasic waveform of the stimulus–spike train reverse correlation (Fig. V.4) for adapting neuron models is similar to that measured in slice neurons (and contrasts with monophasic reverse correlation waveforms obtained for non-adapting leaky integrator models). This suggests that adaptation currents may be responsible for an enhanced sensitivity to stimulus transients described in that study. The variability of spike timing in responses to d.c. stimuli (Mainen and Sejnowski, 1995b) can be attributed in part to measurable drift in recording conditions such

as the cell resting potential and input resistance. Due to adaptation currents, the sensitivity to higher-frequency stimulus components will be high relative to the sensitivity to slower changes (Fig. V.5D). Stimulus time-locking therefore leads to a strong increase in the reliability of spike timing.

Using slow K^+ conductances for spike frequency adaptation, the advantages of operating in a high-gain "balance condition" (Bell, Mainen and Sejnowski, 1995; Tsodyks and Sejnowski, 1995) can be achieved over a wide range of mean stimulus intensities. If rapid variations in input intensity constitute a signal rather than haphazard fluctuations about a slower mean, adaptation should increase the information encoded in the spike train about the input. This prediction remains to be quantified by a more rigorous calculation of the information rate (Bialek et al., 1991).

References

Abeles, M. (1982). Role of the cortical neuron: integrator or coincidence detector? *Israeli J. Med. Sci.*, 18(83-92).

Adams, P. R., Brown, D. A., and Constanti, A. (1982). M-currents and other potassium currents in bullfrog sympathetic neurones. *J. Physiol.*, 330:537–572.

Allen, C. and Stevens, C. F. (1994). An evaluation of the causes for unreliability of synaptic transmission. *Proc. Natl. Acad. Sci. USA*, 91:10380–10383.

Alzheimer, C., Schwindt, P. C., and Crill, W. E. (1993). Modal gating of Na^+ channels as a mechanism of persistent Na^+ current in pyramidal neurons from rat and cat sensorimotor cortex. *J. Neurosci.*, 13:660–673.

Amitai, Y., Friedman, A., Connors, B. W., and Gutnick, M. J. (1993). Regenerative electrical activity in apical dendrites of pyramidal cells in neocortex. *Cerebral Cortex*, 3:26–38.

Angelides, K. J., Elmer, L. W., Loftus, D., and Elson, E. (1988). Distribution and lateral mobility of voltage-dependent sodium channels in neurons. *J. Cell Biol.*, 106:1911–1924.

Bair, W., Koch, C., Newsome, W. T., and Britten, K. H. (1994). Reliable temporal modulation in cortical spike trains in awake monkey. *Soc. Neurosci. Abstr.*, 20:1279.

Baldissera, F., Campadelli, P., and Piccinelli, L. (1982). Impulse coding of ramp currents intracellularly injected into pyramidal tract neurones. *Exp Brain Res.*, 48:455–458.

Baldissera, F. and Gustafsson, B. (1971). Regulation of repetitive firing in motoneurones by the afterhyperpolarization conductance. *Brain Res.*, 30:431–434.

Baldissera, F., Gustafsson, B., and Parmiggiani, F. (1978). Saturating summation of the afterhyperpolarization conductance in spinal motoneurones: a mechanism for 'secondary range' repetitive firing. *Brain Res.*, 146:69–82.

Barlow, H. B. (1972). Single units and sensation: a neuron doctrine for perceptual psychology? *Perception*, 1:371–394.

Bedlack, R. S. J., Wei, M., Fox, S. H., Gross, E., and Loew, L. M. (1994). Distinct electric potentials in soma and neurite membranes. *Neuron*, 13:1187–1193.

Bell, A., Mainen, Z. F., and Sejnowski, T. J. (1995). 'Balancing of conductances' may explain irregularity of cortical spiking. Technical Report 9502, Institute for Neural Computation, La Jolla, CA.

Belluzzi, O. and Sacchi, O. (1986). A quantitative description of the sodium current in the rat sympathetic neurone. *J. Physiol.*, 380:275–291.

Bernander, Ö., Douglas, R. J., Martin, K. A. C., and Koch, C. (1991). Synaptic background activity influences spatiotemporal integration in single pyramidal cells. *Proc. Natl. Acad. Sci. USA*, 88:11569–11573.

Bernander, O., Koch, C., and Usher, M. (1994). The effect of synchronized inputs at the single neuron level. *Neural Computation*, 6:622–641.

Bialek, W., Rieke, F., de Ruyter van Steveninck, R. R., and Warlan, D. (1991). Reading a neural code. *Science*, 252:1854–1857.

Black, J. A., Kocsis, J. D., and Waxman, S. G. (1990). Ion channel oranization of the myelinated fiber. *Tends. Neurosci.*, 13:48–54.

Brown, D. A. (1990a). G-proteins and potassium currents in neurons. *Annu. Rev. Physiol.*, 52:215–242.

Brown, D. A. (1990b). Regulation of cell excitability. *Curr. Opin. Cell Biol.*, 2:221–230.

Bryant, H. L. and Segundo, J. P. (1976). Spike initiation by transmembrane current: A white-noise analysis. *J. Physiol.*, 260:279–314.

Bullock, T. H. (1970). The reliability of neurons. *J. Gen. Physiol.*, 55:565–584.

Burns, B. and Webb, A. C. (1976). The spontaneous activity of neurons in the cat's cerebral cortex. *Proc. Roy. Soc. Lond. B*, 194:211–223.

Burns, B. D. (1968). *The uncertain nervous system*. Arnold E., London.

Bush, P. C. and Sejnowski, T. J. (1994). Effects of inhibition and dendritic saturation in simulated neocortical pyramidal cells. *J. Neurophysiol.*, 71:2183–2193.

Calvin, W. H. (1974). Generation of spike trains in CNS neurons. *Brain Res.*, 84:1–22.

Calvin, W. H. and Stevens, C. F. (1968). Synaptic noise and other sources of randomness in motorneuron interspike intervals. *J. Neurophysiol.*, 31:574–587.

Carr, C. E. and Konishi, M. (1990). A circuit for detection of interaural time differences in the brain stem of the barn owl. *J. Neurosci.*, 10:3227–3246.

Cartling, B. (1993). Control of the complexity of associative memory dynamics by neuronal adaptation. *Int. J. Neural Systems*, 4:129–141.

Chagnac-Amitai, Y., Luhmann, H. J., and Prince, D. A. (1990). Burst generating and regular spiking layer 5 pyramidal neurons of rat neocortex have different morphological features. *J. Comp. Neurol.*, 296:598–613.

Chiu, S. Y. and Schwarz, W. (1987). Sodium and potassium currents in acutely demyelinated iternodes of rabbit sciatic nerves. *J. Physiol.*, 391:631–649.

Connors, B. W. and Gutnick, M. J. (1990). Intrinsic firing patterns of diverse neocortical neurons. *Trends Neurosci.*, 13:99–104.

Cooley, J. W. and Dodge, F. A. (1966). Digital computer simulations for excitation and propagation of the nerve impulse. *Biophys. J.*, 6:583–599.

Coombs, J. S., Curtis, D. R., and Eccles, J. C. (1957). The generation of impulses in motoneurones. *J. Physiol.*, 139:232–249.

Cowan, R. L. and Wilson, C. J. (1994). Spontaneous firing patterns and axonal projections of single corticostriatal neruons in the rat medial agranular cortex. *J. Neurophysiol.*, 71:17–32.

Croner, L. J., Purpura, K., and Kaplan, E. (1993). Response variability in retinal ganglion cells of primates. *Proc. Natl. Acad. Sci. USA*, 90:8128–8130.

Cummins, T. R., Xia, Y., and Haddad, G. G. (1994). Functional properties of rat and human neocortical voltage-sensitive sodium currents. *J. Neurophysiol.*, 71:1052–1064.

De Schutter, E. and Bower, J. M. (1994). An active membrane model of the cerebellar purkinje cell I. simulation of current clamps in slice. *J. Neurophysiol.*, 71:375–400.

Deschênes, M. and Landry, P. (1980). Axonal branch diameter and spacing of nodes in the terminal arborization of identified thalamic and cortical neurons. *Brain Res.*, 191:538–544.

Dodge, F. A. and Cooley, J. W. (1973). Action potential of the motorneuron. *IBM J. Res. Develop.*, 17:219–229.

Douglas, R. J., Martin, K. A. C., and Whitteridge, D. (1991). An intracellular analysis of the visual responses of neurones in cat visual cortex. *J. Physiol.*, 440:659–696.

Ericinska, M. and Silver, I. A. (1989). ATP and brain function. *J. Cereb. Blood Flow Metab.*, 9:2–19.

Fariñas, I. and DeFelipe, J. (1991). Patterns of synaptic input on corticocortical and corticothalamic cells in the cat visual cortex. II. The axon initial segment. *J. Comp. Neurol.*, 304:70–77.

Ferster, D. and Jagadeesh, B. (1992). EPSP-IPSP interactions in cat visual cortex studies with *in vivo* whole-cell patch recordings. *J. Neurosci.*, 12:1262–1274.

Foehring, R. C. and Surmeier, D. J. (1993). Voltage-gated potassium currents in acutely dissociated rat cortical neurons. *J. Neurophysiol.*, 70:51–63.

Frank, K. and Fuortes, M. G. F. (1957). Presynaptic and postsynaptic inhibition of monosynaptic reflexes. *Fed. Proc.*, 16:39–40.

Gerstein, G. and Mandelbrot, B. (1964). Radnom walk models for the spike activity of a single neuron. *Biophys. J.*, 4:41–68.

Gogan, P., Gueritaud, J. P., and Tyc-Dumont, S. (1983). Comparison of antidromic and orthodromic action potentials of identified motor axons in the cat's brain stem. *J. Physiol.*, 335:205–220.

Graham, B. and Redman, S. (1994). A simulation of action potentials in synaptic boutons during presynaptic inhibition. *J. Neurophysiol.*, 71:538–549.

Granit, R., Kernell, D., and Smith, R. S. (1963). Delayed depolarization and the repetitive response to intracellular stimulation of mammalian motoneurons. *J. Physiol.*, 168:100–115.

Gutfreund, Y., Yarom, Y., and Segev, I. (1995). Subthreshold oscillations and resonant frequency in guinea-pig cortical neurons: physiology and modelling. *J. Physiol.*, 483:621–640.

Hamill, O. P., Huguenard, J. R., and Prince, D. A. (1991). Patch-clamp studies of voltage-gated currents in identified neurons of the rate cerebral cortex. *Cerebral Cortex*, 1:48–61.

Harris, K. M. and Stevens, J. K. (1989). Dendritic spines of CA1 pyramical cells in the rat hippocampus: Serial electron microscopy with reference to their biophysical characteristics. *J. Neurosci.*, 9:2982–2997.

Haug, H. (1968). Quantitative elektronenmikroskopische untersuchungen über den markfaseraufbau in der sehrinde der katze. *Brain Res.*, 11:65–84.

Hessler, N. A., Shirke, A. M., and Malinow, R. (1993). The probability of release at a mammalian synapses. *Nature*, 366:569–572.

Hines, M. (1993). NEURON — a program for simulation of nerve equations. In Eeckman, F. H., editor, *Neural Systems: Analysis and Modeling*, pages 127–136. Kluwer Academic Publishers, Boston, MA.

Hodgkin, A. L. and Huxley, A. F. (1952). A quantitative description of membrane current and its application to conduction and excitation in nerve. *J. Physiol.*, 117:500–544.

Huguenard, J. R., Hamill, O. P., and Prince, D. A. (1988). Developmental changes in Na^+ conductances in rat neocortical neurons: Appearance of a slowly inactivating component. *J. Neurophysiol.*, 59:778–794.

Huguenard, J. R., Hamill, O. P., and Prince, D. A. (1989). Sodium channels in dendrites of rat cortical pyramidal neurons. *Proc. Natl. Acad. Sci. USA*, 86:2473–2477.

Jensen, M. S., Azouz, R., and Yaari, Y. (1994). Variant firing patterns in rat hippocampal cells modulated by extracellular potassium. *J. Neurophysiol.*, 71:831–839.

Jester, J. M., Campbell, L. W., and Sejnowski, T. J. (1995). Associative EPSP-spike potentiation induced by pairing orthodromic and antidromic stimulation in rat hippocampal slices. *J. Physiol.*, 484:689–705.

Kaars, C. and Faber, D. S. (1981). Myelinated central vertebrate axon lacks voltage-sensitive potassium conductance. *Nature*, 212:1063–1065.

Kandel, E. R. and Spencer, W. A. (1961). Electrophysiology of hippocampal neuros. I. After potentials and repetitive firing. *J. Neurophysiol.*, 24:243–259.

Kobayashi, T., Storrie, B., Simons, K., and Dotti, C. G. (1992). A functional barrier to movement of lipids in polarized neurons. *Nature*, 359:647–650.

Koch, C. and Segev, I. (1989). *Methods in Neuronal Modeling*. MIT Press, Cambridge, MA.

Korenberg, M. J., Sakai, H. M., and Naka, K. (1989). Dissection of the neuron network in the catfish inner retina. III. Interpretation of spike kernels. *J. Neurophysiol.*, 61:1110–1120.

Lancaster, B. and Zucker, R. S. (1994). Photolytic manipulation of Ca^{2+} and the time course of slow, Ca^{2+}activated K^+ current in rat hippocampal neurones. *J. Physiol.*, 475:229–239.

Larkman, A. U. (1991). Dendritic morphology of pyramidal neurones of the visual cortex of the rat: III. Spine distributions. *J. Comp. Neurology*, 306:332–343.

Larkman, A. U. and Mason, A. (1990). Correlations between morphology and electrophysiology of pyramidal neurons in slices of rat visual cortex. I. Establishment of cell classes. *J. Neurosci.*, 10:1407–1414.

Lass, Y. and Abeles, M. (1975). Transmission of information by the axon. I. Noise and memory in the myelinated nerve fiber of the frog. *Biol. Cybernetics*, 19:61–67.

Levine, M. W., Saleh, E. J., and Yarnold, P. R. (1988). Statistical properties of the maintained discharge of chemically isolated ganglion cells in goldfish retina. *Visual Neurosci.*, 1:31–46.

Li, M., West, J. W., Lai, Y., Scheuer, T., and Catterall, W. A. (1992). Functional modulation of brain sodium channels by cAMP-dependent phosphorylation. *Neuron*, 8:1151–1159.

Lisberger, S. G. and Sejnowski, T. J. (1992). Motor learning in a recurrent network model based on the vestibulo-ocular reflex. *Nature*, 360:159–161.

Lytton, W. W. and Sejnowski, T. J. (1991). Simulations of cortical pyramidal neurons synchronized by inhibitory interneurons. *J. Neurophysiol.*, 66:1059–1079.

Madison, D. V. and Nicoll, R. A. (1984). Control of the repetitive discharge of rat ca1 pyramidal neurones in vitro. *J. Physiol.*, 354:319–331.

Magee, J. C. and Johnston, D. (1995). Synaptic activation of voltage-gated channels in the dendrites of hippocampal pyramidal neurons. *Science*, 268:301–304.

Mainen, Z. F., Joerges, J., Huguenard, J. R., and Sejnowski, T. J. (1995). A model of spike initiation in neocortical pyramidal neurons. *Neuron*, 15. In press.

Mainen, Z. F. and Sejnowski, T. J. (1995a). Dendritic structure determines repetitive firing properties in model neocortical neurons. In review.

Mainen, Z. F. and Sejnowski, T. J. (1995b). Reliability of spike timing in neocortical neurons. *Science*, 268:1503–1506.

Major, G., Larkman, A. U., Jonas, P., Sakmann, B., and Jack, J. J. (1994). Detailed passive cable models of whole-cell recorded CA3 pyramidal neurons in rat hippocampal slices. *J. Neurosci.*, 14:4613–4638.

Malinow, R. and Tsien, R. W. (1990). Presynaptic enhancement shown by whole-cell recordings of long-term potentiation in hippocampal slices. *Nature*, 346:177–180.

Marmarelis, P. Z. and Marmarelis, V. Z. (1978). *Analysis of Physiological Systems: The White Noise Approach*. Plenum Press, New York.

Mason, A. and Larkman, A. U. (1990). Correlations between morphology and electrophysiology of pyramidal neurons in slices of rat visual cortex. II. Electrophysiology. *J. Neurosci.*, 10:1415–1428.

Maunsell, J. H. and Gibson, J. R. (1992). Visual response latencies in striate cortex of the macaque monkey. *J. Neurophysiol.*, 68:1332–1344.

McClurkin, J. W., Optican, L. M., Richmond, B. J., and Gawne, T. J. (1991). Concurrent processing and complexity of temporally encoded neuronal messages in visual perception. *Science*, 253:675–677.

McCormick, D. A., Connors, B. W., Lighthall, J. W., and Prince, D. A. (1985). Comparative electrophysiology of pyramidal and sparsely spiny stellate neurons of the neocortex. *J. Neurophysiol.*, 54:782–806.

Middlebrooks, J. C., Clock, A. E., Xu, L., and Green, D. M. (1994). A panoramic code for sound location by cortical neurons. *Science*, 264:842–844.

Moore, J. W., Stockbridge, N., and Westerfield, M. (1983). On the site of impulse generation in a neurone. *J. Physiol.*, 336:301–311.

Moore, J. W. and Westerfield, M. (1983). Action potential propagation and threshold parameters in inhomogeneous regions of squid axons. *J. Physiol.*, 336:285–300.

Murphy, B. J., Rossie, S., DeJongh, K. S., and Catterall, W. A. (1993). Identification of the sites of selective phosphorylation and dephosphorylation of the rat brain Na^+ channel alpha subunit by cAMP-dependent protein kinase and phosphoprotein phosphatases. *J. Biol. Chem.*, 268:27355–27362.

Noda, H. and Adey, R. (1970). Firing variability in cat association cortex during sleep and wakefulness. *Brain Res.*, 18:513–526.

Otmakhov, N., Shirke, A. M., and Malinow, R. (1993). Measuring the impact of probabilistic transmission on neuronal output. *Neuron*, 10:1011–1111.

Palay, S. L., Sotelo, C., Peters, A., and Orkland, P. M. (1968). The axon hillock and the initial segment. *J. Cell Biol.*, 37:193–201.

Peters, A. and Jones, E. G. (1984). *Cerebral Cortex Vol. 1: Cellular Components of the Cerebral Cortex*. Plenum, New York.

Peters, A., Proskauer, C. C., and Kaiserman-Abramof (1968). The small pyramidal neuron of the rat cerebral cortex: the axon hillock and the initial segment. *J. Cell Biol.*, 39:604–619.

Phillips, J. R., Johansson, R. S., and Johnson, K. O. (1992). Responses of human mechanoreceptive afferents to embossed dot arrays scanned across fingerpad skin. *J. Neurosci.*, 12:827–839.

Pitler, T. A. and Alger, B. E. (1994). Depolarization-induced suppression of gabaergic inhibition in rat hippocampal pyramidal cells: G protein involvement in a presynaptic mechanism. *Neuron*, 13:1447–1455.

Regehr, W. G., Kehoe, J. S., Ascher, P., and Armstrong, C. (1993). Synaptically triggered action potentials in dendrites. *Neuron*, 11:145–151.

Regehr, W. G., Konnerth, A., and Armstrong, C. M. (1992). Sodium action potentials in the dendrites of cerebellar purkinje cells. *Proc. Natl. Acad. Sci. USA*, 89:5492–5496.

Reuveni, I., Friedman, A., and Amitai, M. J. (1993). Stepwise repolarization from Ca^{2+} plateaus in neocortical pyramidal cells: Evidence for nonhomogeneous distribution of HVA Ca^{2+} channels in dendrites. *J. Neurosci.*, 13:4609–4621.

Rhodes, P. A. and Gray, C. M. (1994). Simulations of intrinsically bursting neocortical pyramidal neurons. *Neural Computation*, 6:1086–11100.

Rice, S. O. (1954). Mathematical analysis of random noise. In Wax, N., editor, *Selected Papers on Noise and Stochastic Processes*, pages 133–294. Dover, New York.

Rosenmund, C., Clements, J. D., and Westbrook, G. L. (1993). Nonuniform probability of release at a hippocampal synapse. *Science*, 262:754–757.

Sah, P., Gibb, A. J., and Gage, P. W. (1988). The sodium current underlying action potentials in guinea pig hippocampal CA1 neurons. *J. Gen. Physiol.*, 91:373–398.

Schellart, N. A. and Spekreijse, H. (1973). Origin of the stochastic nature of ganglion cell activity in isolated goldfish retina. *Vision Res.*, 13:337–345.

Schuman, E. M. and Madison, D. V. (1994). Locally distributed synaptic potentiation in the hippocampus. *Science*, 263:532–536.

Schwindt, P. C., Spain, W. J., Foehring, R. C., Chubb, R. C., and Crill, W. E. (1988). Slow conductance in neurons from cat sensorimotor cortex in vitro and their role in slow excitability changes. *J. Neurophysiol.*, 59:450–467.

Shadlen, M. N. and Newsome, W. T. (1994). Noise, neural codes and cortical organization. *Curr. Opin. Neurobiol.*, 4:579–???

Sheng, M., Tsaur, M. L., Jan, Y. N., and Jan, L. Y. (1992). Subcellular segregation of two A-type K^+ channel proteins in rat central neurons. *Neuron*, 9:271–284.

Singer, W. and Gray, C. M. (1995). Visual feature integration and the temporal correlation hypothesis. *Annu. Rev. Neurosci.*, 18:555–586.

Skaugen, E. (1980). Firing behavior in nerve cell models with a two-state pore system. *Acta. Physiol. Scand.*, 109:377–392.

Sloper, J. J. and Powell, T. P. S. (1978). A study of the axon initial segment and the proximal axon of neurons in the primate motor and somatic sensory cortices. *Phil. Trans. R. Soc. Lond. B*, 285:173–197.

Snowden, R. J., Treue, S., and Andersen, R. A. (1992). The response of neurons in areas v1 and mt of the alert rhesus monkey to moving random dot patterns. *Exp. Brain Res.*, 88:389–400.

Softky, W. (1995). Simple codes versus efficient codes. *Curr. Opin. Neurobiol.*, 5:239–247.

Softky, W. R. and Koch, C. (1993). The highly irregular firing of cortical cells is inconsistent with temporal integration of random epsps. *J. Neurosci.*, 13:334–350.

Spruston, N., Jaffe, D. B., and Johnston, D. (1994). Dendritic attenuation of synaptic potentials and currents: the role of passive membrane properties. *Trends Neurosci.*, 17:161–164.

Srinivasan, Y., Elmer, L., Davis, J., Bennett, V., and Angelides, K. (1988). Ankyrin and spectrin associate with voltage-dependent sodium channels in barin. *Nature*, 333:177–180.

Stafstrom, C. E., Schwindt, P. C., and Crill, W. E. (1984). Repetitive firing in layer V neurons from cat neocortex in vitro. *J. Neurophysiol.*, 52:264–277.

Stein, R. B. (1967). The information capacity of nerve cells using a frequency code. *Biophys. J.*, 7:796–826.

Stevens, C. F. and Wang, Y. (1995). Facilitation and depression at single central synapses. *Neuron*, 14:795–802.

Storm, J. F. (1990). Potassium currents in hippocampal pyramidal cells. *Prog. Brain Res.*, 83:161–187.

Stratford, K., Mason, A., Larkman, A., Major, G., and Jack, J. J. B. (1989). The modelling of pyramidal neurones in the visual cortex. In Durbin, R., Miall, C., and Mitchison, G., editors, *The Computing Neuron*. Addison-Wessley, London.

Strehler, B. L. and Lestienne, R. (1986). Evidence on precise time-coded symbols and memory of patterns in monkey cortical neuronal spike trains. *Proc. Natl. Acad. Sci. USA*, 83:9812–9816.

Stuart, G. J., Dodt, H. U., and Sakmann, B. (1993). Recordings from the soma and dendrites of neurones in brain slices using infrared video microscopy. *Pflügers Arch. ges. Physiol.*, 423:511–518.

Stuart, G. J. and Sakmann, B. (1994). Active propagation of somatic action potentials into neocortical pyramidal cell dendrites. *Nature*, 367:69–72.

Stühmer, W., Methfessel, C., Sakmann, B., Noda, M., and Numa, S. (1987). Patch clamp characterization of sodium channels expressed from rat brain cDNA. *Eur. Biophys. J.*, 14:131–138.

Suga, N., Olsen, J. F., and Butman, J. A. (1990). Specialized subsystems for processing biologically important complex sounds: cross-correlation analysis for ranging in the bat's brain. *Cold Spring Harbor. Symp. Quant. Biol.*, 55:585–597.

Thomson, A. M., Deuchars, J., and West, D. C. (1993). Large, deep layer pyramid-pyramid single-axon EPSPs in slices of rat motor cortex display paired pulse and frequency-dependent depression, mediated presynaptically and salf-facilitation, mediated postsynaptically. *J. Neurophysiol.*, 70:2354–2369.

Tolhurst, D. J., Movshon, J. A., and Dean, A. F. (1983). The statistical reliability of signals in single neurons in cat and monkey visual cortex. *Vision Res.*, 23:775–785.

Tomko, G. J. and Crapper, D. R. (1974). Neuronal variability: non-stationary responses to identical visual stimuli. *Brain Res.*, 79:405–418.

Tovee, M. J., Rolls, E. T., and Bellis, R. P. (1993). Information encoding and the responses of single neurons in the primate visual cortex. *J. Neurophysiol.*, 70:640–654.

Traub, R. D., Jefferys, J. G. R., Miles, R., Whittington, M. A., and Tóth, K. (1994). A branching dendrite model of a rodent CA3 pyramidal neurone. *J. Physiol.*, 481:79–95.

Traub, R. D., Wong, R. K. S., Miles, R., and Michelson, H. (1991). A model of a CA3 hippocampal pyramidal neuron incorporating voltage-clamp data on intrinsic conductances. *J. Neurophysiol.*, 66:635–650.

Tsodyks, M. and Sejnowski, T. J. (1995). Rapid state switching in balanced cortical networks. *Network*, 6:1–14.

Vaadia, E., Haalman, I., Abeles, M., Bergman, H., Prut, Y., Slovin, H., and Aertsen, A. (1995). Dynamics of neuronal interations in monkey cortex in relation to behavioral events. *Nature*, 373:515–518.

Vincent, P. and Marty, A. (1993). Neighboring cerebellar Purkinje cells communicate via retrograde inhibition of common presynaptic interneurons. *Neuron*, 11:885–893.

Wang, Z. and McCormick, D. A. (1993). Control of firing mode of corticotectal and corticopontine layer V burst-generating neurons by norepinepherine, acetylcholine, and 1 *S*,*3R*-ACPD. *J. Neurosci.*, 13:2199–2216.

Waxman, S. G. and Ritchie, J. M. (1993). Molecular dissection of the myelinated axon. *Ann. Neurol.*, 33:121–136.

Westenbroek, R. E., Merrick, D. K., and Catterall, W. A. (1989). Differential subcellular localization of the R_I and R_{II} Na^+ channel subtypes in central neurons. *Neuron*, 3:695–704.

Westrum, L. E. (1970). Observations on the initial segments of axons in the prepyriform cortex of the rat. *J. Comp. Neurol.*, 139:337–356.

Wollner, D. A. and Catterall, W. A. (1986). Localization of sodium channels in axon hillocks and initial segments of retinal ganglion cells. *Proc. Natl. Acad. Sci. USA*, 83:8424–8428.

Wong, R. K. S. and Prince, D. A. (1978). Participation of calcium spikes during intrinsic burst firing in hippocmapal neurons. *Brain Res.*, 159:385–390.

Xing, J. and Gerstein, G. L. (1994). Simulation of the dynamic receptive fields in primary visual cortex. *Vision Res.*, 34:1901–1911.

Yuste, R., Gutnick, M. J., Saar, D., Delaney, R. D., and Tank, D. W. (1994). Ca^{2+} accumulations in dendrites of neocortical pyramidal neurons: An apical band and evidence for two functional compartments. *Neuron*, 13:23–43.

Zucker, R. S. (1989). Short-term synaptic plasticity. *Annu. Rev. Neurosci.*, 12:1213–1231.